Theses & Dissertations   Graduate Studies

Spring 5-9-2020

Delivery for Hydrophobic Drugs for Treating Pancreatic Cancer

Saud Almawash
University of Nebraska Medical Center

DELIVERY OF HYDROPHOBIC DRUGS FOR TREATING PANCREATIC CANCER

by

Saud A. Almawash

A DISSERTATION

Presented to the Faculty of

the University of Nebraska Graduate College

in Partial Fulfillment of the Requirements

for the Degree of Doctor of Philosophy

Pharmaceutical Sciences Graduate Program

Under the supervision of Professor Ram I. Mahato

University of Nebraska Medical Center

Omaha, Nebraska

February, 2020

Supervisory Committee:

Rakesh K. Singh, Ph.D.	Jered Garrison, Ph.D.
Rongshi Li, Ph.D.	Apar Kishor Ganti, M.D.

ACKNOWLEDGMENTS

Finally, I would like to dedicate this work to parents Mr. Abdulaziz and Mrs. Hala, my wife, Mrs. Raneem, and my adorable, loving daughter Nora for their endless love and continued support.

ABSTRACT

The main objective of this dissertation is to treat pancreatic cancer by developing an amphiphilic biodegradable polymer that is capable of carrying small hydrophobic molecules. These polymers were used to prepare micelle or nanoparticles. They were characterized and evaluated in vitro settings and pancreatic cancer mouse model (In vivo).

In chapter 1, an overview of pancreatic cancer pathogenesis, the implicated pathways, and current treatments will be highlighted

In chapter 2, small molecules Docetaxel (DTX) or cyclopamine (CYP) were conjugated into methoxy poly(ethylene glycol)-block-poly(2-methyl-2-carboxyl-propylene carbonate-graft-dodecanol) to form polymeric conjugate of docetaxel (P-DTX) or polymeric conjugate of cyclopamine (P-CYP). Polymeric micelles were prepared and characterized for particle size, cytotoxicity, and synergism. Micelles containing both DTX and CYP were assessed in an orthotopic pancreatic tumor model. The combination treatment of P-DTX micelles and P-CYP effectively inhibited tumor growth compared to monotherapy, either P-DTX micelle or P-CYP micelle. In immunohistochemical analysis, tumor sections of mice treated with combined-therapy revealed a low level of tumor cell proliferation markers, a high level of apoptotic cell markers compared to either P-DTX micelles or P-CYP micelles.

In chapter 3, a small molecule targeting two different pathways SF2523 was loaded into nanoparticles prepared by using a biodegradable copolymer mPEG-b-p(CB-co-LA). Polymeric nanoparticles containing SF2523 were characterized for particle size, drug loading, encapsulation efficiency, microsomal stability, and cytotoxicity in vitro. Polymeric nanoparticles loaded with SF2523 were tested in an orthotopic pancreatic cancer mouse model. It inhibited tumor growth effectively compared to SF2523 as a free

drug. Mice treated with polymeric nanoparticle containing SF2523 showed better restoration of the interstitial fluid pressure of the pancreas compared to mice treated with SF2523 as a free drug. In the immunohistochemical assay, the Tumor section of mice treated with Polymeric nanoparticles loaded with SF2523 showed a lower level of tumor cell proliferation markers and a high level of apoptotic cell markers. Furthermore, polymeric nanoparticles containing SF2523 significantly decrease the level of desmoplasia (Collagen-1 and α-SMA) in the tumor section compared to SF2523 as a free drug.

In chapter 4, all results from the first and second projects will be summarized and, future research direction will be provided.

TABLE OF CONTENTS

List of Figures

List of Tables

LIST OF ABBREVIATIONS

α-smooth muscle actin (α-SMA)

β-nicotinamide adenine dinucleotide phosphate (NADPH)

Bromodomian and extra-terminal (BET)

cyclin-dependent kinase inhibitor (CDKN1A)

cancer stem cells (CSCs),

c-Jun N-terminal kinases (JNK)

cancer-associated fibroblast (CAF)

Cyclopamine (CYP)

Carbon Nanotubes (CNTs)

Dodecanol (DC)

Dichloromethane (DCM)

Docetaxel (DTX)

Dulbecco's modified eagle medium (DMEM)

Epidermal Growth Factor Receptor (EGFR)

Extracellular matrix (ECM)

Encapsulation efficiency (EE)

Enhanced Permeability and Retention (EPR)

FAK-protein kinase B (AKT)

Fetal bovine serum (FBS)

Gemcitabine (GEM)

Guanosine triphosphate (GTP)

Guanosine diphosphate (GDP)

HEDGEHOG (Hh)

Hairy and enhancer of split-1 (Hes1)

Hematoxylin and eosin (H&E)

Human liver microsomes (HLM)

Interstitial fluid pressure (IFP)

Intraepithelial neoplasias (PanINs)

Iron Oxide Nanoparticles (IONP's)

Intravenous (IV)

Liposomal irinotecan (nal-IRI)

Methoxy poly (ethylene glycol)-b-poly (carbonate-colactide) [mPEG-b-P(CB-co-LA)]

Methoxy poly(ethylene glycol)-block-poly(2-methyl- 2-carboxylpropylenecarbonate-graftdodecanol-graft-cyclpamine) (P- CYP)

Methoxy poly(ethylene glycol)-blockpoly(2-methyl- 2-carboxylpropylenecarbonate-graftdodecanol-graft-docetaxel) (P-DTX)

3-(4,5-dimethyl-thiazol-2-yl)-2,5-diphenyl tetrazolium bromide (MTT)

Nanoparticles (NPs)

nuclear factor of activated T-cells (NFAT)

Pancreatic cancer (PC)

12-pass transmembrane protein receptor PATCHED (PTCH)

7-pass transmembrane protein receptor SMOOTHENED (SMO)

phosphoinositol-3 kinase (PI3K),

PBST Phosphate Buffered Saline with Tween

Pancreatic stellate cells (PSCs)

Phosphoinositide 3-kinases (PI3K)

pancreatic intraepithelial neoplasias (PanINs)

poly(ethylene oxide)-block-poly(lactic acid) (PEO-b-PLA)

Propidium Iodide (PI)

Paclitaxel (PTX)

Pancreatic ductal adenocarcinoma (PDAC)

Reactive oxygen species (ROS)

rat sarcoma virus (Ras)

SHh Sonic hedgehog

SF2523 nanoparticles (SF2325-NP)

tumor microenvironment (TME)

vismodegib (GDC-0449)

zinc finger E-box binding homeobox 1 (ZEB1)

1 CHAPTER 1. AN OVERVIEW OF PANCREATIC CANCER AND CURRENT TREATMENT

1.1 INTRODUCTION

Pancreatic ductal adenocarcinoma (PDAC) is the third responsible reason for cancer-related death in the west, with a 5-year survival rate of less than 10% [1]. Since 1975, the death rate has continually increased by 0.3% per year [2]. By 2040, the number of incidences is expected to increase and reach 355,317 new cases [3]. The specific causes of PDAC are not well defined; however, people who are smoker, diabetic, obese, physically inactive, are at higher to develop PDAC [4-7]. Furthermore, 80% of PDAC patients developed cancer between 60 and 80 years old [8].

1.2 Genetic alteration in PDAC

Around 97% of pancreatic cancer patients have gene mutations such as deletions, amplifications, inversions, translocations, substitutions, and frameshifts [9]. Alterations of several genes in PDAC are common, and around 70-98% of patients have these mutations [10-12]. However, alteration of other genes is less common, and some of them are obtained from inherited germline [13, 14]. These alterations of the gene can be classified as an enhancer of protein functions or diminisher of protein functions.

Consequently, disruptions of protein functions lead to uncontrolled cell division, mobility, preventions from apoptosis/autophagy, and issues with DNA repair. All the mentioned processes promote cancer progression [9]. The most commonly mutated genes will be discussed in the next subsection.

1.2.1 KRAS

It is a small GTPase with a molecular weight of 21 kDa and known as c-Ki-ras c-K-ras, Ki-Ras, or K-Ras 2. It is mutated in more than 90% of pancreatic cancer patients [**Table 1.1**] [15]. Its function is to bind guanosine triphosphate (GTP) and diphosphate nucleotides (GDP), and it gets activated when binds to GTP and deactivated if binds to

GDP. KRAS (active form) stimulates RAF family kinases, ARAF, BRAF, and RAF1[16]. Once RAFs are activated, it will activate MEK1 and MEK2 kinases, and then ERK1 and ERK2 kinases got activated as a subsequent step. In the end, ERKs activate and phosphorylate different nuclear-cytosolic proteins, including c-JUN and ELK1, which lead to cell proliferation [17]. Because of KRAS alteration, uncontrolled cell proliferation and other cellular processes will be promoted that support tumor development and metastases [15]. Furthermore, KRAS regulates other signaling pathways such as RAL, PLC-PKC, and PI3K-AKT. These signaling pathways are known as one of the prominent players in cancer progression [15].

1.2.2 TP53

It is a tumor suppressor gene and knowns as P53 or antigen NY-CO-13. Its functions are to transcriptionally activate target genes as a defense response to cellular stress events such as DNA damages and oxidative stress. Therefore, it induces cellular apoptosis and cell growth arrest [18]. Moreover, it increases the expression of cyclin-dependent kinase inhibitor (CDKN1A) and then helps in arresting cell cycle progression [18]. This gene is one of the most commonly altered genes in pancreatic cancers, which counts for around 70% of pancreatic cancer patients [Table 1.1] [19]. The mutated TP53 leads to failure of DNA binding ability and In subsequently, gene transcription activation [20].

1.2.3 CDKN2A

It is a tumor suppressor gene and knowns as CDK4I, MTS-1, or p16-INK4a. It can regulate cell cycle progression via preventing cyclinD-CDK4 and cyclinD-CDK6 complexes, which are responsible for beginning the G1/S phase transition [21]. It is one of the most mutated genes in various types of tumors, and the incidence of alterations in sporadic pancreatic cancer is remarkable, with 98% inactivation occurrence in pancreatic

cancer patient cases **[Table 1.1**][22]. The alteration of CDKN2A happens through various mutation mechanisms such as the promoter silencing, homozygous deletion, or loss of heterozygosity.

1.2.4 SMAD4

It is a tumor suppressor protein and knowns as MADH4 or DPC4. It translocates as heterotrimeric SMAD2/SMAD3-SMAD4 complex to the nucleus after activating of TGFβ family receptors. In the end, it leads to activation and expression of targeted genes and causes tumor growth inhibition [23, 24]. Alterations of SMAD4 happen in 50% of pancreatic cancer cases [Table 1] [25]. The mechanisms of SMAD4 mutation occur through homozygous deletion. It has been shown that genetic alterations of SMAD4 are associated with poor prognosis of pancreatic cancer patients **[Table 1.1**] [26, 27]

1.2.5 BRCA1

It is also a tumor suppressor gene and known as **RNF53**. It mediates the formation of Lys-6-linked polyubiquitin chains formation by acting as E3 ubiquitin-protein ligase [28]. It controls cellular responses to the damage of DNA. Therefore, it is essential for repairing DNA and G2/M cell cycle progression [29]. This gene is often mutated in familial cancer such as breast cancer, with 45% of the incidence of occurrence, ovarian cancer with 80% of the incidence of occurrence; however, it accounts for 6.6% of pancreatic cancer patients with familial history **[Table 1.1**][30].

1.2.6 BRCA2

It is a tumor suppressor gene and known as **FANCD1**. In the S-phase of the cell cycle distribution. This gene is involved in double-strand break repair via activating RAD51 recombinase. Additionally, it plays a crucial role in centrosome duplication, cytokinesis, and cell death [31]. Alterations of BRACA2 causes a high risk of developing stomach, prostate, ovarian, breast, and familial pancreatic cancers[32, 33]. Around 7.3% of

pancreatic cancer patients with familial background have a mutation in BRCA2, and they are at high risk by 20-folds [13].

Table 1.1 Summary of genes alterations in PDAC

Gene	Frequency	Mechanism of alterations
KRAS	70%-95%	Substitution at codons G12, G13, K117, A146, or Q61
TP53	20%-76%	Substitution at codons R175, R284, R273, or R282
CDKN2A	49%–98%	loss of heterozygosity, homozygous deletion, promoter silencing
SMAD4	19%–50%	homozygous deletion
BRCA1	6.6%–14%	11-base pair deletion, a 1-base pair insertion, a stop codon, a missense substitution

1.3 Implicated signaling pathways in PDAC

1.3.1 HEDGEHOG (Hh) Signaling pathway

The Hh signaling pathway is involved in the critical role of PDAC development and progression. The downstream signaling of this pathway is controlled through 12-pass transmembrane protein receptor PATCHED (PTCH), which usually acts as suppressor function over the 7-pass transmembrane protein receptor SMOOTHENED (SMO) in the absence of the ligand. The PTCH decreases its suppression effect on SMO after binding of Hh ligand to the PTCH protein receptor. As a result, the downstream signaling pathway continues and becomes active. The final product of losing suppression effect on SMO leads to release and activate of the GLI family transcription factors such as GLI1, GLI2, or GLI3. These transcriptional factors play an essential role in cellular response processes. Therefore, The Hh signaling pathway plays a crucial role in activating genes involved in apoptosis and cell cycle progression.

This pathway plays an essential role in the epithelial and stromal compartments. Several changes in the Hh signaling pathway have been shown in pancreatic tumor cells (epithelial compartment). In the global genomic analysis, it has been shown that there is at least one alteration in Hh signaling genes [34]. It has been found that Hh is highly expressed in a large number of PDAC patients [35, 36]. Another compartment, which can be affected by Hh signaling pathway is the stroma of PDAC. The Hh signaling pathway is triggered in a stromal cell connected with a pancreatic cancer cell that has a high expression level of Hh ligands such as SHH or IHH, suggesting a paracrine function [37, 38]. Another study in an orthotopic model from PDAC cells overexpressing SHH showed that a high level of desmoplasia (stroma), whereas the level of stroma was low after treatment with a SHH-specific antibody [39]. Moreover, the SMO has a high expression in

cancer-associated fibroblasts, and thereby activation of the Hh pathway leads to GLI1 overexpression [40]. In *Pdx-1-Cre; Trp^{R172H/+}; Kras^{G12D/+}* mouse model, a group of scientists, found a low level of stroma and collagen-1 deposition in mice treated with a Hh inhibitor [41]. Taken together, these results suggest that the Hh signaling pathway plays a significant role in tumor growth and desmoplasia support.

1.3.2   NOTCH signaling pathway

NOTCH is mainly active in the embryogenesis stage. However, this pathway has been seen to be active in various types of cancers, including PDAC. The primary function of NOTCH in development is to prevent the terminal differentiation of cells until appropriate [42]. In addition, it maintains the population of undifferentiated cells in normal tissue to serve as s progenitor cells. The interaction between transmembrane ligands of neighboring cells and NOTCH receptors either NOTCH-1 or NOTCH-2 leads to the cleavage of the intracellular domain of the receptors by an enzyme called γ-SECRETASE. After that, the cleaved part of the receptor moves in the cytoplasm and crosses the nuclear membrane to interact with transcription factors to stimulate the expression of targeted genes. It has been shown that high expression of NOTCH receptors and ligands in early PanIN lesions compared to the normal pancreas [43]. It was seen that high expression of NOTCH in pancreatic cancer is not only needed for tumor initiation but also required for tumor maintenance [44]. The NOTCH-1 and NOTCH-2 have different functions on pancreatic cancer. It has been found that the NOTCH-1 was expressed on normal acinar cells, whereas it was rarely expressed in PanIN lesions; however, NOTCH-2 was found in the ductal cells [45]. The loss of NOTCH-2 in the *Kras^{G12D}* mouse model was seen to inhibit PanIN progression [45]. In the *Pdx1-Cre; Kras^{G12D}; p53^{lox/+}* mouse model, the NOTCH signaling pathway was seen to be overexpressed, which results in support of the progression of PDAC lesions, and treating these mice with GSI (γ-SECRETASE inhibitor)

showed inhibition of early-stage progression [46]. Therefore, the NOTCH signaling pathway plays a critical role in promoting PDAC tumorigenesis.

1.3.3 WNT Signaling pathway

The WNT signaling pathway plays a primary role in cell growth, development, and differentiation. This pathway is activated when ligands interact with the WNT protein receptor on the cell membrane. This interaction leads to β-Catenin release onto the cytoplasm. Generally, β-Catenin is inactive. This form is activated by phosphorylation by GSK3-β kinase and binding to axon and APC. This phosphorylation enhances β-Catenin ubiquitination and degradation by proteasomes. A free form of β-Catenin can cross through the cytoplasm and translocate into the nucleus to interact with transcription factors T-cell factor (TCF) and lymphocyte-enhancer (LEF) to activate target genes. A high level of β-Catenin has been seen in most PDAC but was not high in the normal pancreas [47, 48]. The siRNA that knockdowns β-Catenin, decrease the pancreatic cancer proliferation by increasing the apoptosis [48]. Thus, the WNT Signaling pathway supports tumor growth, development, and differentiation.

1.3.4 The nuclear factor-κB (NF-κB) proteins

NF-κB is a family of transcription factors that correlated with controlling inflammatory responses, genes responsible for cell proliferation, cell apoptosis, and cell development. These transcription factors regulate both tumor and stromal cells of PDAC. In the normal state, NF-κB factors including c-Rel, p100/p52, p65 (RelA0), p105/p50, and RelB are present in the cytoplasm of cells as homodimeric or heterodimeric form. These factors typically are inactive form because of their linkage with IκB-α, which prevents them from being localized in the nucleus. Once the appropriate signals are received by cells, it allows phosphorylation and degradation of IκB-α, followed by a nuclear movement of NF-κB to regulate transcription of the targeted genes [49]. A study has shown that the

incidence of PDAC is highly increased in patients who have chronic pancreatitis compared to those who have not [50].

Furthermore, the presence of immune cells in the tumor microenvironment (TME) is associated with the promotion of NF-κB activity in stromal cells due to the secretion of cytokines. Thereby, it will activate NF-κB in the tumor cells, which support tumor progression [49]. It has been demonstrated that the NF-κB subunit RelA is highly activated in PDAC; however, it is not activated in normal pancreatic cells [51]. Another study has revealed that NF-κB subunits such as p105, p100, and cRel have a high-level of expression in PANC-1 and BxPC-3 cells compared to nonmalignant cells [52]. Therefore, it is evidence that NF-κB factors play a significant role in supporting PDAC.

1.3.5 C-MYC

C-MYC is an essential regulator of several aspects of cell growth. It is an oncogene that facilitates cell growth and cell transformation [53]. It can activate or repress the transcription of the targeted genes based on the other cellular stimuli, and it provokes the transcription of genes that involved in cellular metabolism, cell cycle progression, and inhibition of checkpoint [54]. The activation of C-MYC can be achieved by several signaling pathways, such as WNT [54]. Using Ela-1-myc transgenic mice showed a high expression C-MYC support the development of acinar cell lesions, and ductal cell lesions [55]. Another study showed that a 30% amplification of C-MYC was seen highly increased in PDAC patients, and most of them have concurrent gene activations that support tumor growth [56]. The nuclear factor of activated T-cells (NFAT) is a family of transcriptions factors that are implicated to be active in C-MYC-dependent growth of pancreatic cancer. It has been shown that NFAT is overexpressed in pancreatic cancer and supports tumorigenesis through activating the C-MYC gene expression [57]. Nuclear translocation of NFAT and interaction with C-MYC promoter increases the activity of p300-dependent

histone acetylase, then binding of other factors to stimulate the activity of C-MYC transcription [58].

1.3.6 Epidermal Growth Factor Receptor (EGFR)

EGFR family consists of a cytoplasmic receptor tyrosine kinases that contain human EGF receptor or HER1 (ErbB-1 or EGFR1), Her2 (ErbB-2 or EGFR2), Her3 (ErbB-3 or EGFR3), and Her4 (ErbB-4 or EGFR4). Typically, the interaction between a ligand and receptor results in conformational changes in the receptor (dimerization) and activation that felicitate the initiation of the downstream signaling pathways. This can induce other signaling pathways such as phosphoinositol-3 kinase (PI3K), Ras, and phospholipase C pathways. These pathways have intersecting players, which play a vital role in stimulating the transcriptions of targeted genes. These genes promote cell growth, proliferation, and survival [59]. Increased expression of the EGFR2 has been revealed to be existent in pancreatic cancer cells [60]. Researchers have evaluated a sample of human PDAC tissues and shown high expression of EGFR2 [60, 61]. The expression of EGFR2 is significantly higher in PanIN lesions and carcinoma compared to normal pancreatic ducts [62]. Based on what was mentioned, EGFR has an essential role in PDAC progression and development.

1.3.7 PI3K signaling pathway

The PI3K signaling pathway is a vital downstream target of the rat sarcoma virus (Ras) family. This family is a group of proteins that are responsible for cell proliferation. It was estimated that 60% of PDAC cases have dysregulation of the PI3K signaling pathway [63-66]. The PI3K belongs to a family called lipid kinase, that respond to trigger from the Ras family to regulate several cellular responses such as cell growth, motility, transformation, proliferation, and survival [67, 68].

1.4   Pathogenesis of PDAC

The PDACs are derived from the epithelial cells that are present in the pancreatic duct (gland-like shape) [69]. The development of PDAC can be achieved by developing the hyperplastic lesions called pancreatic intraepithelial neoplasias (PanINs) [70]. PanINs are histologically defined as the microscopic mucinous pancreatic ductal lesions (<0.5 cm) [71]. According to the degree of nuclear and cellular atypia, this non-cancerous lesion is sub-classified into low- (PanIN-1A/B) to high- (PanIN-3) degree lesions [72]. This process is accompanied by huge genetic alterations, which accumulate over time and drive PDAC development through PanIN stages (PanIN1–3). In the PanIN-1 stage, miRNAs (oncogenic) are overexpressed. The KRAS is alerted, and stromal factors are activated [73]. In the PanIN-2 stage, Mucin 1 (MUC1) is highly expressed, and the p16/CDKN2A gene has mutations. Finally, PanIN-3 stage is associated with mutation in TP53, BRCA2, and SMAD4 [74-77]. Furthermore, the TME has a critical role in PDAC pathogenesis and failures of therapeutic attempts. PDAC composed of different types of cells such as fibroblasts, immune cells and endothelial cells, which serve different roles in supporting tumorigenesis [78-80]. A CXCL12 is a cytokine produced by stromal-derived cells, which is taken up by pancreatic tumor cells and supports tumor growth invasion and chemoresistance. Pancreatic cancer cells secreted SHH ligand that stimulates desmoplasia of the tumor through a paracrine mechanism, and boost pancreatic tumorigenesis [81, 82]. In contrast, It has been reported that depletion of stroma makes the disease worse [83, 84]. The mechanism of stroma in supporting tumor growth is still unanswered. Therefore, the dual effect of TME open the door for scientists to investigate how TME supports the PDAC progression.

1.5   Characteristic of PDAC

1.5.1   Chemoresistance

Most of the researches on chemoresistance of PDAC focuses on gemcitabine [85]. Resistance to chemotherapies is one of the primary barriers in the treatment of the PDAC. Chemoresistance can be classified into intrinsic or acquired mechanisms. The intrinsic mechanism defines as the ability of cancer cells to bypass the toxic effect of the chemotherapies through drug breakdown, change the expression of drug target, reduce the drug transporter channels across the cell membrane, or decrease the interaction efficiency between drug and its molecular target [86, 87]. This resistance mechanism can be mediated by nuclear receptors such as sxr or ATP-dependent membrane transporters [88].Moreover, some cellular metabolic (ceramide glycosylation) processes reduce the efficacy of chemotherapies [89].

On the other hand, the acquired mechanism is irresponsive to chemotherapies after multiple treatments. This mechanism is influenced by environmental and genetic factors that help in the development of chemo-resistant cancer close or promote enzymatic mutations that play an essential role in metabolic pathways [87, 90].

1.6   Factors implicated in developing resistance to chemotherapies

The development of resistance to chemotherapies in PDAC is multifactorial and might be attributed to the interaction between cancer stem cells (CSCs), non-coding RNAs, and TME.

1.6.1   Cancer stem cells (CSCs)

CSCs are a small subclass of tumor cells that act as the driving force of cancer development. CSCs have some distinct features, such as their ability to self-renew, initiate cancer development, and develop drug resistance. CSCs develop chemoresistance against gemcitabine and 5-FU through overexpression of c-Jun N-terminal kinases (JNK)

[91]. Another study has shown that retinoic acid (RA) was able to decrease the mRNA expression of CSCs markers such as CD44, CD24, CD133, and ALDH1 [92]. Pancreatic CSCs have a high expression of EMT activator zinc finger E-box binding homeobox 1 (ZEB1). ZEB1 controls the chemoresistance and stemness of CSCs by epigenetic silencing of the miR-203 [93, 94]

1.6.2 Non‑coding RNAs

It is an RNA molecule, which is transcribed from DNA, such as miRNA. The miRNAs can regulate gene expressions in most of the cellular biological processes. They also play an essential role in developing resistance against standard chemotherapies [95-101]. It has been shown that the downregulation of miR‑497 might lead to chemoresistance; however, the upregulation of miR‑497 increases pancreatic cancer sensitivity to gemcitabine and erlotinib [95] . Moreover, Overexpression of miR-33a enhances the sensitivity of pancreatic cancer cells to standard chemotherapy (gemcitabine), and it also inhibits tumor growth by blocking of Pim‑3 kinase expression [96]. Another study showed that both miR‑29a and miR‑330‑5p serve as tumor suppressor genes by decreasing MUC1 expression level and increasing pancreatic cancer cells' sensitivity toward gemcitabine [97].

1.6.3 The tumor microenvironment

It is an interstitial tissue that surrounds cancer cells and, it consists of cellular compartments such as nerve cells, endothelial cells, fibroblasts, pancreatic stellate cells, and inflammatory cells and non-cellular components such as fibrous proteins and proteoglycans [102]. These components interact with cancer cells and promote desmoplastic reactions, which prompt chemoresistance [103]. Around 90% of the tumor volume is the fibrous stroma that acts as a barrier for proper delivery of chemotherapeutic agents to cancer cells. However, depletion of the stroma is associated with tumor

progression, which means stroma has some components that inhibit tumor growth [84, 104]. Some soluble proteins that are secreted by fibroblast in the stroma are implicated in promoting chemoresistance in cancer cells [105]. One study has shown that the SOM230 analog activates somatostatin receptor 1 in cancer‑associated fibroblasts and inhibits protein synthesis by rapamycin/4E‑BP1 pathway. This activation leads to improving the efficacy of gemcitabine treatment [105].

1.6.4 Pancreatic stellate cells (PSCs)

These cells are one of the critical components of the tumor stroma and play a significant role in cancer proliferation. There are two different states (quiescent state PSCs or activated state). The quiescent state usually presents in the normal tissue; however, it can be activated via the inflammatory signals (e.g., TGF-β1, and present as a myofibroblasts-like phenotype [102]. Once those PSCs got activated, it can secrete the ECM proteins including laminin, fibronectin and collagen, resulting in the formation of a dense desmoplasia. PSCs support tumor growth, chemoresistance in the pancreatic cancer cells. One study performed using the co-culture methodology of PANC-1 or BxPC-3 cells with PSCs showed increased resistance to gemcitabine by increasing the expression of hairy and enhancer of split-1 (Hes1) via the NOTCH pathway. The knockdown of the NOTCH or Hes1 leads to reverse chemoresistance [106].

Furthermore, PSCs produce soluble stromal cell-derived factor-1α, that suppresses the apoptotic effect of gemcitabine in pancreatic cancer cells (PANC-1) through binding to C-X-C chemokine receptor type 4 to activate FAK-protein kinase B (AKT) and ERK ½ pathways [107]. The vitamin D receptor is expressed on PSCs, and it gets activated after its interaction with vitamin D receptor ligand and regulates tumor stroma reprogramming thorough restoring PSCs nature state [108]. The activated PSCs

have a low expression level of miR-29a and miR-29b. These two miRNAs are associated with a high ECM deposition [109].

1.7   The FDA approved treatment for PDAC

1.7.1   Gemcitabine (GEM)

GEM is an analog of deoxycytidine that is a pyrimidine antimetabolite [110]. This compound is a pro-drug, once it gets inside the cells; it is converted to the active forms gemcitabine diphosphate and gemcitabine triphosphate by phosphorylation using deoxycytidine kinase. Both forms can incorporate into the DNA, resulting in inhibition of the processes that are required for DNA synthesis [111]. It showed better clinical outcomes in treating pancreatic cancer patients over 5-FU [112]. Even though it suffers from being metabolized in the human body (short-half-life) and less cell membrane permeability, it received the FDA approval to be used as a treatment option for pancreatic cancer patients [113, 114]. It has been the first option for two decades until combination chemotherapies showed a better survival rate and longer median overall survival than GEM [115-117]. These two combinations (FOLFIRINOX or gemcitabine/nab-paclitaxel) become the first-line treatment for advanced pancreatic cancer [118].

1.7.2   FOLFIRINOX

This combination regimen consists of 5-FU, leucovorin, oxaliplatin, and irinotecan. The mechanism of action of 5-FU is to inhibit thymidylate synthase that is important for pyrimidine thymidine synthesis (required for DNA replication). Leucovorin is similar to folic acid, and not chemotherapy by nature. It is added to the chemotherapy regime to improve the anticancer effect of 5-FU. Oxaliplatin is platinum-based chemotherapy and exhibits the anticancer effect through DNA damage by forming the DNA lesions, stop DNA synthesis, and block RNA synthesis [119]. Irinotecan acts as an antineoplastic enzyme inhibitor. It stops DNA strand re-ligation through binding to topoisomerase I-DNA complex and

initiates double-strand DNA damage and cell killing [120]. The superiority of FOLFIRINOX over GEM was after some pre-clinical and clinical studies, which suggested the synergistic effect and no overlapped toxic effect [121-128]. The PRODIGE6 is a clinical trial, which compared FOLFIRINOX to GEM. There were 171 patients in each arm, and FOLFIRINOX arm has improved the median overall survival by around 4.3 months [116]. It is well known that FOLFIRINOX causes a grade 3-4 adverse events such as neutropenia, febrile neutropenia, thrombocytopenia, diarrhea, and peripheral neuropathy compared to GEM; however, the quality of life of the patient was not statistically significant compared to GEM [129].

1.7.3   Gemcitabine/nab-Paclitaxel

Another clinical trial study, which makes the combination of GEM and nab-Paclitaxel better option for treating pancreatic cancer as first-line therapy, is called the MPACT study. The median overall survival was around 8.5 months for patients treated with combined-therapy of GEM and nab-paclitaxel; however, the median overall survival was around 6.7 months for patients treated with GEM alone [117]. In terms of toxicities, patients treated with combination therapy experienced toxicity more than GEM alone. These toxicities are as follow neutropenia, febrile neutropenia, fatigue, peripheral neuropathy, and diarrhea. In comparison between GEM/nab-paclitaxel and FOLFIRINOX regarding neuropathy toxicity, GEM/nab-paclitaxel causes less neuropathy compared to FOLFIRINOX.

1.7.4   Gemcitabine and erlotinib

The EGFR is highly overexpressed in the pancreatic tumors, and it plays a vital role in tumor progression [130, 131]. The overexpression of this molecule is correlated with a low prognosis. A combination of gemcitabine and erlotinib was tested in phase 3 clinical trial and showed moderate and significant improvement in overall survival 6.2

months compared to 5.9 months in gemcitabine arm [132]. The FDA approved this combination after the phase III clinical trial. This combination has become a good option for treating advanced and unrespectable pancreatic tumor patients [133].

1.7.5   Liposomal irinotecan (nal-IRI), 5-Fu, and leucovorin

Nal-IRI is a liposomal formulation of irinotecan. This chemotherapy acts as a topoisomerase I inhibitor [134]. It has been shown that nal-IRI have a better therapeutic profile than conventional irinotecan because the active metabolite (SN-38) was achieved at a lower dose in liposomal formulation compared to free form [135]. The combination of nal-IRI with 5-fluorouracil and leucovorin was approved by the FDA for metastatic PDAC patients, who failed on gemcitabine-based therapy. Based on NAPOLI-1 trial (phase III), this combination significantly improved the overall survival rate of 6.1 months compared to 4.2 months in 5-fluorouracil and leucovorin arm [136].

1.8   The nanotechnology in cancer

It is the idea that small sized materials can be designed and introduced to the human body in order to perform cellular damages or repairs at molecular levels [137]. The ultimate goal of using nanotechnologies/nanomedicine in cancer treatment is to improve drug absorption and permeability plus controlled released manner of the drug and increase site specificity [138]. The nanotechnologies/nanomedicine are capable of interacting with the biological molecules inside cells or outside cells, which is useful for cancer therapy and diagnosis [139, 140]. The advantages of nanotechnologies/nanomedicine over the traditional excipient approach such as emulsions and surfactants are that avoid physiological barriers, prevent fast drug metabolism or degradation, can passively target the drug to tumor vasculature by the enhanced permeability and retention phenomenon (EPR), and can actively target to specific site after functionalizing with specific target moiety [141-143].

Furthermore, the nanotechnology carriers are easy to be synthesized, inexpensive, and modifiable to perform specific applications. For example, adding a reactive functional group can help in incorporating targeting moiety to improve the delivery to specific sites or linking fluorescent moiety that will be helpful in better diagnosis. It has been shown that loading or incorporating the cytotoxic agents in nanocarrier can improve tumor penetration and enhance the therapeutic efficacy [144-146]. Loading anticancer drugs in nanocarrier has several benefits. First, it increases the circulation time of the loaded drug and protects the loaded drug from being cleared quickly by the kidney or liver. Second, the small size of the nanocarrier causes passive extravasation of drug called the EPR phenomenon. It happens when an improper formation of vasculatures in the tumor site. These vasculatures have tiny pores where nanoformulations can passively diffuse inside the tumor and accumulated because of poor lymphatic drainage on the tumor site. Therefore, these nanoformulations are less likely to go back to systemic circulation; as a result, a higher drug concentration at the tumor site is accomplished. Finally, the side effect of co-solvents is absent because hydrophobic drugs can be effortlessly loaded or encapsulated onto the nanoparticle systems.

Active targeting is another advantage of using nanoformulations. Specific targeting moieties such as antibodies, aptamers, or peptides can be attached to the surface of the nanocarrier that would lead to favored binding on specific receptors on the targeted cell. Thus, this interaction ensures that nanoformulation reach the targeted cells and avoid other cells, leading to more effective treatment [141]. There are plentiful researches on using nanocarriers for treating different type of cancers such as prostate, colorectal, ovarian, breast cancer [147-152]. In the next section, we will highlight the uses of different types of nanocarriers in pancreatic cancer.

1.8.1 Polymer-Drug Conjugates

The polymer-drug conjugates consist of chemotherapy molecules or targeting moieties that are conjugated onto the polymers by forming a covalent chemical bond between chemotherapy molecules or targeting moieties and a hydrophilic polymeric carrier. They could be applied in tumor diagnosis or detection [153]. Most of the chemotherapeutic agents are hydrophobic, that feature acts as a challenge or barrier against clinical trial testing. Therefore, conjugating the chemotherapy into the backbone of hydrophilic polymer would lead to the core-shell aggregate formation by which the lipophilic drug exists in the hydrophobic micellar core. Consequently, this conjugation enhances the water solubility of chemotherapies and alters the pharmacokinetic profile of chemotherapies at the whole body and even subcellular level [154, 155]. Thus, It improves the therapeutic effect of chemotherapies. There are many good examples of this method has been reported in the literature. SN-38 is an active metabolite that can not be administered as a free form to patients because of its poor solubility in water and other co-solvents [156]. Conjugating of SN-38 onto the poly(ethylene glycol) based polymer improves its water solubility and bioavailability. Furthermore, vismodegib (GDC-0449) was encapsulated into the lipophilic core that offers the dual therapy strategy. This dual system showed in vitro that GDC-0449 (Hh inhibitor) restored fibroblast, which is responsible for SN38 resistance. Finally, the potent in vivo chemotherapeutic effect was achieved after using the conjugation approach [154].

1.8.2 Amphiphilic Polymers

The amphiphilic polymers consist of both lipophilic and lipophobic parts. They spontaneously or favorably aggregate to form the core-shell structures in the aqueous solution [157]. This polymer is extensively used in drug delivery to improve the water solubility of the hydrophobic drug inside the lipophilic core of the formed aggregate. Based

on the molecular formation, there are many different architectures of amphiphilic polymers, which will be discussed in the following paragraphs.

1.8.2.1 Block Copolymers

They are the most common type of amphiphilic polymers. This kind of polymers is made-up of polymerizing of two or more kinds of monomer units in the linear style [158]. In general, one hydrophilic and one hydrophobic monomer are polymerized, which leads to the amphiphilic diblock copolymer such as poly(ethylene oxide)-block-poly(lactic acid) (PEO-b-PLA) [159]. In aqueous environments, the block copolymers can spontaneously form polymeric micelles. The micelles characters depend on the hydrophilic and hydrophobic monomer blocks. Poly(ethylene glycol) is the most commonly used hydrophilic polymer because it is biocompatible, offers efficient steric hindrance protector, increases the circulation time of the micelles in the blood [160-162]. Polymeric micelles stability depends on the molecular weight and types of the hydrophobic block. Higher molecular weight and more hydrophobic blocks have greater stability than low molecular weight and less hydrophobic block [141]. There are several reports in the literature showing that using mixed micelles to incorporate various chemotherapeutic agents such as paclitaxel, 5-fluorouracil, gemcitabine, and doxorubicin improves pancreatic cancer treatment [163].

1.8.2.2 Graft Polymers

They are branched polymer consist of the hydrophilic homopolymer backbone and hydrophobic pendant moieties attached to the hydrophilic backbone [164]. This type of polymer favorably forms aggregates in aqueous solutions due to the reduction in Gibbs's free energy. It was shown in the literature that developing a chitosan grafted polymer with poly(ethyleneimine) and candesartan conjugate and complexed with w-p53 genes are beneficial for targeting pancreatic cancer cells [165].

1.8.2.3 Dendrimers

They are a grouping of repetitive, very branched, and symmetrical polymers. Dendrimer branches act as a selective door to control the entry of the small molecules and show the smallest size by far [141]. The number of branches points is traced from the center of the dendrimer to the periphery of the dendrimer, and it is called the generation [166]. The solubility of the dendrimer can be managed by the terminal groups on the dendrimer border [167]. These terminals also can be used as an anchor to link with polymers, antibodies, and drugs [168, 169]. The mechanism of aggregation depends on the molecular composition of the system, and it could include hydrogen bonding, electrostatic, or hydrophobic interaction [170]. The hydrophobic drugs can be loaded in the hydrophobic core of the dendrimers, and achieve sustained release profile [171]. It has been shown that poly(amidoamine) (PAMAM) dendrimers with the conjugation of hyaluronic acid improve the water solubility of 3,4-difluorobenzylidene curcumin [172].

1.8.2.4 Smart Polymers

Smart polymer or stimuli-responsive polymer undergoes conformational changes due to the changes in the surrounding environmental factors. These factors can be either biological (biomolecules), physical (light, temperature, ultrasound), or chemical (pH) [173-176]. It is known that the metabolic rate of the tumor tissue is higher than the healthy tissue. The temperature on tumor tissue is ranged from 40-44 ^{o}C [177]. In 2017, a group of people developed a thermos-responsive copolymer composed of hydrophobic blocks and hydrophilic thermos-responsive blocks (poly[(di(ethylene glycol) methyl ether methacrylate-co-poly(ethylene glycol) methyl ether methacrylate 300)-b-poly(2-ethylhexyl methacrylate)] [poly(diEGMAco-OEGMA300)-b-PEHMA]). This polymer could easily self-assembled in the aqueous environment, and was used to deliver gemcitabine derivatives and paclitaxel. The conformational change happened when the temperature reaches 40

^{o}C. This study showed that thermos-responsive polymers have a high potential in pancreatic cancer treatments [178].

Another type of smart polymer is pH-responsive micelles. It has been reported that the pH of the tumor tissue is around 6.75, while the pH of the healthy tissue is around 7.4 [175, 179]. A group of people in Canada developed amphiphilic polymers that can self-assembled and encapsulate the curcumin. Once the reduction in pH occurs, the micellar structure was destabilized, and drug release occured. The authors have concluded that this system has a high potential for delivering chemotherapies specifically to cancer cells with the help of pH-responsive polymers [180].

1.8.3   Albumin

It is well known as an excellent drug delivery system for hydrophobic drugs [181]. The advantage of albumin is that long half-life around 19 days [182]. In 2013, the FDA approved Abraxane®, which nanoparticle-albumin bound paclitaxel to treat metastatic pancreatic cancer patients. An international study (Phase III study) showed that the combination of Gemcitabine and Abraxane® significantly improved the overall survival rate in pancreatic cancer patients compared to gemcitabine only [117].

1.8.4   Inorganic Nanoparticles

It has useful properties that are suitable for novel systemic delivery due to their electrochemical, optical, and electrical properties [183]. In the next sections, the list of inorganic nanoparticles will be discussed, and their applications in pancreatic cancer treatments.

1.8.4.1   Carbon Nanotubes (CNTs)

They have several advantages that made them useful for the drug delivery system. The high degree of biocompatibility, high target specificity, and target sensitivity are the main reason for CNTs to be attractive as a delivery system in pancreatic cancer [184,

185]. CNTs can be used to deliver a broad range of molecules such as small molecules, small peptides, proteins, vaccines, nucleic acid, and carbohydrates. These molecules can be loaded onto the inner cavity of the tubes, or linked onto the outer surface of the tubes. One study showed that encapsulating of the MRI contrast agent gadolinium nanoparticles with CNTs could map and ablate the primary tumors and metastatic lymph nodes [186].

1.8.4.2 Quantum Dots

They are semiconductor crystal in nano-sized range and have distinctive electronic and optical features. They also exhibit intensive and bright fluorescence that is not quenched easily compared to conventional fluorescent labels [187]. The quantum dots have different applications in pancreatic cancer (therapeutics or diagnostics). One study showed that coating Cadmium telluride quantum dots (CdTeQDs) with mercaptopropionic acid could eradicate pancreatic cancer cells after UV illumination through generating reactive oxygen species (ROS) [188]. Another application is the pancreatic cancer diagnosis. The pancreatic cancer diagnosis is a challenge due to the absence of apparent biomarkers or detection methods for these markers. A group of people in South Korea has developed a QDs containing Cadmium Selenide (CdSe) in the core and (Cd, Zn)S in the shell. The surface of the QDs was conjugated with claudin-4 and mesothelin (MSLN), and prostate stem cell antigen (PSCA) to ensure the target specificity to pancreatic cancer cells. The QDs showed a high target selectivity with low non-specific binding level [189]. These results offer a new method of diagnosis of pancreatic cancers.

1.8.4.3 Iron Oxide Nanoparticles (IONP's)

They have various applications in the medical field, such as cell labeling, magnetic cell sorting, drug transportation, cancer detection, and cancer treatment [190]. They are different shapes for IONP's including rods, cubic, hexagonal, and spherical. Furthermore, IONP's with particle size less than 20 nm are superparamagnetic [191, 192]. This feature

allows the IONPs to be beneficial as MRI contrast agent that would be useful in cancer imaging and diagnosis [193]. Arachchige's group has developed dextran-coated IONPs. This system was tagged with red fluorescing doxorubicin and green fluorescing fluorescein to track the nanoparticles inside the MIP PaCa-2 cells. This study revealed that the cellular uptake of doxorubicin was 20 times higher than the free drug [194]. Another group has developed poly (lactic-co-glycolic acid) (PLGA) coated with 17AAG (heat shock protein inhibitor) and loaded with IONPs. This system has decreased the cell viability by 75% compared to control cells due to magnetic hyperthermia subjected to MIA PaCa-2 cells [195].

1.8.4.4 Hybrid Iron Oxide-Gold Nanoparticles

The hybrid nanoparticles consist of gold shells covering the iron oxide core. These nanoparticles have a mix of physical characters including magnetism (iron oxide core) and nano-heater plus biocompatibility (gold shell) [141]. Larson's group has reported that using a GoldMag, which is hybrid nanoparticles, decreased the cell viability of Panc-1 by 47%; however, after cellular uptake of the nanoparticles and irradiation for 5 mins at 808 nm, only 2.3% of the cell was viable because the thermal raised to 79.51 $^{\circ}$C. Therefore, the mixture of thermal generation and cytotoxicity of hybrid nanoparticles showed a significant reduction in cell proliferation of Panc-1 cells [196]. Hoskins's group have developed hybrid iron nanoparticles coated with poly(ethylene glycol) that have potential as a theragnostic because of its capability to image using MRI, deliver drugs, heating up after irradiation. They showed in this study hybrid nanoparticles increase the thermal by 9 $^{\circ}$C, and heat shock proteins (HSPs), that indicate tumor cells have stresses because of generated heat [197]

1.8.4.5 Gold Nanoparticle

They are useful vehicles for targeted delivery systems. They also have various shapes such as tetrapods, rods and spheres. Gold metal is relatively non-toxic and resistant to corrosion, oxidation, and acidic condition because it is noble metal. Due to its biocompatibility, easy to synthesize and carry drugs, gold has powerful tools in pancreatic cancer therapy. Additionally, absorbing near-infrared (NIR) radiation, and generating heat through surface plasmon resonance (SPR) make the gold as a powerful tool to eradicate tumor but not healthy tissue because the laser emitting NIR radiation can be targeted to an area (pancreas) where the gold nanoparticles are located.[198-201]. It was reported that gold nanoparticles could interfere with mitochondrial electron transfer chain in pancreatic cancer cells (1.4E7 cells) and depolarize mitochondrial cell membranes, resulting in cell lysis. Further, these nanoparticles inactivated the Bcl-2 anti-apoptotic proteins after cellular uptake and irradiation nanoparticles [202]. Another study showed that gold nanoparticles could interrupt the communicating between pancreatic cancer cells (Panc-1 or AsPC-1) and fibroblast cells, resulting in reprograming the TME and hindering tumor growth [203].

2   Chapter 2. Coadministration of Polymeric Conjugates of Docetaxel and Cyclopamine synergistically inhibits Orthotopic Pancreatic Cancer Growth and Metastasis

2.1   Introduction

Pancreatic ductal adenocarcinoma (PDAC) is among the most devastating diseases, with a 5-year survival rate of less than 6% [204] . The curative therapeutic option is surgical resection; however, because of the lack of early symptoms, the vast majority of patients present in the clinic at a very advanced stage, and less than 25% of patients are surgically resectable by the time of diagnosis [205, 206]. By 2030, pancreatic cancer is expected to be the third leading cause of cancer-related death [207]. In 1996, the Food and Drug Administration (FDA) approved gemcitabine hydrochloride as a first line chemotherapy for locally advanced and metastatic pancreatic adenocarcinoma, but its clinical outcomes are indigent due to inefficient delivery and rapid metabolic inactivation [208]. In addition, a new combination therapy FOLFIRINOX (5-fluorouracil [5-FU], leucovorin, irinotecan and oxaliplatin) has shown improvement in overall survival compared to gemcitabine alone. However, there were significantly more grade 3-4 toxicities such as cytopenia and neutropenia fever with this therapy [209].

One of the characteristic features of PDAC is development of a dense desmoplastic (abundant fibrotic stroma around the cancer cells) that affect tumorigenesis, therapy resistance and possibly metastasis of tumor cells [210]. Desmoplasia is composed of extracellular matrix (ECM) including collagen and fibronectin. These proteins play a vital role in supporting cancer cell growth, invasion and metastasis [155, 211]. Hedgehog (Hh) signaling pathway promotes desmoplasia by causing pancreatic stellate cells to differentiate into myofibroblasts, which hinder the delivery of chemotherapeutic agents by forming a barrier from fibrotic cells around the tumor cells. By blocking the Hh pathway to

inhibit desmoplasia formation, extravasation of chemotherapeutic agents can be facilitated, and chemotherapeutic activity may be improved.

Cyclopamine (CYP) is a natural steroidal alkaloid, which can inhibit the Hh signaling pathway by blocking the 12-transmembrane protein smoothened (Smo) that inactivates the transcription factor glioma-associated oncogene family zinc finger-1 (GLI-1) [212]. As a result, CYP downregulates the target genes that are responsible for dense desmoplastic formation. CYP has been shown to inhibit cell proliferation of E3LZ10.7 and L3.6pl pancreatic cancer cell lines and growth of tumors in mice [213]. Docetaxel (DTX) acts as a microtubule stabilizer by binding to the β-tubulin and results in mitotic arrest and subsequent apoptosis. DTX is a second-line therapy for advanced pancreatic cancer [214]. However, DTX alone is not effective due to chemoresistance. Accordingly, we hypothesized that a combination of CYP and DTX might have a synergistic therapeutic efficacy in treating pancreatic cancer. However, both CYP and DTX are hydrophobic drugs that need an appropriate carrier system to improve their aqueous solubility. One of the strategies to improve water solubility is to use a co-solvent such as cremophor and Tween 80. The drawbacks of using these chemicals are their severe toxicity such as peripheral neuropathies, acute hypersensitivity reactions and alteration of pharmacokinetic profiles [215]. Therefore, polymeric micelle delivery systems, which either physically encapsulate drugs or conjugate to amphiphilic polymer can overcome these drawbacks. Physical drug-encapsulated micelles often have poor drug loading, premature drug release and unwanted toxicity. In contrast, covalently linked polymer drug conjugate micelles are more stable in circulation and can release drugs in a controlled manner at the tumor site with a therapeutically effective concentration [216]. Furthermore, drug conjugation to an amphiphilic polymer covalently accomplished higher drug payload compared to physically encapsulated micelles. In addition, the nano-size range confirm accumulation of these

conjugates in tumor site through the enhanced permeability and retention (EPR) effect [217].

Previously, we synthesized methoxy poly (ethylene glycol)-block-poly (2-methyl-2-carboxyl-propylene carbonate (mPEG-b-PCC) as a polymer delivery system and conjugated CYP and paclitaxel (PTX) to the carboxyl pendant groups of mPEG-b-PCC [218, 219]. In the present study, we conjugated CYP and DTX to the carboxyl pendant groups of mPEG-b-PCC. DTX was used instead of PTX because DTX is more potent than PTX. The final polymeric conjugates with CYP or DTX contained biocompatible PEG blocks to contribute stealth property, dodecanol (DC) as lipid chains, and polycarbonate as the biodegradable backbone. The polycarbonate backbone exhibits low toxicity to humans because its byproducts are carbon dioxide (CO_2) and alcohol. Furthermore, DC increases the hydrophobicity of the polymer, which promotes self-assembly into nano-sized micelles. The polymer drug conjugates were tested for their effect on the proliferation of MIA-PaCa-2 pancreatic cell lines , which highly express sonic hedgehog (Shh) and Smo receptor [220]. Finally, this formulation was administered intravenously into mice bearing orthotopic pancreatic tumors to determine whether P-DTX and P-CYP conjugates inhibit tumor growth associated with dense desmoplasia.

2.2   Materials and methods

2.2.1   Materials

CYP was purchased from Logan Natural Product (Plano, TX), and DTX was obtained from LC Laboratories (Woburn, MA). Dodecanol (DC), 1-ethyl-3-(3-(dimethylamino)propyl carbodiimide, N,N′-dicyclohexylcarbodiimide (EDC), N,N-dimethylpyridin-4-amine (DMAP), N,N′-Dicyclohexylcarbodiimide (DCC), Boc-β-alanine, dichloromethane (DCM), and hydroxybenzotriazole (HOBT) were obtained from Sigma-Aldrich (St. Louis, MO). Primary antibodies Shh (rabbit polyclonal antibody sc-9024), Bax

(rabbit polyclonal antibody sc-6236) and GAPDH (mouse monoclonal antibody sc-365062) were purchased from Santa Cruz Biotechnology, Inc. (Dallas, TX). Secondary antibodies goat anti-rabbit IgG-HRP (sc-2054) and goat anti-mouse IgG-HRP (sc-2055) were purchased from Santa Cruz Biotechnology, Inc. (Dallas, TX). Matrigel® matrix basement membrane was obtained from Corning (Chicago, IL). All other chemicals were analytical grade and were purchased from Sigma-Aldrich (St. Louis, MO).

2.2.2 Synthesis of mPEG-PCC-g-DTX-g-DC (P-DTX)

Previously, ring opening polymerization was utilized to synthesize monomer 2-methyl-2-benzyloxycarbonyl-propylene carbonate and its copolymer with mPEG (mPEG-b-PBC) followed by reduction to obtain the copolymer containing carboxyl pendent groups (mPEG-b-PCC) [219]. Carbodiimide coupling reaction was used to conjugate DTX and DC to the carboxyl groups of mPEG-b-PCC polymer. mPEG-b-PCC (150 mg, 0.0158 mmol) was dissolved in anhydrous dichloromethane (DCM) followed by the addition of DTX (108 mg, 0.134 mmol), DCC (130 mg, 0.62 mmol) and DMAP (58 mg, 0.48 mmol). This reaction mixture was stirred for four to five days under nitrogen atmosphere at 4°C. Then, DC (47 mg, 0.24 mmol) was added, and the reaction was allowed to proceed for another two days **[Figure 2.1A].** The product was purified by precipitation method in excess cold diethyl ether followed by dialysis against methanol for 4 days using a regenerated cellulose membrane with 7 K MWCO.

2.2.3 Synthesis of mPEG-b-PCC-g-CYP-g-DC (P-CYP)

Previously, secondary amine terminal was intoduced to CYP structure [218]. Briefly, Boc-β-Ala-TT was synthesized by reacing the following chemicals together. Boc-β-Ala-OH, 2-mercaptothiazoline and DMAP were dissolved in DCM under nitrogen protection. The solution was first stirred for 5 min −10°C followed by the addition of EDC and the solution was stirred at −10°C for 3 h and another 14 h at room temperature. After

reaction, 40 mL DCM was added and the solution was washed with NaHCO3 aq. (0.1 M),
HCl (0.1 M) and then NaCl aq. Then, the organic layer was deried by adding Na2SO4,
and the product was purified by column chromatography (silica gel 60 Å, 200–400 mesh,
EtOAc: CH3OH 15: 1) and then recrystallized from DCM to find yellow powder. The
structure was confirmed by 1H–NMR spectroscopy. Second step is the synthesis of Boc-
β-Ala-CYP. Briefly, the final product from the first step (Boc-β-Ala-TT 53 mg 0.185 mmol)
and CYP (38 mg, 0.09 mmol) were dissolved in pyridine under nitrogen. The reaction
mixture was stirred at 50°C for 18 h. The solvent was removed by rotary evaporation. The
resulted product was cleaned by column chromatography (silica gel 60 Å, 70–230 mesh,
EtOAc: Hexane 7:3) to give solid of Boc-β-Ala-CYP in 75% yield. The structure was
confirmed by 1H NMR spectroscopy. Third step is the synthesis of NH2-β-Ala-CYP.
Briefly, the final product from the previuos step (Boc-β-Ala-CYP) was dissolved in
anhydrous DCM (3 mL) and TFA (3 mL) was added at 0 °C. Then, the solvent was
removed by N2 flashing. The crude product was dissolved in chloroform (20 mL) and
washed with aqueous saturated NaHCO3 (3 × 25 mL) and brine (1 × 25 mL). The organic
layer was dried over anhydrous sodium sulfate and filtered. NH2-β-Ala-CYP was obtained
after the solvent was removed by rotary evaporation. The structure was confirmed by 1H
NMR spectroscopy and LC-MS. Final step was to synthesize P-CYP. Briefly, mPEG-PCC
(185 mg, 0.0195 mmol) was dissolved in anhydrous DCM followed by the addition of NH2-
β-Ala-CYP (75 mg, 0.15 mmol), EDCl (75 mg, 0.375 mmol), HOBt (53 mg, 0.375 mmol).
The reaction was stirred for two days under nitrogen at the room temperature. Then, DC
(72.45 mg, 0.375 mmol) was added and the reaction was allowed to proceed for another
two days [**Figure 2.1B**]. After completion of the reaction, the final product was purified by
precipitation in large excess of diethyl ether and then by dialysis against ethanol using a
regenerated cellulose membrane of 3500 MWCO.
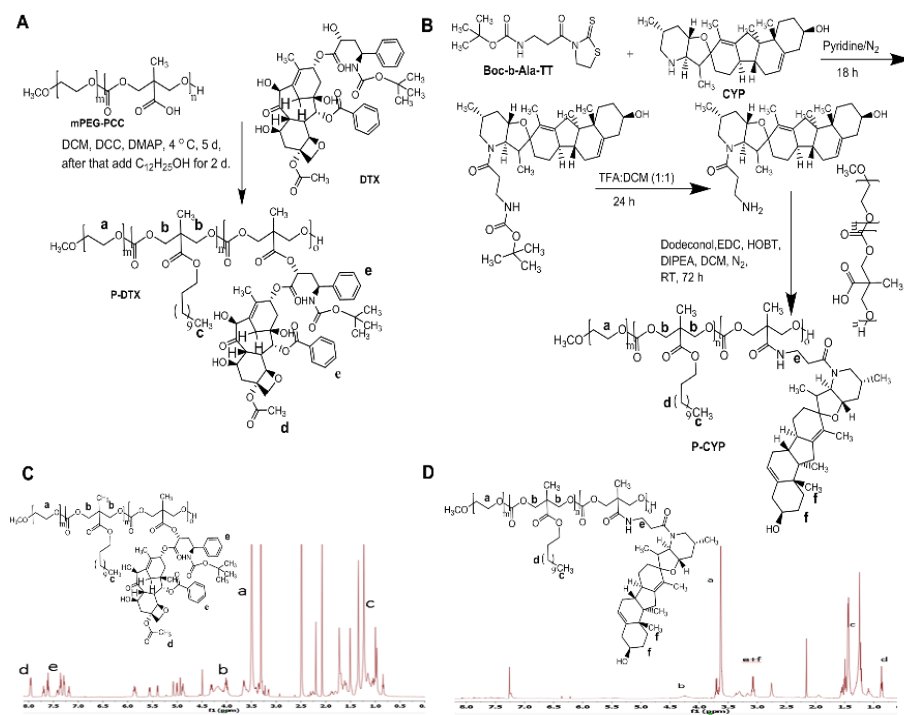
Figure 2.1 Synthesis schemes and 1H NMR analysis of polymer-drug conjugates.

(A) Synthesis scheme of P-DTX, (B) synthesis scheme of P-CYP, (C) 1H NMR spectrum of P-DTX, and (D) 1H NMR spectrum P-CYP.

2.2.4 Preparation and characterization of P-CYP and P-DTX micelles

Briefly, 15 mg of P-CYP or P-DTX was dissolved in 500 µL of DCM and the solvent was removed under reduced pressure to obtain a film, which was vacuum dried overnight. The film was hydrated by adding one mL of phosphate-buffered saline (PBS; pH 7.4) followed by probe sonication for 6 min and filtration by using a 0.22 µm filter. A zetasizer Nano ZS90 (Malvern, Worcestershire, UK) was used to determine the mean particle size at a scattering angle of 90. Particle size distribution is reported as the mean ± S.D.

2.2.5 Cell Culture

The human pancreatic cancer cell line MIA PaCa-2 was obtained from ATCC (ATCC® CRL-1420™), and cultured in DMEM medium containing 10% FBS and 1% penicillin/ streptomycin. Cells were maintained in an incubator with 5% CO_2 at 37°C.

2.2.6 Isobologram Analysis

To assess the synergistic effect of combination of P-CYP and P-DTX, dose-response curves were plotted for the effect of P-CYP and P-DTX on MIA PaCa-2 and BxPC-3 cell viability separately. Both cells were treated with P-CYP (0,1.5625, 6.25, 25 and 100 µM) and P-DTX (0, 1, 4, 16 and 64 nM) for 48 h. From these curves, The IC_{50} values were determine for P-CYP micelles and P-DTX micelles in MIA PaCa-2 and BxPC-3 cells. Then, Isobologram method of analysis of Steel and Peckham were applied to check the synergism. The combination index was calculated based on the following equation

$$CI = \frac{d1}{D_{50}1} + \frac{d2}{D_{50}2}$$

Where $D_{50}1$ is the dose of P-DTX that produce 50% inhibition effect alone, *d*1 is the dose of P-DTX that produce same 50% inhibition effect in combination with P-CYP, $D_{50}2$ is the dose of P-CYP that produce 50% inhibition effect alone, and *d*2 is the dose of

P-CYP that produce same 50% effect inhibition in combination with P-DTX. The interpretation of CI was done as follow: < 1.0 synergism, =1.0 additive, >1 antagonism. The parameter $d1$ was obtained by using constant dose of P-DTX in combination varied dose of P-CYP (1.5625, 6.25, 25 and 100 µM). The $d2$ was determine when the dose of P-CYP combined with $d1$ produced the 50% inhibition in cell growth.

2.2.7   Cell Viability Assay

To determine the effect of P-CYP micelles, P-DTX micelles and their combination on cell viability and tumor spheroid formation, MIA PaCa-2 cells were seeded in a 96-well plate (5000 cells/well) and incubated for 24 h. The culture medium was replaced with medium containing either empty polymer micelles as a negative control, 25 µM P-CYP micelles, 16 nM P-DTX micelles, or a mixture of 25 µM P-CYP and 16 nM P-DTX micelles in 200 µL; cells were then grown for 48 h. Cell viability was evaluated by an MTT assay at 560 nm absorbance and 630 nm for the cell debris. The absorbance results from 630 nm were deducted from 560 nm to eliminate cells debris effects. The cell viability for all groups was calculated according to the following formula:

$$\textbf{Cell viability } (\%) = \frac{\textbf{absorbance of test sample}}{\textbf{absorabnce of control}} \textbf{ x 100}$$

For 3D spheroid formation, MIA PaCa-2 cells were seeded in Perfecta3D® 96-Well Hanging Drop Plates (3D Biomatrix, Inc., Ann Arbor MI) in triplicate and incubated at 37°C, 5% CO_2 over the course of time. The cell number per well was 3000 cells in 40 µL of DMEM. The tumor spheroids were treated with empty polymer micelles as negative control, 25 µM P-CYP micelles, 16 nM P-DTX micelles, or a combination of 25 µM P-CYP micelles and 16 nM P-DTX micelles on day 4, 6 and 8 after forming tumor spheroid. The image under light microscope were taken in the day before starting the treatment, and the

day after each treatment (day 5th, 7th and 9th) to check the cyctotoxic effect of diferent formulations on 3D tumor model.

2.2.8 Colony Formation Assay

To evaluate the ability of P-CYP micelles, P-DTX micelles or their combination to inhibit cells undergoing cell division, MIA PaCA-2 cells were plated in 6-well plate (500 cells/well), and cultured for 24 h to adhere in the bottom of the plate. Thereafter, the medium was replaced with the medium containing empty micelles as control, 25 µM P-CYP micelles, 16 nM P-DTX micelles or a mixture of both conjugates in 2 mL then incubated for 14 days. Visible colonies, which are consisted of at least 50 cells, were fixed with 10% formalin and stained with 0.5% crystal violet. All colonies were counted following the staining, and the percentage of colonies was calculated with respect to the control colonies as described earlier [221].

2.2.9 Apoptosis Assay

To assess apoptosis, MIA PaCa-2 cells were seeded into 6-well plates (3.5×10^5 cells/well) and incubated for 24 h. The culture medium was replaced with medium containing either plain polymer micelles, 25 µM P-CYP micelles, 16 nM P-DTX micelles, or a mixture of both in 2 mL and incubated for 48 h. Then, the cells were stained with an Annexin-V and propidium iodide (PI) by using a Vybrant® Apoptosis Assay Kit according to the manufacture's protocol (Molecular Probe, Waltham, MA). Apoptotic cells were quantified by flow cytometry (Becton, Dickison, NJ, USA).

2.2.10 Cell Cycle Analysis

To determine the effect of treatment on cell cycle distribution, 3.5×10^5 MIA PaCa-2 cells were plated into 6-well plates with no FBS for 24 h. Cells were then incubated with empty polymer micelles as a negative control, 25 µM P-CYP micelles, 16 nM P-DTX, or their mixture in 2 mL for 48 h. Then, cells were detached and fixed in 90% ice-cold ethanol

overnight. Cells were washed with cold PBS twice and stained with propidium Iodide (PI) (Molecular Probes, Waltham, MA). Cell cycle analysis was assessed by flow cytometry, with 10,000 fluorescent events per analysis.

2.2.11 Western Blot Analysis

MIA PaCa-2 cells were seeded in 6-well plates (3.5×10^5 cell/well) for 24 h. Cells were then treated with various micelles for 48 h. Next, RIPA buffer (Sigma-Aldrich, St. Louis, MO) was used to lyse the cells, and a bicinchoninic acid (BCA) Protein Assay Kit (Pierce, Rockford, IL) was used to measure protein concentrations. The lysate was denatured by heating at 90°C for 5 min, and then subjected to 15% SDS-PAGE. Thereafter, the lysate was transported to a PVDF membrane using the iBlot™ system (Invitrogen, Carlsbad, CA). Membranes were blocked with Odyssey® blocking buffer for 1 h at room temperature. Then, membranes were incubated with primary antibodies for Shh (sc-9024) BAX (sc-6236), and GAPDH (sc-365,062) overnight at 4°C followed by washing with PBS with 0.05% Tween 20 (PBST). The membranes were then incubated with their corresponding horseradish peroxidase-conjugated secondary antibodies (sc-2055, and sc-2054). Target proteins were detected by ImmunoCruz Western blotting luminol reagent kit (Santa Cruz Biotechnology, Dallas, TX).

2.2.12 Evaluation in Orthotopic Pancreatic Cancer-Bearing Nsg Mice

All animal experiments were performed according to the NIH animal use guidelines, and the protocol was approved by the Institutional Animal Care and Use Committee (IACUC) at the University of Nebraska Medical Center, Omaha, NE. The orthotopic pancreatic tumor was created in NSG mice 6–8 weeks old by implanting 2×10^6 MIA Paca-2-GFP-luciferase cells into the dorsum of the pancreas using PBS: Matrigel (1:1 *v*/v, 50 μL). The tumor size was monitored by noninvasive bioluminescence. In brief, 150 mg/kg of D-luciferin was administered intraperitoneally, and an IVIS imaging system

(Caliper Life Sciences, Waltham, MA) was used to measure the intensity of bioluminescence. All animals were then divided randomly into four groups with six animals in each group once the radiance of the tumor reached 2 X10^7 p/s/cm^2/sr: saline as control, P-CYP micelles, P-DTX micelles, or a mixture of P-CYP and P-DTX micelles. Those formulations were given intravenously through the tail vein, 3 times per week for 2 weeks and the maximum volume injected was 200 µL based on the mouse body weight. Group 1 was injected with saline as the vehicle control. Group 2 received six doses of formulated P-CYP micelles in 2 weeks, and the equivalent dose of P-CYP was 20 mg/kg of free CYP. Group 3 received 6 doses of P-DTX micelles in 2 weeks equivalent to 5 mg/kg of free DTX. Group 4 received a combined-chemotherapy of P-CYP and P-DTX with respect to their actual therapeutic doses of 5 mg/Kg and 20 mg/Kg P-DTX and P-CYP, respectively. Bioluminescent radiance of the tumor and body weight were measured every other day following cells implementation for 45 days. After finishing the study, all animals were sacrificed, and the tumor and all vital organs (liver, spleen, kidney, heart) were collected and stored in −80°C.

2.2.13 Immunohistochemical and Immunofluorescences Assay

Tumor tissue was fixed with 10% buffered formalin for 24 h. The samples were embedded in the paraffin, and thin sections of 4 µm were prepared and immunostained for cell proliferation marker (Ki-67), apoptosis (cleaved caspase 3), tissue morphology hematoxylin and eosin (H&E), total collagen (Masson's trichomes), epithelial–mesenchymal transition (EMT) modulator (ZEB-1) and metastatic marker (E-cadehrin).

To detect tumor cell apoptosis induced by different micelle formulation, a TUNEL assay kit (Abcam, Cambridge, MA) was used according to the manufacturer's protocol. PI was used to counterstain the tumor sections and then imaged under a fluorescence microscope(zeiss, Germany).

2.2.14 Statistical Analysis

Data are represented as the mean ± standard deviation (SD). The statistical comparisons of the data were performed by student's *t* test. *P*-value <0.05 was considered statistically significant.

2.3   Results

2.3.1   Synthesis and Characterization of Polymer-Drug Conjugates

P-DTX was synthesized by direct carbodiimide coupling of DTX to one of the carboxylic acid groups on the hydrophobic block of mPEG-b-PCC copolymer. The esterification took place favorably at 2′-hydroxyl group due to its less steric hindrance. In ^{1}H NMR spectra of mPEG-b-PCC, protons corresponding to $–CH_2 – CH_2 – O–$ of PEG were observed at δ 3.4–3.6, and $–CH_2–$ units of PCC δ 4.2–4.4 and –COOH were observed at δ 12–14 as reported earlier by our group. After conjugation of DTX to mPEG-b-PCC, protons related to DTX were all seen in ^{1}H NMR spectra and DTX content in the conjugates was determined to be 30.4 ± 3.7% (*w*/w), as calculated from the peak intensities of all phenyl proton signals from 7.3 to 8.4 ppm **[Figure 2.1 A,C]**. Conjugation of CYP was done through a Boc-b-Ala linker because the secondary amine on CYP was not easy to conjugate with carboxylic acid group on mPEG-b-PCC. Therefore, after Boc-removal the primary amine on the linker made the conjugation of CYP to the copolymer much easier. After conjugation of CYP to mPEG-b-PCC, protons corresponding to CYP were seen in 1H NMR spectra and CYP content in the conjugates were 25 ± 1.6% (w/w) calculated from proton signal 1.7–2.4 ppm **[Figure 2.1 B,D]**. P-DTX and P-CYP micelles were prepared by film hydration method, and the mean particle sizes of P-DTX and P-CYP were 66.18 ± 0.4 nm (PDI 0.190) and 73.11 ± 0.7 nm (PDI 0.209), respectively [Figure 2.2]
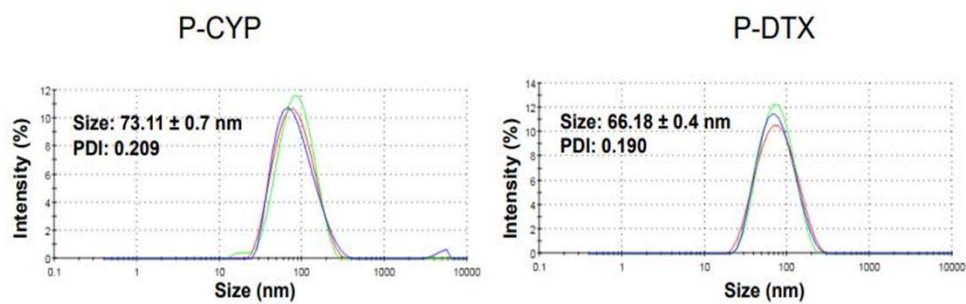
Figure 2.2 Particle size distribution of P-CYP and P-DTX micelles using dynamic light scattering (DLS).

2.3.2 Combined Treatment with P-CYP and P-DTX Synergistically Inhibits the Growth of Pancreatic Cancers Cells

To determine whether the combination of P-CYP and P-DTX could have a synergistic effect, a combination index (CI) was determined after treating 5000 MIA PaCa-2 or BxPC-3 cells with P-CYP, P-DTX and combination of P-CYP and P-DTX. MIA PaCa-2 and BxPC-3 were treated with P-DTX (0–64 nM) to produce dose-response curves using MTT assay, with 50% inhibitory concentration (IC50) 39 nM and 34 nM, respectively **[Figure 2.3 A]**. In addition, MIA PaCa-2 and BxPC-3 were treated with P-CYP (0–100 µM) to produce the dose-response curve. Form these curves, the (IC50) were 55 µM and 70 µM, respectively **[Figure 2.3B]**. The CI was calculated by using this formula: CI = (d1/D501) + (d2/D502). As shown in Table 2.1, CI value was calculated to be 0.86 and 0.89 when MIA PaCa-2 and BxPC-3 were treated with 25 µM P-CYP and 16 nM P-DTX combination, respectively.

2.3.3 Combined-Treatment with P-CYP and P-DTX Decreases the Proliferation of Pancreatic Cancer Cells

Cell viability after incubation of MIA PaCa-2 and BxPC-3 cells with empty micelles, 25 µM P-CYP, 16 nM P-DTX micelles or their combination for 48 h was measured by an MTT assay. Combination treatment for 48 h reduced MIA PaCa-2 cell viability by 64% and BxPC-3 cell viability by 60% **[Figure 2.4 A].** However, both P-CYP and P-DTX micelles as monotherapy did not achieve the same level of cell viability reduction when 100 µM P-CYP and 64 nM P-DTX were used **[Figure 2.3 A,B]**. Thus, combination of P-CYP and P-DTX micelles had a better effect on decreasing the cell viability of pancreatic cancer cells.
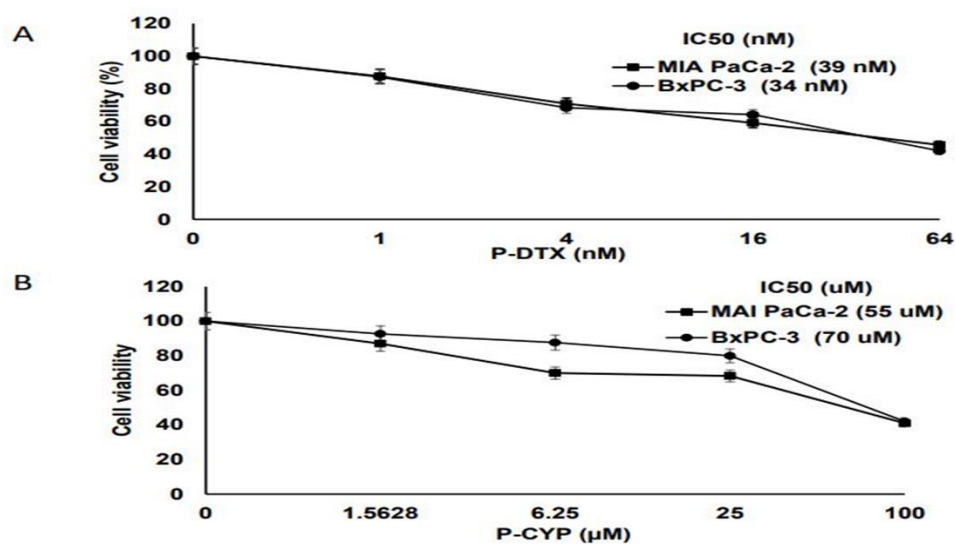
Figure 2.3 Effect of micelle formulations on pancreatic cancer cells (dose-response curve).

(A) MIA PaCa-2 and BxPC-3 cells were treated with an increased concentrations of P-DTX micelles (0-64 nM) for 48h zero is the empty micelles, (B) MIA PaCa-2 and BxPC-3 cells were treated with an increased concentrations of P-CYP micelles (0-100 µM) for 48h.

Table 2.1 Synergistic Anticancer Activity of P-CYP and P-DTX in Human Pancreatic Cancer

Drug combination	Cell line	D501 (nM)	d 1 (nM)	D502 (μM)	d 2 (μM)	CI
P-DTX + P-CYP	MIA PaCa-2	39	16	55	13.7	0.66
					25	0.86
	BxPC-3	34		70	16.34	0.7
					25	0.83

2.3.4 Combined Treatment with P-CYP and P-DTX Reduces Colony Formation Ability of MIA PaCa-2 Cells

The efficacy of combination treatment with 25 µM P-CYP and 16 nM P-DTX to inhibit 50 of MIA PaCa-2 cells to come close together and form one colony for 14 days was evaluated by unaided eye after staining with 0.5% crystal violet. The combination treatment had more effect on MIA PaC-2 cells in terms of decreasing the percentage of colonies to 12% compared to 34% and 67% in case of P-DTX micelles and P-CYP, respectively **[Figure 2.4b**].

2.3.5 Combination of P-CYP and P-DTX Reduced the Size of MIA PaCa-2 Spheroid Structure

To simulate the real pancreatic tumor structure, 3D model was performed by using handing drop method. Combination treatment with 25 µM P-CYP and 16 nM P-DTX had the smallest spheroid size compared to either P-DTX or P-CYP only **[Figure 2.4c].**
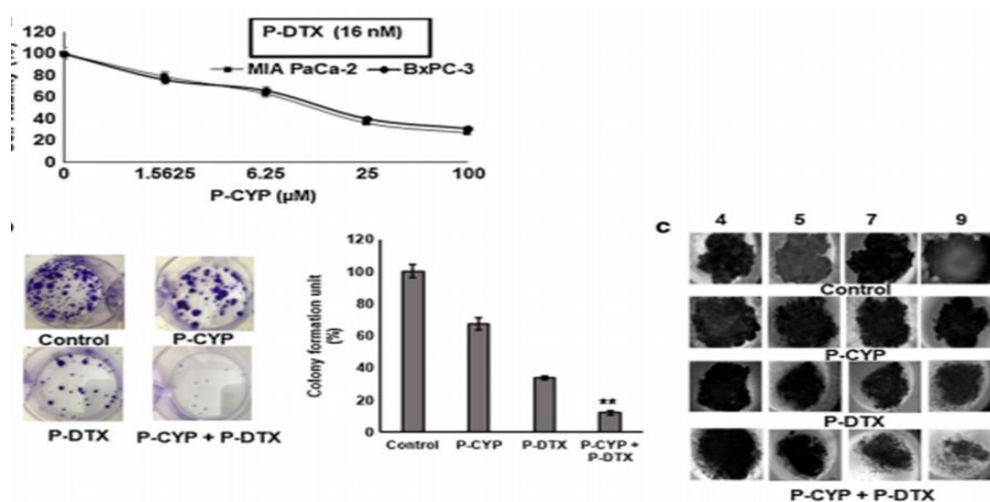
Figure 2.4 Cell viability assay at 48 h post-incubation of MIA PaCa-2 and BxPC-3 cells with a combination of 16 nM P-DTX and 25 *μ*M P-CYP

(**a**). Colony formation potential of MIA PaCa-2 cells. 500 cells were seeded to 6-well plate. After 24 h, formulations were added and at day 14 the colonies were fixed, stained and counted (**b**). Treatment of tumor spheroids of MIA PaCa-2 with the same formulation at days 4, 6 and 8 and images were taken at days 4, 5, 7 and 9 under inverted microscope at 40 x magnification (**c**). Results are presented as the mean ± S.D. (*n* = 5).

2.3.6 Combined Treatment with P-CYP and P-DTX Enhances Cell Cycle Arrest at G2/M Phase

The ability of the combination treatment with 25 µM P-CYP and 16 nM P-DTX on cell cycle arrest was measured by flow cytometry using PI staining. Treatment for 48 h with the combination of P-CYP and P-DTX increased the fraction of cells in the G2/M phase compared to that of their monotherapies. The combination treatment resulted in increased number of cells in G2/M phase from 22.0 ± 0.2% in control to 63.3 ± 2.5%. However, the increase in the number of cells in the G2/M phase with P-CYP or P-DTX alone was 30.2 ± 0.2% and 50.9 ± 1.3%, compared to 22.0 ± 0.2% in control respectively **[Figure 2.5a].**

2.3.7 Combination of P-CYP and P-DTX Enhances Apoptosis in Pancreatic Cell Lines

The ability of combined-treatment with 25 µM P-CYP and 16 nM P-DTX to enhance apoptosis over 48 h was measured by an Annexin V binding assay. Combined-treatment with P-CYP and P-DTX resulted in more apoptotic cells compared to the single treatments **[Figure 2.5b,c].** The percentage of cell death in the combination treatment group was 64 ± 2%, whereas in the case of P-CYP or P-DTX, the percent of cell death was 33 ± 1.5% and 51 ± 2%, respectively.

2.3.8 Combination Treatment with P-CYP and P-DTX Downregulates Their Respective Target Proteins

The effect of combination treatment of MIA PaCa-2 cells with 25 µM P-CYP plus 16 nM P-DTX, vs. 25 µM P-CYP or 16 nM P-DTX CYP and DTX alone on their target proteins, such as Shh and BAX were determined by Western blot analysis at 48 h post-treatment. Combined treatment of P-CYP and P-DTX significantly decreased Shh expression more than their monotherapies. On the other hand, combined-treatment of P-CYP and P-DTX significantly increased BAX expression compared to monotherapies **[Figure 2.5 d].**
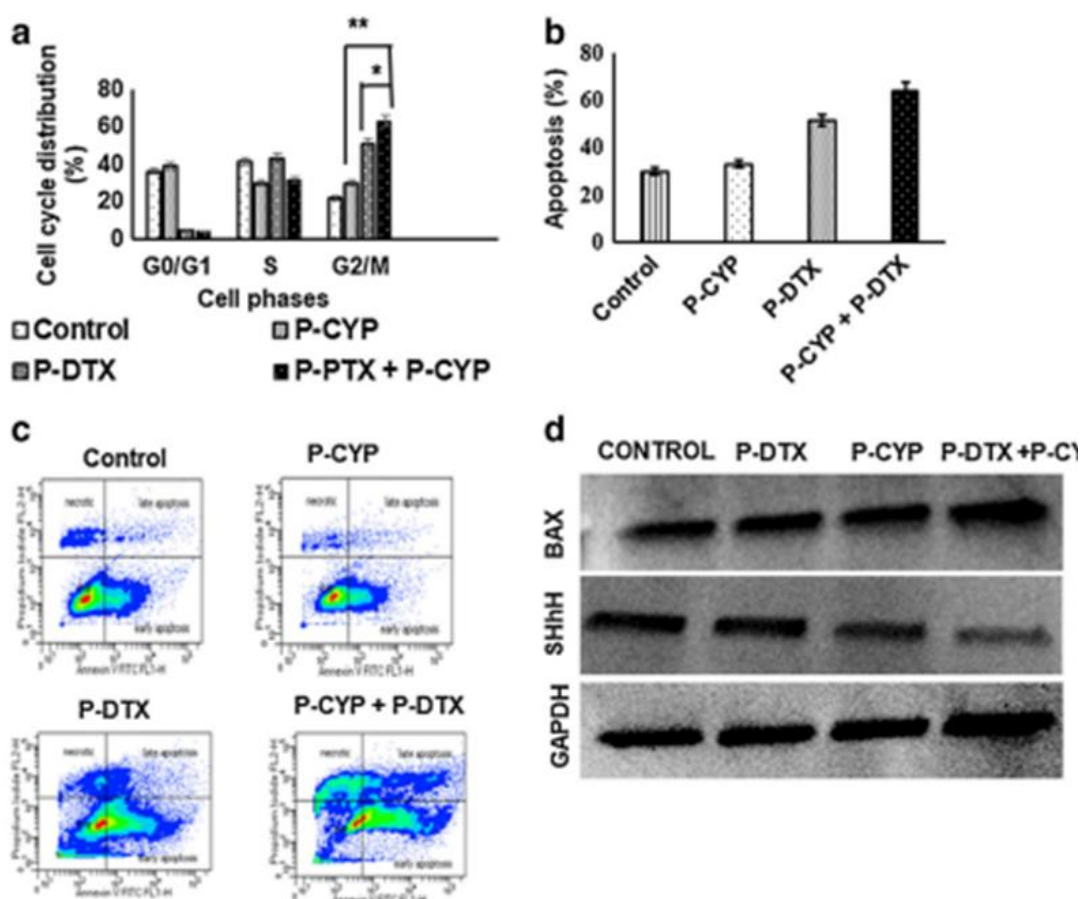
Figure 2.5 Cell cycle, apoptosis and Western blot analysis of MIA PaCa-2 cells after 48 h exposure to empty micelles, 25 µM P-CYP micelles, 16 nM P-DTX micelles, and their combination.

(a) Cells were grown in 6-well plate (3.5 × 105 cells/well), and cell cycle analysis were evaluated by flow cytometry after staining with propidium iodide (PI). (b-c) Apoptotic cells were measured by flow cytometry after staining with Annexin-V and PI. (d) BAX and SHH protein levels were assessed by Western blot analysis. All data were presented as the mean ± S.D. (n = 3) (*) $P < 0.05$, (**) $P < 0.001$.

2.3.9 *In vivo* **Evaluation**

To investigate the efficacy of combination therapy with P-CYP and P-DTX, orthotopical pancreatic cancer mouse model was established by implementing stably luciferase expressing MIA PaCa-2 cells in the pancreas. Once the tumor radiance reached around 2×10^7 $p/s/cm^2/sr$, mice were injected intravenously with the following formulations via the tail vein thrice a week for 2 weeks: saline, 20 mg/Kg of P-CYP micelles, 5 mg/Kg of P-DTX micelles, or a mixture of 20 mg/Kg P-CYP and 5 mg/Kg P-DTX micelles. After 12 days of cell implementation in the pancreas, all mice were imaged for luciferase bioluminescence to determine the tumor growth and divided the mice randomly into different groups. At day 33, the final bioluminescence images were recorded and showed significant tumor growth inhibition in mice receiving the combination therapy to monitor the tumor burden over time **[Figure 2.6a**]. Luciferase bioluminescence intensity was measured throughout the study from day 12 to day 33. After plotting the photon intensity values of different mouse groups versus time, mice administered combination therapy had the lowest photon intensity value compared to other groups receiving saline, P-CYP micelles, or P-DTX micelles **[Figure 2.6b**]. At the end of the study, all mice were sacrificed and the tumors and vital organs were collected. Then, the tumor weight and volume were measured, and we found that mice receiving combination therapy had the lowest tumor weight (0.23 ± 0.03 g) compared to the mice which were injected with P-DTX micelles (0.58 ± 0.16 g), P-CYP micelles (0.78 ± 0.10 g), or PBS (1.13 ± 0.04 g) [Figure 2.7A] Furthermore, the combination therapy had the lowest- tumor volume (202 ± 52 mm3) compared to P-DTX micelles (661 ± 112 mm3), P-CYP micelles (732 ± 104 mm3), or PBS (1596 ± 394 mm3) [Figure 2.6c & Figure 2.7B]. To evaluate the general toxicity profile of the formulation, mouse body weights were monitored throughout the treatment. No significant differences was observed in body weights in the treatment groups compared to the control **[Figure 2.7C**]. In addition, the acute toxicity was evaluated in vital organs (liver,

spleen, heart, or kidney). There was no huge histological changes post treatment for all groups [**Figure 2.8**]

To expound the remarkable effect of combination therapy, immunofluorescence and immunohistochemistry experiments were carried out. Tumors from mice treated with combination therapy had loosen groups of epithelial cells; however, mice treated with P-CYP micelles or P-DTX micelles had dense epithelial cells. Treatment with combination of P-CYP and P-DTX had the lowest staining of Ki-67 that reflects the cancer cell proliferation [**Figure 2.9**]. Moreover, mice receiving the mixture of P-CYP and P-DTX had the highest staining of cleaved caspase-3 that reflect the apoptosis of cancer cells **[Figure 2.9**].

To investigate whether treatment with the combination therapy of P-CYP and P-DTX micelles can enhance the ECM degradation, tumor section slides were stained with Masson's trichome. Combination treatment with P-CYP and P-DTX micelles degraded the components of ECM much more efficiently than either P-CYP micelles or P-DTX micelles alone **[Figure 2.10]**. An increase in E-cadherin signal was detected in the mice treated with the combination therapy of P-CYP and P-DTX micelles compared with the control or monotherapies. Furthermore, ZEB-1, which regulates the EMT was seen in low expression in mice treated with combination therapy of P-CYP and P-DTX micelles **[Figure 2.10]**. TUNEL assay was performed to evaluate the tumor growth inhibition. The apoptotic cells were stained with green fluorescence. P-CYP micelles or P-DTX micelles treated group had small number of apoptotic cells, but the combination of P-CYP and P-DTX micelles treated group had significant number of apoptotic cells **[Figure 2.11]**.
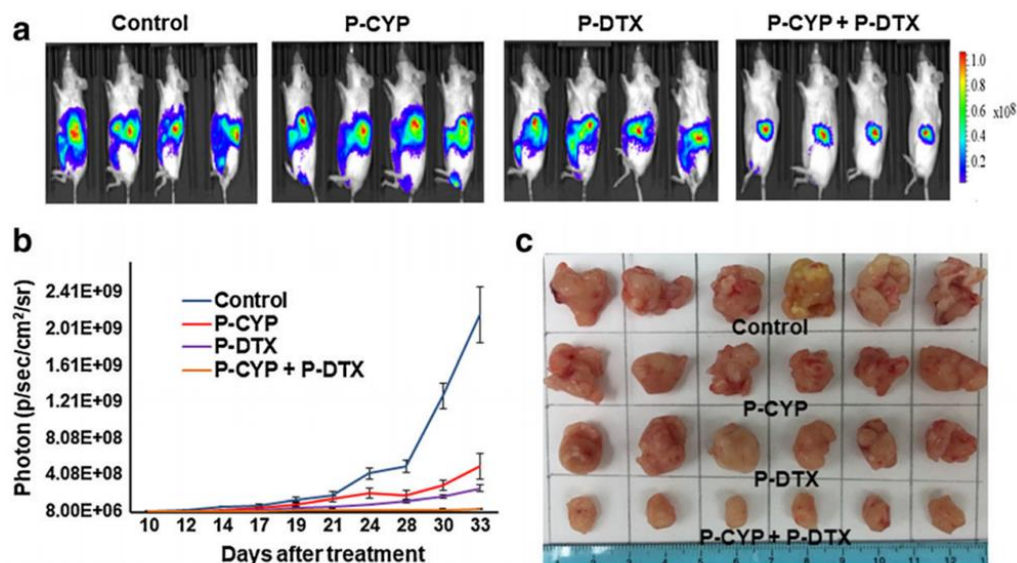
Figure 2.6 In vivo efficacy of combined-treatment of P-CYP and P-DTX after I.V. injection in NSG mouse bearing MIA PaCa-2-GFP-LUC cells inserted pancreatic tumor

(a) In vivo representative bioluminescence image at last day from mice treated with free saline (control), P-CYP, P-DTX, and P-CYP + P-DTX. **(b)** Photon intensity of orthotopically implanted pancreatic tumor was measured by IVIS machine at various times post treatment. **(c)** a representative tumor image after sacrificing all mice at the end of experiment.
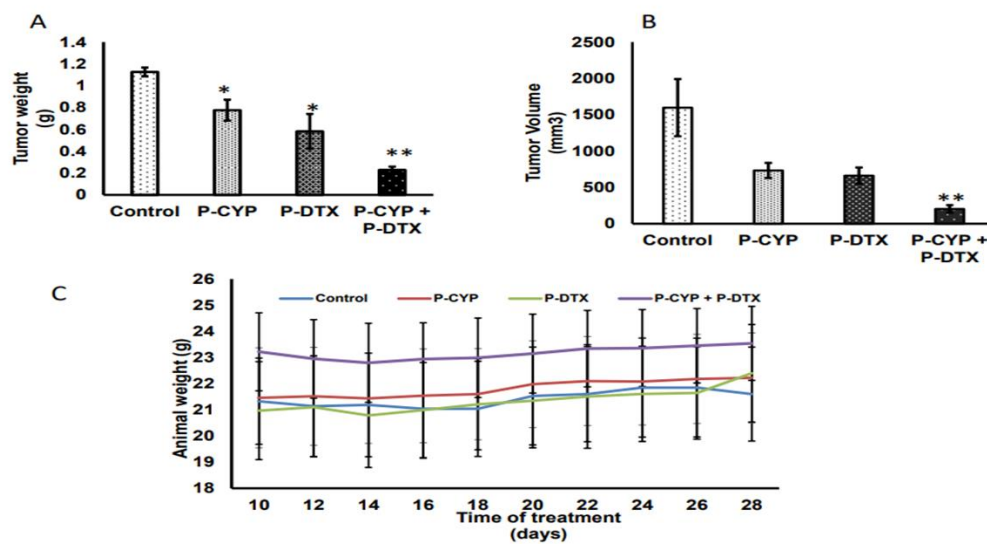
Figure 2.7 tumor weight and volume at the end of the study, and mice body weight during treatment

Tumor weight **(A)** and volume **(B)** at 3 weeks post treatment. (**C**) Animal body weight during the treatment period. Results are presented as the mean ± S.D. for 6 mice per experimental group (*) $P < 0.001$ (**) $P < 0.0001$.
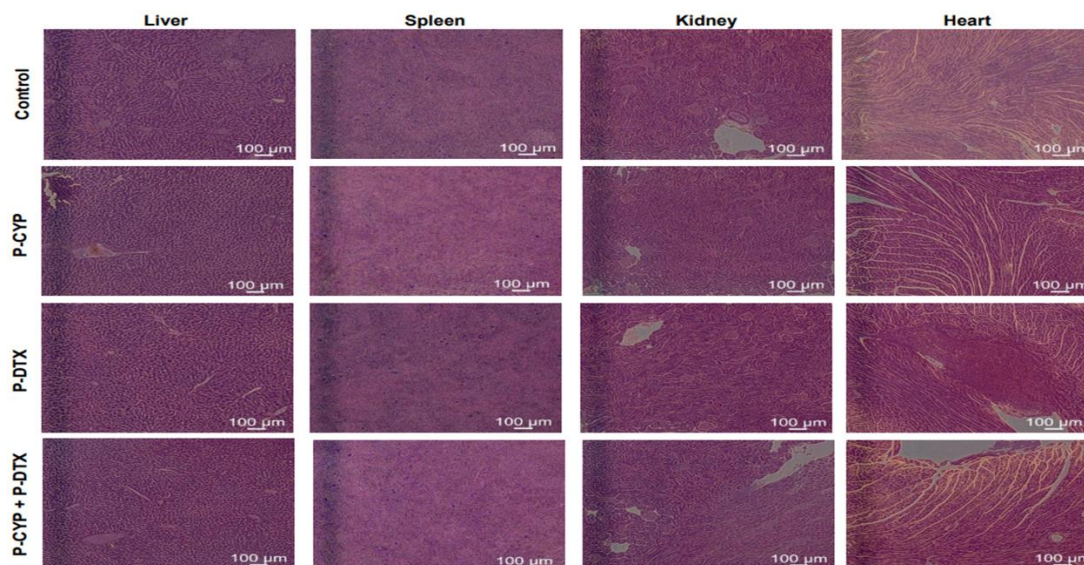
Figure 2.8 In vivo toxicity assessment.

H & E staining of vital organs, such as liver, spleen, kidney and heart at two weeks after systemic administration (three times a week for two weeks) of saline as control, P-CYP, P-DTX and their combination. Scale bar 100 μM.
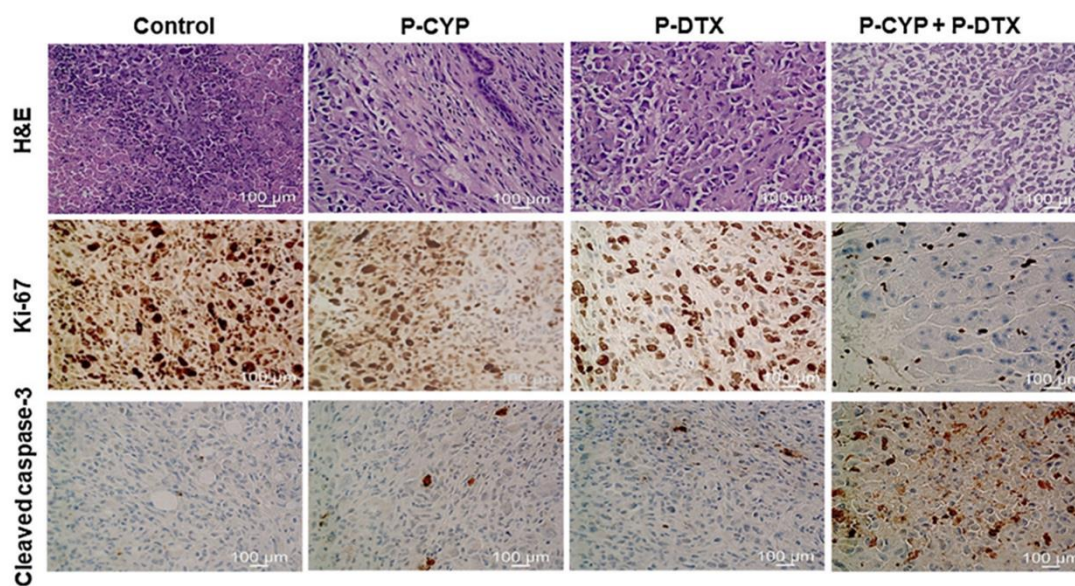
Figure 2.9 Immunohistochemical assay-1

Immunohistochemical staining of tumor section for hematoxylin and eosin (H&E), Ki-67 (proliferation related marker), and cleaved caspase-3 (apoptotic marker). The apoptotic cells are stained brown. Images were taken at 40× magnification.
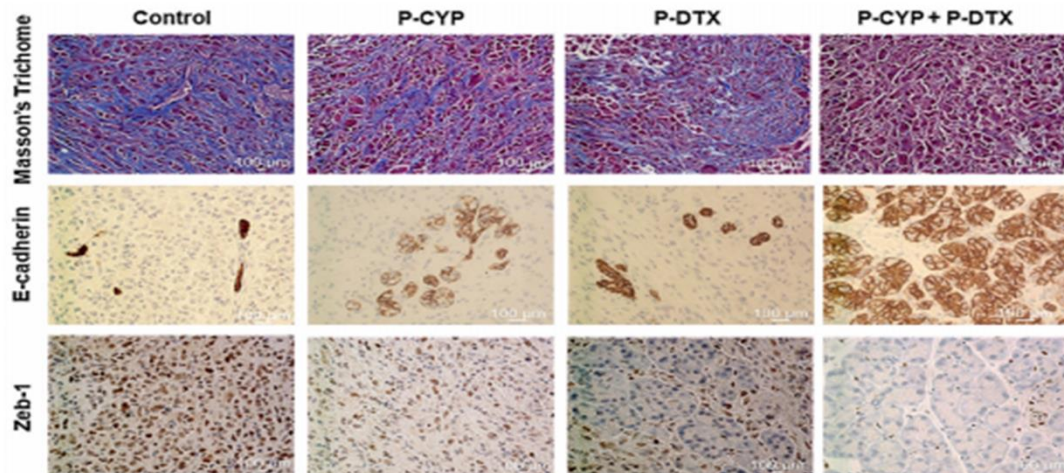
Figure 2.10 Immunohistochemical assay-2

Immunohistochemical staining of tumor section with Masson's Trichome (related to collagen deposition and desmoplasia), E-cadherin (related to metastasis maker) and ZEB-1 (EMT modulator)
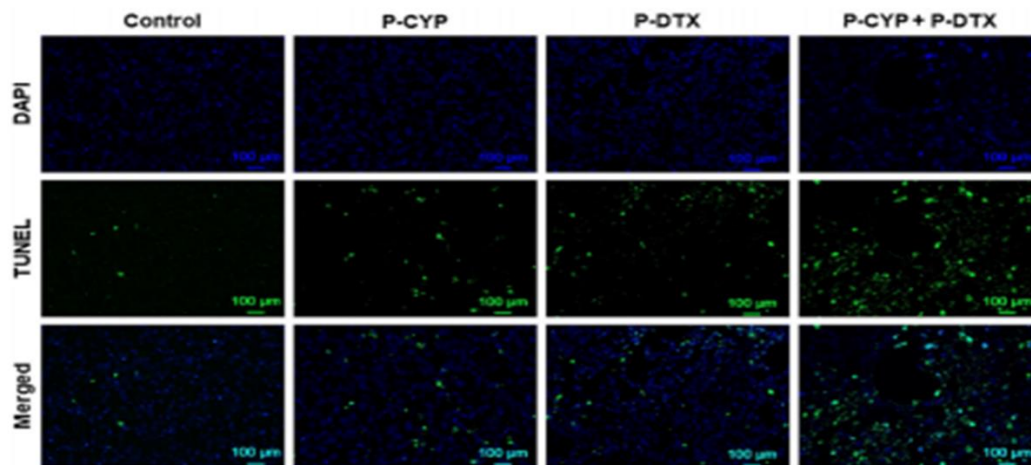
Figure 2.11 TUNEL assay of tumor specimens of orthotopic MIA PaCa-2 cells derived tumor bearing mice treated with P-CYP, P-DTX and their combination

Tumor tissues were fixed, paraffin cryosectioned and immunostained for TUNEL to detect apoptotic tumor cells. TUNEL positive nuclei (green), DAPI positive nuclei (blue), scale bar 100 μM.

2.4 Discussion

PDAC is a highly aggressive cancer usually diagnosed at an advanced state and poses a medical challenge due to its insensitivity to the majority of chemotherapeutic agents after long-term treatment. Hh signaling promotes pancreatic cancer cell proliferation by promoting EMT and decreasing apoptosis by regulation of Bcl-2 and Bcl-X. Hh pathway also promotes cell invasion, migration, and chemoresistance. Therefore, inhibition of Hh signaling using CYP has the potential to synergistically inhibit tumor growth and metastasis.

Unlike physically encapsulated drugs into polymeric micelles, which are released faster due to the dynamic instability of micelles, bioconjugation to amphiphilic polymers prevents drug release in the circulation and provides sustained drug release. Therefore, in this study, we conjugated DTX and CYP to a biodegradable amphiphilic diblock copolymer mPEG-b-PCC with pendant carboxyl acid groups. We previously conjugated a water soluble drug gemcitabine as well as dodecanol to mPEG-b-PCC, which self-assembled into micelles and showed an enhanced drug delivery to pancreatic tumor, which resulted in significant reduction in tumor growth [222-224]. In this study, DTX was conjugated to mPEG-b-PCC through an ester bond at its 2′-OH position. For CYP conjugation to mPEG-b-PCC, we used a linker containing thiazolidine-2-thione to react with secondary amine in CYP [218]. The attachment of DC enhanced requisite hydrophobicity and assisted in the self-assembly of polymer-drug-conjugate micelles. Combination of P-CYP and P-DTX micelles significantly inhibited MIA PaCa-2 and BxPC-3 cell viability [**Figure 2.4a**]. Isobologram method of analysis of Steel and Peckham suggests that the combination of P-CYP and P-DTX have a synergistic effect on the growth inhibition of pancreatic cell lines (MIA PaCa-2 and BxPC-3) since the CI values were less than one [**Table 2.1**]. This combination therapy inhibited colony formation, enhanced apoptosis and cell cycle arrest in G2/M phase, upregulated BAX proteins, and

downregulated the Shh ligand much more than micelles with either CYP or DTX micelles alone [**Figure 2.4b,c & Figure 2.5**].

In vivo efficacy of P-DTX and P-CYP conjugate micelles was determined in orthotopic pancreatic tumor model developed by MIA PaCa-2-luc-GFP cells in NSG mice. Promising results were obtained in three treated groups wherein the combination therapy of P-DTX and P-CYP resulted in a significant reduction in tumor growth rate and tumor size compared with the control group [Figure 2.6] In addition, the significantly low level of cellular proliferation and high level of apoptotic cells found in combination group demonstrated combined P-DTX and P-CYP reduces tumor growth synergistically [Figure 2.9, 2.10 and 2.11]. Furthermore, our formulation carrying P-DTX and P-CYP conjugate micelles were well tolerated as the vital organs such as livers, spleens, kidneys and hearts did not show any histological changes after treatments **[Figure 2.8**]. The tumor tissues of mice treated with combination therapy were loosened epithelial cells aggregate with a high amount of interspersed mesenchymal cells, whereas compact epithelial cells were seen in the control group. Ki-67 is a specific nuclear protein for cancer cell proliferation. Since the overexpression of this protein is linked to high cancer cell proliferation with low survival of the patients in many kinds of malignancies such as brain cancer [225]. A low expression of Ki-67 was seen in mice treated with a mixture of P-CYP and P-DTX mice, indicating low tumor cell proliferation. Cleaved caspase 3 is a hallmark of programmed cell death. The expression of this protein after immunostaining was higher in-group treated with combination of P-CYP and P-DTX micelles compared to other groups. Masson's trichome staining method was used to test where this combination has better effect on reducing ECM deposition. Mice treated with the mixture of P-CYP and P-DTX micelles had lowest Masson's trichome staining compared to either control or monotherapies groups. This finding supports that using combination of P-CYP and P-DTX micelles deceases the stress

in the cancer microenvironment because of reducing the ECM deposition. Moreover, measurement of E-cadherin expression of the mice treated with the combination therapy showed significant enhancement in the expression that explain metastasis to the liver is low compared to other treated groups. High expression of ZEB-1 was observed in mice treated with combination of P-CYP and P-DTX micelles compared to either control group or their monotherapies. The number of apoptotic cells were seen very high in mice treated with the combination of P-CYP and P-DTX micelles, whereas these cells were found to be in small number in the control group or monotherapies group. Thus, the possibility to reduce the proliferation and increase the apoptosis of cancer cells *in vitro* and *in vivo* by using the combination therapy of P-CYP and P-DTX micelles may be a potential advantage to improve chemotherapy outcomes.

We recently reported higher drug loading and prolonged drug release of P-CYP and P-PTX conjugate micelles than physically drug encapsulated micelles [218]. In the present study, we replaced PTX with DTX, since DTX is more potent than PTX [226]. Using CYP as an Hh signaling pathway inhibitor in combination with DTX as a microtubule stabilizer has the potential to chemosensitize resistant cells and improve the efficacy of DTX by targeting both desmoplastic cells and bulk tumor cells. In our recent study, CYP and paclitaxel were conjugated as well as dodecanol to mPEG-b-PCC, and drug release was in sustained manner. Furthermore, drug loading of PTX and CYP was high and there their release from the micelles was significantly prolonged, compared to physically drug encapsulated micelles [218]. Olive *et al.* showed that the inhibition of Hh signaling pathway using IPI-926 improved gemcitabine delivery to pancreatic cancer KPC mouse model [218]. Similarly, the Jiang group demonstrated that CYP disrupts the ECM and enhances the delivery and efficacy of nanoparticles in pancreatic cancer [41].

2.5 Conclusion

In conclusion, these studies show that P-CYP and P-DTX combination therapy has the potential to treat advanced pancreatic cancer associated with dense desmoplasia. Although tumor regression phenomenon could be achieved by the synergistic effect of CYP and DTX, the mechanistic regression pathway needs further investigation.

3 Chapter 3. Nanoparticulate Delivery of BRD4/PI3K Dual Inhibitor SF2523 for Pancreatic Cancer Treatment

3.1 Introduction

Delivering of hydrophobic chemotherapeutic agents is a severe issue in the treatment of the majority of solid tumors, especially pancreatic cancer (PC) because most of the drugs have a short half-life, drug resistance, and poor cellular uptake due to desmoplasia [227, 228]. All these factors require drug to be administered in high doses to be effective, which lead to unacceptable toxicity [229-231]. Moreover, low-water solubility is an issue and requires co-solvent such as *cremophor* (CrEL) and Tween 80 should be used in the formulations. However, including these co-solvents have their own complications. For instance, commonly administered co-solvents (e.g., *cremophor* and Tween 80) with paclitaxel (PTX) are known alter its pharmacokinetic profile and cause severe toxicity, including hypersensitivity reactions and peripheral neuropathies [232]. Therefore, non-toxic delivery means for lipophilic chemotherapies are urgently needed.

Further, the nature of PC makes the delivery of chemotherapeutic agents nearly impossible due to the excessive amount of stromal elements (i.e. extracellular matrix (ECM), fibronectin, and hyaluronans) [233]. Quiescent pancreatic stellate cells (PSCs) activated by growth factors (e.g.TGF-ß1 and PDGF) and pro-inflammatory cytokines (e.g. TNFα, IL1, and IL6), are the main source of desmoplasia in the PC [234, 235]. Desmoplasia ultimately leads to the hypovascular microenvironment and resist drug penetration into the tumor [236]. Moreover, desmoplasia has been shown to induce IFP in the tumor, which results in low chemotherapeutic uptake and vascular capillary collapse, and ultimately leads to ineffective chemotherapy. A high IFP leads to reducing molecular uptake of chemotherapies, and vascular capillaries collapse [237-240]. As a consequence of desmoplasia, a high IFP has a negative impact on efficacy chemotherapies due to a lower rate of chemotherapeutic agents' perfusion[241]. PI3K plays a vital role in the

desmoplastic formation through the interaction between mitogen and cholecystokinin and their receptor on stellate cells. This interaction leads to the activation of PI3K signaling pathway for regulating fibrosis and collagen production [242, 243]. The phosphoinositide 3-kinases (PI3K) signaling pathway is one of the main pathways that is involved in cancer growth and resistance. PI3K signaling pathway regulates different cellular responses such as cell proliferation, transformation, motility, and survival of PC cells [67, 68, 244].

Another implicated signaling pathway in PC is Bromodomain and extra-terminal (BET) motif proteins. BET has a critical role in regulating the transcription of genes that are involved in tumor growth and fibrosis [245-250]. BET proteins include BRD2, BRD3, BRD4, and BRDT that bind to acetylated lysine on histone tails and enhance gene transcriptions during RNA transcription of MYC proteins. It has been shown that using JQ1 as a selective inhibitor of BET protein was beneficial in the regression of solid tumors via decreasing oncogene c-MYC [246, 251-254]. Another group showed that BRD4 positively regulates collagen production in primary and immortalized PSCs [255]. Therefore, both PI3K and BRD4 signaling pathways are implicated in the failure of chemotherapies because they support tumor growth, desmoplasia formation, and IFP elevation.

SF2523, a small molecule, dual inhibits PI3K, and BRD4 [256]. It has been shown that SF2325 has a significant high level of inhibition to the PI3K and BRD4 pathways besides the low toxicity level to the host compared to the combination of the single PI3K inhibitor and BRD4 inhibitors [256]. Furthermore, SF2523 was shown to be more potent in inhibiting chondrosarcoma cells and prostate cells than the only BRD4 inhibitor JQ1[257, 258]; However, SF2523 is a hydrophobic drug that has shorter half-lives due metabolic instabilities [259].

Given the aforementioned limitations, delivering chemotherapeutic agents in polymeric nanoparticles (NP) has gained considerable attention for three reasons. NPs

protect drug molecules from drug metabolism and degradation in the blood [141]. NPs increase the circulation time of loaded drugs, which could subsequently improve drug penetration in the tumor and accumulation by the enhanced permeability and retention (EPR) effect [142, 144-146]. NPs provides low toxic profile due to the sustained release of drugs [141]. Therefore, we hypothesized that using NP to encapsulate SF2523 could increase its water solubility, half-life, and delivery to the tumor site.

Previously, we synthesized copolymer mPEG-b-P(CB-co-LA) that formed NPs to deliver several therapeutic agents for the treatment of metastatic melanoma, prostate cancer, and liver fibrosis [260-262] Recently, we have also shown that encapsulating LY293 or QW296 into the [mPEG-b-P(CB-co-LA)] as NP significantly inhibits proliferation and metastasis of melanoma in the lung metastasis mice model [262]. Therefore, we prepared SF2523 loaded mPEG-b-P(CB-co-LA) NPs and characterized in vitro. Finally, SF2523 NPs were injected into tail veins of mice bearing orthotopic pancreatic tumor to and compared its therapeutic efficacy in inhibiting tumor proliferation, reducing pancreatic desmoplasia, and lowering IFP compared to free SF2523.

3.2 Materials and methods
3.2.1 Materials

SF2523 was obtained from MedKoo Biosciences, Inc. (Morrisville, NC). Thiazolyl blue tetrazolium bromide was purchased from CHEM-IMPEX INT'L. (Wood Dale, IL). FxCycle™ PI/RNase staining solution and penicillin/streptomycin were obtained from Invitrogen (Waltham, MA). Human microsomes and Dulbecco's modified eagle medium (DMEM) were purchased from Gibco™ (Waltham, MA). β-nicotinamide adenine dinucleotide phosphate (NADPH), reduced form, tetra sodium salt trihydrate was purchased from RPI (Mt. Prospect, IL). Fetal bovine serum (FBS) was bought from Atlanta Biologicals (Flowery Branch, GA). The PI3-kinase primary antibody (sc-293115) and p-

AKT primary antibody were bought from Santa Cruz Biotechnology, Inc.(Dallas, TX). The c-MYC primary antibody was obtained from Proteintech (Manchester, UK). Collagen-1 (ab-34710), α-SMA (ab5694) and BDR4 (ab128874) primary antibodies were obtained Abcam (Cambridge, MA). Matrigel® matrix basement membrane was purchased from Corning (Chicago, IL). All other chemical reagents were of analytical grade and obtained from Sigma-Aldrich (St. Louis, MO).

3.2.2 Cell culture

The human pancreatic cancer cells MIA PaCa-2 and PANC-1 were purchased from the American Type Culture Collection (Manassas, VA). These cells were cultured in DMEM containing 10% FBS and 1% penicillin/streptomycin at 37°C in a humidified atmosphere containing 5% CO_2.

Human pancreatic stellate cells (PSCs), and stellate cell growth medium were purchased from iXcells Biotechnologies USA, Inc (San Diego, CA). Cells were cultured in stellate cell growth medium containing 10% FBS and 1% penicillin/streptomycin and incubated at 37°C in a humidified atmosphere containing 5% CO_2. The growth media were changed every two days.

3.2.3 SF2523 polymeric nanoparticle preparation

In this study, we used our previously synthesized copolymer mPEG-b-P(CB-co-LA) to prepare SF2523 nanoparticles (SF2325-NP) Polymer was characterized by ^{1}H NMR to confirm its successful synthesis [260-262]. NPs were formulated using oil/water (o/w) emulsification in the presence of 1% polyvinyl alcohol (PVA, emulsifier agent). Briefly, 10 mg of mPEG-b-P(CB-co-LA) and 0.5 mg of SF2523, which is equivalent to 5% theoretical drug loading, were solubilized in 1 mL of a solvent mixture composed of DCM and acetone (1:1). Then, 4 mL of 1% PVA solution was added to the mixture containing mPEG-b-P (CB-co-LA) and SF2523. A probe sonicator (Newtown, CT) was used to

perform to disperse NP at the following condition; amplitude 20W, pulse on and off time 5 sec, and the duration 5 min. Acetone and DCM were removed using a rotary evaporator. The aqueous formulation was centrifuged using Sorvall Legend X1 Centrifuge Thermo Fisher Scientific (Waltham, MA) for 10 min at 5000 rpm to remove unloaded SF2523. The supernatant was retaken and centrifuged at 24,000 rpm for 30 min to remove 1% of PVA.The sediments were washed with PBS three times, and re-disperse SF2523-NP in the desired volume.

3.2.4   Nanoparticle characterization

The particle size distributions of SF2523-NPs was determined using a Malvern Zetasizer Nano ZS90 (Worcestershire, UK). The mean particle size was determined at a scattering angle of 90, and particle size distribution is presented as the average ± S.D (n=3).

The actual drug loading (w/w) and encapsulation efficiency (EE) were determined using HPLC using the following conditions; λ_{max} 214 nm using a Inertsil ODS-3 C18 (250 mm × 4.6 mm, 5 µmm) column (temp 30 °C), mobile phase was mixture of acetonitrile (ACN) and water (70:30 v/v), injection volume of 20 µL, and flow rate of 1 mL/min. For determining SF2523 content, 100 µL of SF2523-NP solution was mix with 200 µL of ACN and mixture was bath sonicated for 5 min at RT followed by centrifugation for 5-10 min at 11,000 rpm. 200 µL of the supernatant was filtered through a 0.2 µm syringe filter (Acrodisc, Waters, USA) and injected to HPLC.

SF2523 release profile from the formulated nanoparticle was determined using a dialysis method, and concentration was determined by HPLC using method described above. In brief, SF2523-NPs (containing 500 µg equivalent of drug) was placed in a dialysis bag (1,000 MWCO) and suspended into 50 mL of the release medium (PBS, pH 7.4, 1% Tween 80). The study was performed in a closed chamber orbital shaker at 37°C,

with a rotation speed of 100 rpm. At regular time intervals (between 0 and 100h), 1 mL sample was taken and volume was replaced with fresh release medium. Each sample was mixed with 2 mL of ACN; then bath sonicated for 5 min at RT, centrifuged at 11,000 rpm for 5-10 min, filtered using 0.2µm filter, and analyzed with HPLC.

3.2.5 SF2523-NP half-life determination

We determined the effect of NP formulation on $t_{1/2}$ of SF2523 in presence of human liver microsomes SF2523 content in the samples was quantified using LC-MS/MS. The SF2523-free and SF2523-NP were incubated with the reaction media composed of human liver microsomes (HLM, 1 mg/mL), 40 mM $MgCl_2$, 1.0 mM NADPH, and phosphate buffer (100 mM, pH 7.4) to make the final concentration of 1 µM. The samples (100 µL) were taken at 0-60 min for SF2523-Free, and at 0-180 min for SF2523-NP. All samples were mixed with 300 ACN in a 1.5 mL centrifuge tube, centrifuged at 12,000 for 15 min. Then, 150 µL of the supernatant was filtered and transferred into HPLC via to be analyzed by LC-MS/MS. Based on the area under the curve, the percentage of SF2523 remaining was quantified each time points and transformed into natural log values(Y-axis) and plotted against time (X-axis).

3.2.6 Cell viability study

To determine the effect SF2523-Free and SF2523-NP on cell viability, MIA PaCa-2 cells or PANC-1 cells were seeded in a 96-well plate (4000 cells/well) and incubated for 24 h. The culture medium was replaced with 200 µL of growth medium containing either 2 µL of DMSO, 0.1, 1, 5, 10, 25, and 50 µM of SF2523-Free, or empty NP, 0.1, 1, 5, 10, 25, and 50 µM of SF2523-NP. The cell viability assays were performed in both cell lines at different time point 24, 48, and 72h. At each time point, 25µL of 5 mg/ml 3-(4,5-dimethyl-thiazol-2-yl)-2,5-diphenyl tetrazolium bromide (MTT) solution in PBS were added to cells. and incubated for 4 h at 37 °C. The growth media and MTT solution were aspirated after

centrifugation (1,500 rpm for 2 min) to help formazan crystal to sediment. The formazan crystals were solubilized in 100 µL of the DMSO. The formazan absorbance corresponding to viable cells was measured at 560 nm and subtracted from absorbance of cell debris at 630 nm. The cell viability of SF2523-Free and SF2523-NP at 48h was calculated based on the following equation.

$$Cell\ viability\ (\%) = \frac{absorbance\ of\ SF2523}{absorabnce\ of\ DMSO}\ x\ 100$$

The IC$_{50}$ for both SF2523-Free and SF2523-NP were plotted after transforming the concentration into log value for accurate IC$_{50}$.

3.2.7 Cellular uptake analysis

The cellular uptake efficiency study was determined using the flow cytometry [263]. In brief, MIA PaCa-2 cells (0.3 X 10^6) were seeded in 6-well plates and in incubated for 24h. Then, MIA PaCa-2 cells were treated with 2 mL of freshly prepared cultured medium containing coumarin-6, a free drug (coumarin-6-Free), and coumarin-6 loaded nanoparticles (coumarin-6-NP) equivalent to 30 µg/mL for both of them and incubated for 2 hours in incubator. As a negative control, cells were treated only culture media. After 2 hours, cells were washed three times with cold PBS, trypsinized, centrifuged at 1000 rpm for three mins, and rewashed once again before going to FACS analysis. The free particles and cell debris were excluded via setting the gate on the plot of the side-scattered light (SSC) versus forward-scattered light (FSC). A total of 10,000 events were analyzed. An increase of fluorescent intensity in cells treated with coumarin-6-Free and coumarin-6-NP compared to that in negative control was expressed as median fluorescence intensity compared to negative control.

3.2.8 Cell cycle analysis

To determine the effect SF2523-NP on cell cycle distribution, MIA PaCa-2 cells (3.5×10^5 cells/well) were plated in the 6-well plate for 24h with no FBS. Then, the cells were treated with empty NP, 5 µM SF2523-NP, and 10 µM SF2523-NP for 48h. Cells were trypsinized and fixed in ice-cold ethanol (70%) overnight. Cells were washed twice with ice-cold PBS, stained with FxCycle™ PI/RNase solution for 15 min at RT in the dark according to the manufacturer's protocol. Cell cycle distributions were assessed by a flow cytometer (BD FACS Calibur, NJ) with 10,000 fluorescent events per assessment.

3.2.9 Colony formation assay

To evaluate the ability of SF2523-NP to inhibit colony formation capability of MIA PaCa-2 cells, cells were plated in the 6-well plate (500 cells/well), and cultured for 24 h to adhere to the bottom of the plate. Next, the medium was replaced with the medium containing empty NP, 5 µM SF2523-NP, and 10 µM SF2523-NP in 2 mL then incubated for 14 days. A single colony consists of at least 50 cells, were fixed with 4% paraformaldehyde, washed with ice-cold PBS twice, stained with 0.5% crystal violet, and washed with ice-cold PBS thrice. Colonies were counted manually, averaged, and calculated the percentage of colonies with respect to the controlled group colonies as described previously[221].

3.2.10 In vivo evaluation of SF2523-NP in orthotopic pancreatic cancer-bearing NSG mice

All in vivo experiments were performed according to the NIH animal use regulations and protocol approved by the Institutional Animal Care and Use Committee (IACUC) at the University of Nebraska Medical Center (UNMC), Omaha, NE. The NSG mice (6-8 weeks old) were used to establish the desmoplastic orthotopic pancreatic tumor according to our established method [264]. In brief, stable luciferase expressing MIA Paca-2-GFP-luciferase positive cells and human pancreatic stellate cells (hPSCs) were mixed

at a 1:1 ratio in Matrigel (1:1 v/v, 50µL) and implanted into the dorsum of the pancreas using PBS. The tumor growth was monitored via bioluminescence measurement using IVIS. Briefly, D-luciferin (150 mg/kg) was injected in the peritoneum cavity of the mice, and then an IVIS imaging machine (Caliper Life Sciences, Waltham, MA) was used to quantify the intensity of bioluminescence. Once the intensity of the bioluminescence in tumors reached 1.5 X 10^7 p/s/cm^2/sr, mice were divided randomly into three groups, empty NP control, SF2523-Free, and SF2523-NP. Both SF2523-Free and SF2523-NP were administered as I.V. through tail vein injection. Each mouse received six doses, through two weeks (3 doses per week). The maximum volume of the injection was 200 µL. SF2523-Free group was injected with SF2523 at the dose of 30 mg/kg dissolved in 35% of co-solvent (30% Cremophor® EL, 20% ethanol & 50% propylene glycol) in addition to 65% of dextrose solution. SF2523-NP group was injected 30 mg/kg equivalent to free drug. The bioluminescent intensity and mice's body weight were monitored every other day after start of the treatments. At day 30, the terminal experiment was performed to measure the interstitial fluid pressure (IFP). Then, mice were sacrificed, tumor and other vital organs such as liver, spleen, kidney, and heart were collected for other experiments.

3.2.11 Interstitial fluid pressure (IFP) measurement

IFP was measured on the last day of the experiment using a Millar Mikro-Tip® pressure catheter transducer (SPR-1000, 0.33 mm diameter) with a dynamic pressure range from −50 to 300 mmHg, possessing a shielded side-mounted sensor. The catheter was linked to the pressure control unit (PCU-2000), and ADInstruments PowerLab® data acquisition system (Millar Instruments, Inc.) [237, 265, 266]. LabChart software was used to record and analyze the data. Before each measurement, the recording system was calibrated to 0, 25, and 100 mmHg according to manufacture's protocol. In brief, All mice were anesthetized by using Isoflurane, and then the abdominal cut was performed to make the pancreas ready for measuring the IFP. The 25 gauge needle with around double the

diameter of the probe, was introduced first into the pancreatic tumor. Thereafter, the probe was inserted into the same space after removing the needle.

3.2.12 Immunohistochemical assay

After collecting the tumor and other vital tissues, a small piece from each tissue was taken and fixed with 10% buffered formalin for 24 h. All tissues were embedded in the paraffin. A thin section (4 µm) of each tissue was sliced to perform immunohistochemical experiments; histology (hematoxylin and eosin, H&E) apoptotic cells (cleaved caspase 3) (1:200 dilution), and proliferative cells (Ki-67) (1:200 dilution). Moreover, immunohistochemistry staining was used to test the effect of SF2523-Free and SF2523-NP on its target proteins, including BDR4 (1:50 dilution), c-MYC (1:100 dilution), PI3K (1:100 dilution), p-AKT (1:500 dilution), α-SMA (1:500 dilution), collagen-1 (1:500 dilution), HIF-1α (1:100 dilution). The signals were quantified using Definiens Tissue Studio dual software.

3.2.13 Statistical analysis

Data were represented as average ± S.D. (n=3) Two-tailed Student's t-test was utilized for comparison between two groups. *P <0.05 and #P <0.01 were considered as statistical significance.

3.3 Results
3.3.1 Preparation and characterization of SF2523-NP

The polymer used for preparing NPs was mPEG-b-P(CB-co-LA). This polymer was synthesized and characterized according to previously reported methods [260-262]. NPs were successfully prepared by emulsion solvent evaporation method [267]. The encapsulation efficiency (EE) for 2.5%, 5%, and 7.5% of theoretical SF2523 loading was found to be 81 ± 9.4, 82.15 ± 3.8 and 60.41 ± 4.38, respectively **[Table 3.1].** The average particle size of SF2523-NP was 162.1 ± 10.3 nm based on DLS characterization **[Figure**

3.1A]. The in vitro drug release was sustained and only 63 ± 12.3 % of SF2523 was release over 96 hours at 7.4 pH, **as shown in figure 3.1B**.

3.3.2   SF2523-NP microsomal stability and half-life determination

To determine the effect of SF2523-NP on its metabolic stability, SF2523-Free and SF2523-NP were incubated in HLM for up to 180 min. The amount of SF2523 depleted after 60 min incubation in HLM was 4.5% for SF2523-Free versus 36.6% for SF2523-NP as determined by LC-MS/MS **[Figure 3.2A].** Under the same condition, the metabolic rate constant was 0.0504 fraction/ min for SF253-DMSO; however; It was 0.0105 fractions/min for SF2523-NP. The half-life of SF2523-Free was 14 min, whereas it was 67 min SF2523-NP **[Figure 3.2B].**

3.3.3   SF2523-NP Inhibit the growth of pancreatic cancer cells in a dose-dependent manner

We determined the growth inhibitory activities of SF2523-Free and SF2523-NP in pancreatic cancer cell lines MIA PaCa-2 and PANC-1. A dose-response curve was determined after treating cells with SF2523-Free (0.1- 50 μM) or SF2523-NP (0.1, - 50 μM) for 48 h. Both SF2523-Free and SF2523-NP

Table 3.1 Determination of drug loading and encapsulation efficiency of SF2523-NP

Theoretical loading (%)	Encapsulation efficiency (%)
2.5	81 ± 9.4
5	82.15 ± 3.8
7.5	60.41 ± 4.38
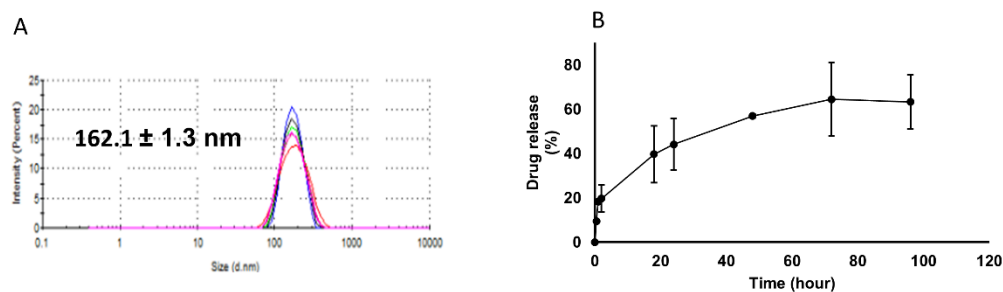
Figure 3.1 Polymeric nanoparticles characterization.

The particle size distribution of SF2523-NP was measured using dynamic light scattering (DLS), **(B)** the release of SF2523 from nanoparticles at pH7.4, The amount of released drug were quantified using HPLC after establishing standard curve for SF2523.

A

B

	SF2523- DMSO	SF2523-NP
Metabolic rate constant (-k)	0.0504 /min	0.0104 /min
Half-Life	14 min	67 min
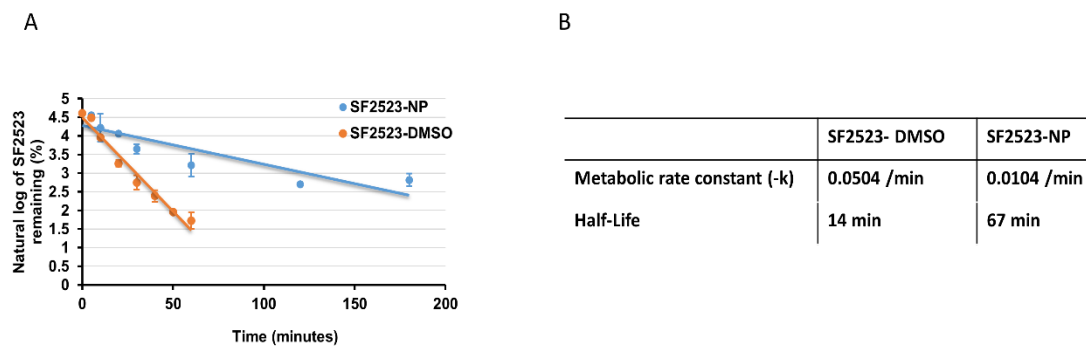
Figure 3.2Metabolic stability of SF2523-NP and SF2523-Free in human liver microsomes (HLM).

(A) Time-dependent depletion of SF2523 by NADH*-supplemented HLM. The data are expressed as percentage of SF2523 remaining at each time compared with time 0 min and represent the mean ± SD (n=3). **(B)** The metabolic rate constant (-k) and $t_{1/2}$ of SF2523-Free and SF2523-NP.

decreased the percentage of PC cell viability in a dose-dependent manner as shown in **figure 3.3 A&B.** However, SF2523-NPs showed significant higher cytotoxicity than free drugs in MIA PaCa-2 cells with IC_{50} of 5.22 µM Vs. 9.16 µM respectively in 48h. However, IC_{50} of SF2523-Free (4.9 µM) and SF2523 NPs (5.60 µM) were not significantly different in PANC-1 cells after 48h of treatment.

3.3.4   Coumarin-6-NP had high cellular uptake by MIA PaCa-2 cells.

To determine whether coumarin-6-NP or coumarin-6-Free have higher cellular uptake, the median fluorescent intensity was measured using flow cytometry. As shown in **figure 3.3C**, the median fluorescent intensity in coumarin-6-NP (2978 ± 61.54 MFI) was significantly higher than that of the coumarin-6-Free (1039.67 ± 60.93 MFI) treated group.

3.3.5   Treatment with SF2523-NP Enhances Cell Cycle Arrest at G_0/G_1 phase

The capability of SF2523-NP (5 µM & 10 µM) to cause cell cycle arrest was evaluated after treatment for 48h using Flow Cytometry. Treatment of MIA PaCa-2 cells with 5 µM SF2523-NP significantly increased the percentage of cells in G_0/G_1 from 55.71 ± 0.09% in empty-NP to 71.47 ± 0.27% and 10 µM SF2523-NP significantly increased the percentage of cells in G0/G1 from 55.71 ± 0.09% in empty-NP to 75.69 ± 0.42% **[Figure 3.4].**

3.3.6   Treatment with SF2523-NP Decreases Colony Formation Ability of MIA PaCa-2 cells

The efficacy of 5 µM and 10 µM SF2523-NP to inhibit 50 singlet cells of MIA PaCa-2 from forming a single colony by coming close to each other was assessed by using colony formation assay. The number of colonies was evaluated via unaided eye right after staining with crystal violet (0.5%). SF2523-NP (5 µM) decreased the percentage of MIA PaCa-2 colonies to 49 ± 3.26%, and SF2523-NP (10 µM) reduced the percentage MIA PaCa-2 colonies to 34 ± 2.49% **[Figure 3.5].**
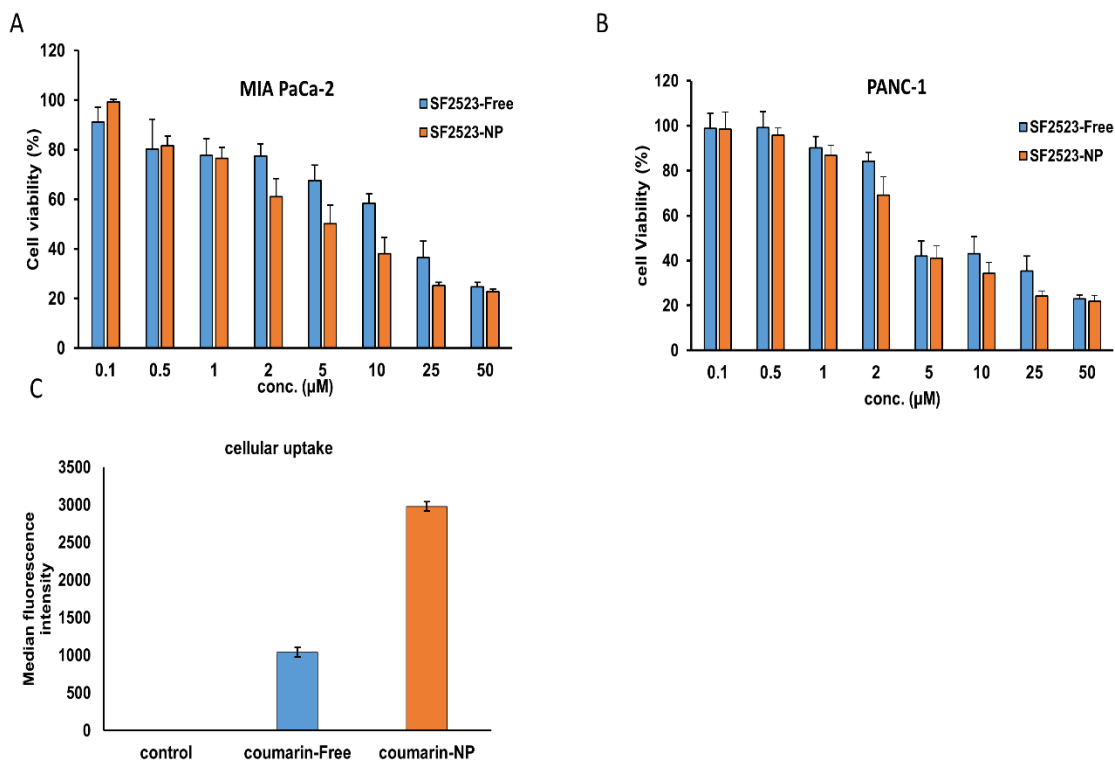
Figure 3.3 Effect of SF2523-Free or SF2523-NP on cell viability and cellular uptake.

(A&B) Cells viability assessment in MIA PaCa-2 or PANC-1 cells treated with SF2523-Free and SF2523-NP after 48h of treatment. All treatments were performed in triplicate (n=3), and data were presented as average ± S.D. (C) Intracellular uptake of analysis of coumarin-Free and coumarin-NP in MIA PaCa-2 cells through flow cytometry.
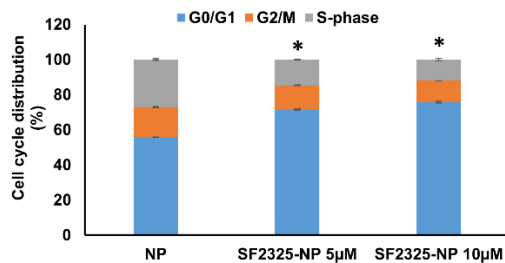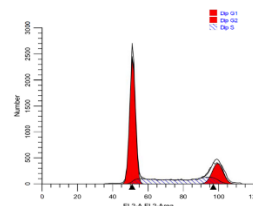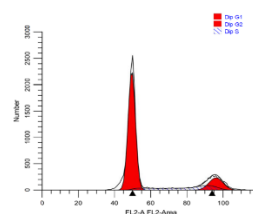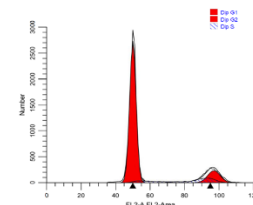
 Figure 3.4 The effect of SF2523-NP on cell cycle distribution.

Cell cycle distributions were analyzed by flow cytometry after staining with PI. All data were presented as the average ± S.D (n=3) (*) P<0.05.

3.3.7 SF2523-NP inhibits tumor growth in an orthotopic pancreatic cancer mouse model

To investigate the efficacy of SF2523-NP, an orthotopic pancreatic cancer mouse model was created via injecting MIA PaCa-2 cells expressing stable luciferase and human pancreatic stellate cells (hPSCs) in 1:1 ratio. When the tumor bioluminescence intensity reached 1.0×10^7 p/s/cm^2/sr. Mice were randomly divided into three groups, and injected the following different treatments: empty-NP, SF2523-Free, (30 mg/kg) or SF2523-NPs (30 mg/kg). All the formulations were administered intravenously through tail vein injection three times a week for two weeks. Both the treatments; SF2523-Free and SF2523-NP showed inhibition of tumor growth, however SF2523-NP showed higher tumor growth inhibition as determined by IVIS imaging [**Figure 3.6A**]. The quantitation the bioluminescence photon intensity readings values (p/s/cm^2/sr) of different mouse groups versus time (days) showed that SF2523-NP treated group had significantly low bioluminescence photon intensity value compared to control or SF2523-Free groups **[Figure 3.6B]** Accordingly, SF2523-NP treated group had the lowest tumor weight (0.30 ± 0.03 g) compared to control (1.42 ± 0.27 g) or SF2523-Free group (0.52 ± 0.09), and SF2523-NP treated group had the lowest tumor volume compared to either control or SF2523-Free groups **[Figure 3.6C- D].** The general toxicity of all formulations was assessed by monitoring mice's body weight during treatment. There was no more than 5% reduction in mice's body weight in control, SF2523-Free, and SF2523-NP compared mice's body weight before starting treatments **[Figure 3.7A].**
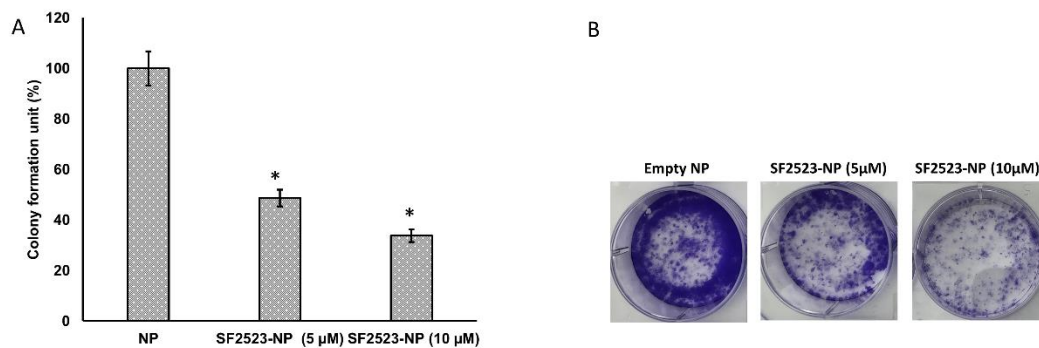
Figure 3.5 The potential of MIA PaCa-2 cell to form colonies after treating SF2523-NP (5 µM) and SF2523-NP (10 µM).

500 cells were plated in a 6-well plate for 24h. Then, empty NP 5 & 10 µM SF2523-NP were added for 14 days. The formed colonies were fixed, stained and counted **(A)**. Comparative analysis of colony formation percentages. This experiment was carried out in triplicate (n = 3). The data is presented as average ± S.D. **(B)** A representative pictures of empty-NP, SF2523-NP (5 µM) and SF2523-NP (10 µM) (*) $P<0.05$
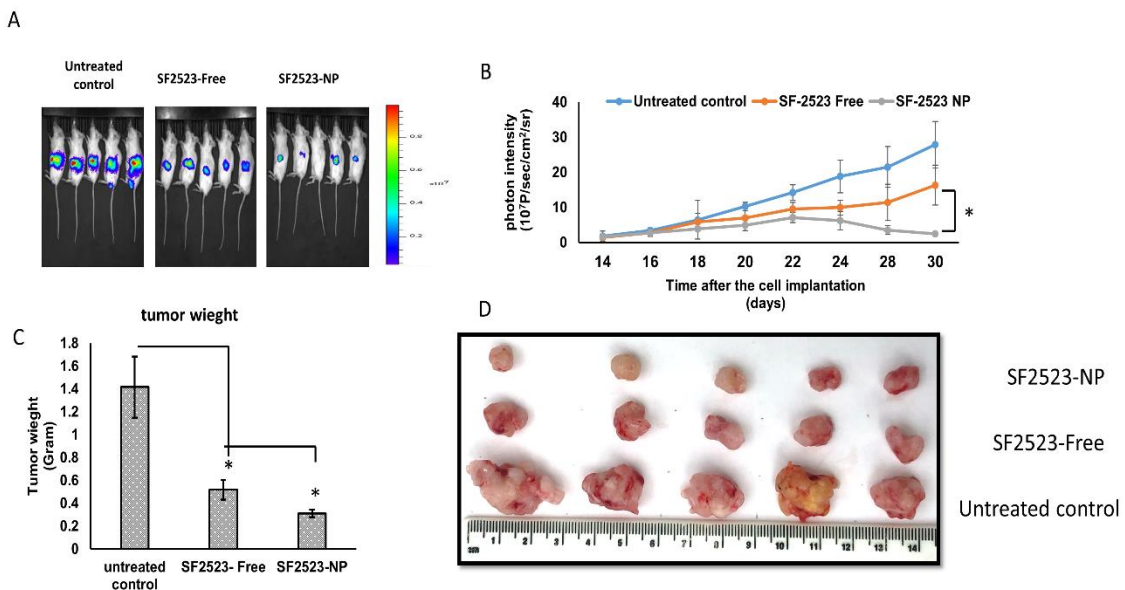
Figure 3.6 The therapeutic effect of SF2523-Free (30 mg/Kg) versus SF2523-NP (30 mg/Kg) in orthotopic pancreatic tumor-bearing NSG mice.

(A) A representative bioluminescence image at the end of the treatment. **(B)** Quantitation of photon intensity of tumor at different time points during treatment. **(C)** The tumor weight from different treatment groups. **(D)** An illustrative tumor picture from different groups. The data were represented as average ± S.D (n=5), *P < 0.05

3.3.8 SF2523-NP restores the IFP in an orthotopic pancreatic cancer mouse model

On the last day of in vivo experiments, and under anesthesia, mice in different groups were used to measure IFP. The IFP was significantly lower (50.60 ± 3.71 mmHg) in SF2523-NP treated mice compare to SF2523-Free treated mice (110.96 ± 38.05 mmHg). The control group had the highest IFP (132.84 ± 32.50 mmHg) among these **[Figure 3.7B].** Furthermore, there was no significant change in the histology of vital organs including the liver, spleen, heart, or kidney **[Figure 3.8].**

Immunohistochemistry experiments were further performed to evaluate the effect of SF2523-NP on cancer-related markers. SF253-NP significantly decreased the percent of Ki-67 positive cells (53.98 ± 9.57%) compare to either SF2523-Free (70.88 ± 6.33%) or control groups (74.69 ± 5.24) **[Figure 3.9].** The Ki-67 staining reflects that the SF2523-NP inhibited the cancer cell proliferation more effectively. Additionally, SF2523-NP significantly increased the percentage of the cleaved caspase-3 positive area (11.51 ± 2.82%) compared to for SF2523- Free (4.99 ± 1.19%) group, and (1.63 ± 0.39%) for the control group **[Figure 3.9].** The cleaved caspase-3 staining represents the apoptotic cells in the tumor tissue section.

A   B
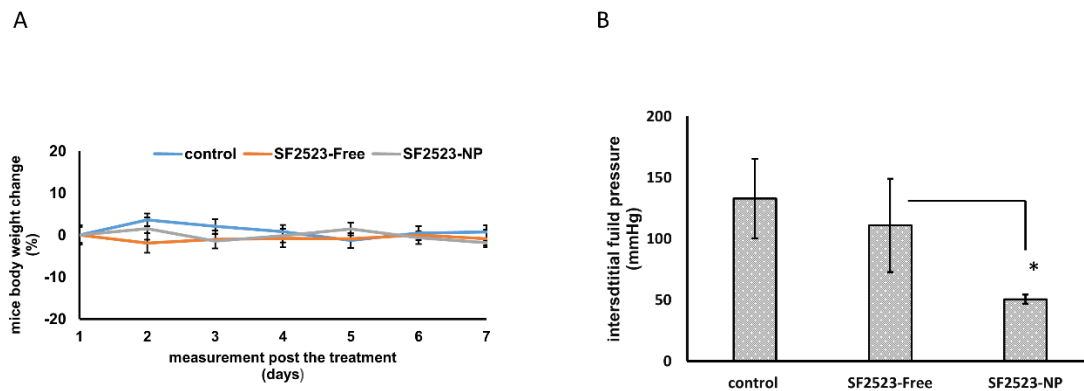
Figure 3.7 The body weight of mice were taken at the day of the first treatment and during the treatments and Interstitial fluid pressure measurement

Data were presented as the average ± S.D. Number of mice per group was 5 mice each group (n = 5, *P < 0.05) **(B)** Assessment of intra-tumoral interstitial fluid pressure (IFP). After the end of treatments, the IFP was measured using a Millar Mikro-Tip® pressure catheter transducer (SPR-1000, 0.33 mm diameter) with a dynamic pressure range from −50 to 300 mmHg. SF2523-NP treatment significantly reduced the IFP compared to SF-2523-Free treatment.(*P < 0.05, n=5)
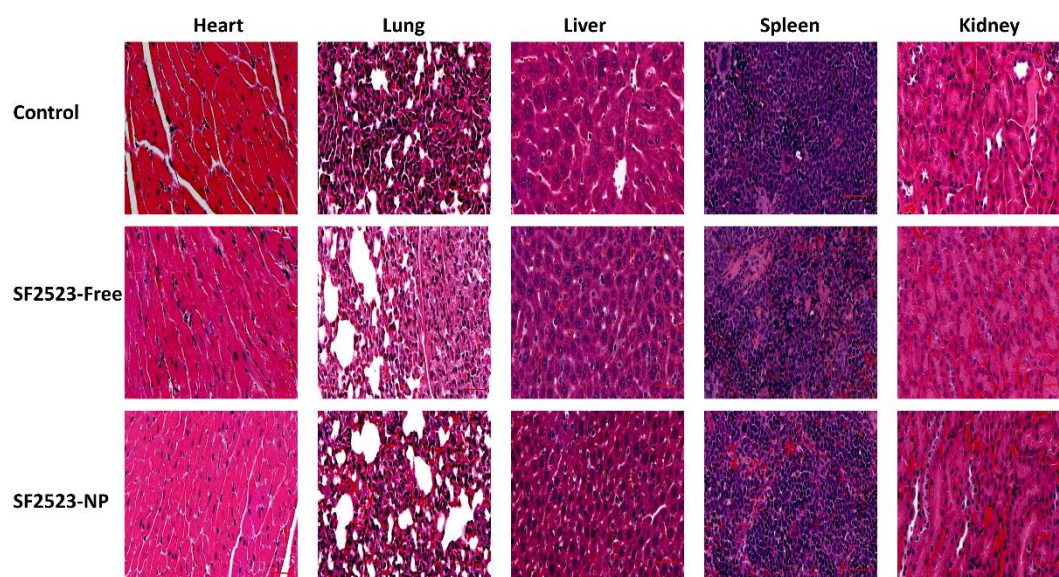
Figure 3.8 In vivo SF2523-NP toxicity assessment

The H&E staining of vital organs, such as heart, lung, liver, spleen, and kidney after treatment with empty-NP, SF2523-Free and SF2523-NP.Scale bar 50 µM.
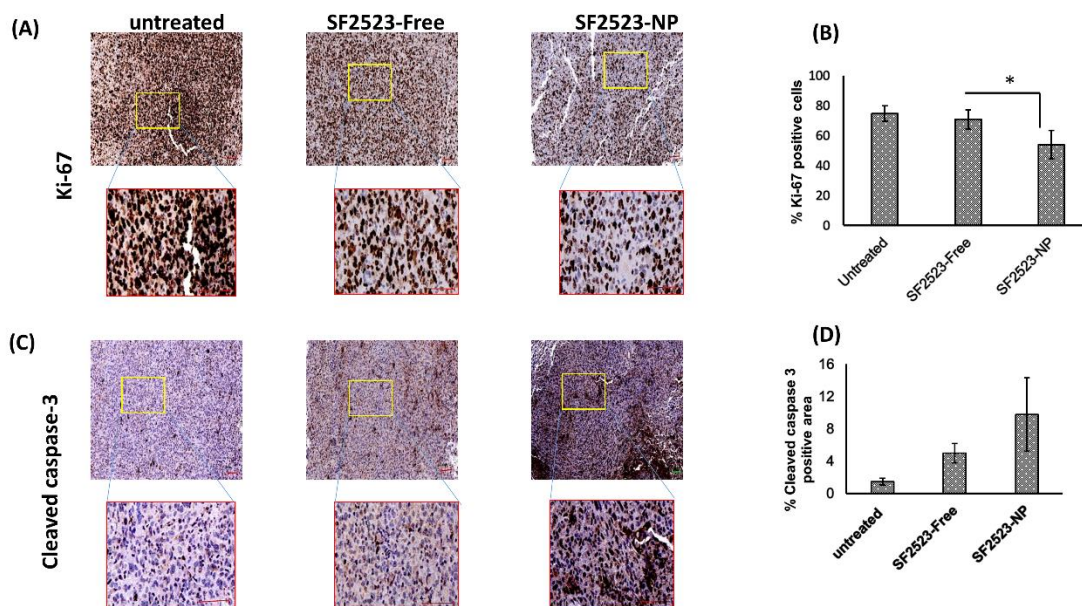
Figure 3.9 Immunohistochemical staining of tumor sections for proliferation and apoptotic markers.

(A) Stains of tumor sections for the cell proliferation marker Ki-67. **(B)** Quantification of Ki-67-positive cells in the tumor sections. **(C)** Stains of tumor sections for cleaved caspase-3. **(D)** Quantification of the cleaved caspase-3-positive area in the tumor sections. The representative images were taken at 10X magnification and 40X for image with the red edges. (*) $P < 0.05$

To assess whether SF2523-NP has an inhibitory effect on BDR4/Pi3K pathways, tumor tissue sections were immunostained for the respective proteins including BDR4, c-MYC, PI3K, and p–AKT. SF2523-NP significantly reduced the percentage of BDR4 positive cells (25.0 ± 5.0%) more than SF2523-Free (36.86 ± 3.0%), or control group (43.17 ± 5.0%), and significantly decreased the percentage of c-MYC positive cells (41.42 ± 3.85%) whereas the percentage of c-MYC positive cell was 49.36 ± 2.53% in SF2523-Free group and 63.79 ± 10.84% in control group **[Figure 3.10]**. Moreover, SF2523-NP showed a greater reduction of percentage of PI3K positive (9.21 ± 1.21%) and p-AKT (8.16 ± 1.25%) either compare to SF2523-Free group (26.63 ± 3.42% for Pi3K and 14.41 ± 4.71%) or control group (28.78 ± 6.73% for Pi3K and 19.63 ± 3.07% for p-AKT) **[Figure 3.11]**.

In addition, desmoplasia markers including α-SMA and Collagen-1 were immunostained with the respected primary antibodies, and it was found that SF2523-NP reduced the percentage of α-SMA positive area (26.96 ± 1.31%); compared to (34.91 ± 1.95%) for SF2523-Free group and (41.53 ± 2.97%) for control group **[Figure 3.12]** SF2523-NP decreased the percentage of the collagen-1 positive area (6.51 ± 0.92%) whereas in SF2523-Free or control groups the percentage of the collagen-1 positive was (8.55 ± 0.79%) and
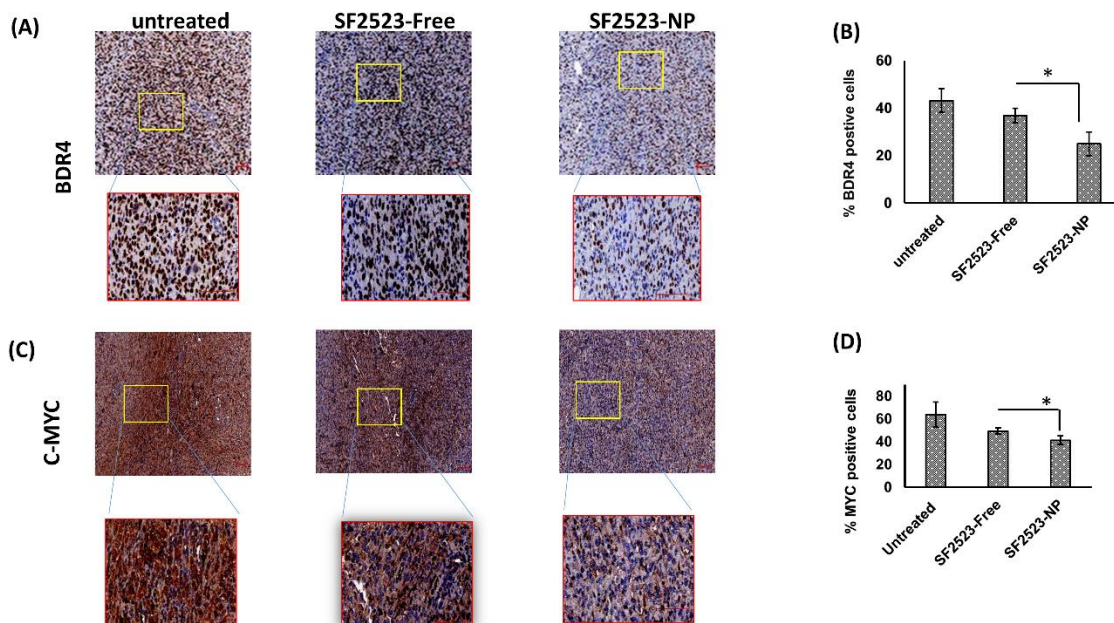
Figure 3.10 Immunohistochemical staining of tumor sections for BDR4 and c-MYC proteins marker.

(A) Stains of tumor sections for the BDR4 proteins marker. **(B)** Quantification of BDR4 positive cells in the tumor sections. **(C)** Stains of tumor sections c-MYC proteins marker. **(D)** Quantification of c-MYC positive cells in the tumor sections. The representative images were taken at 10X magnification and 40X for image with the red edges. All sections were quantified using Definiens Tissue Studio software. (*) $P < 0.05$
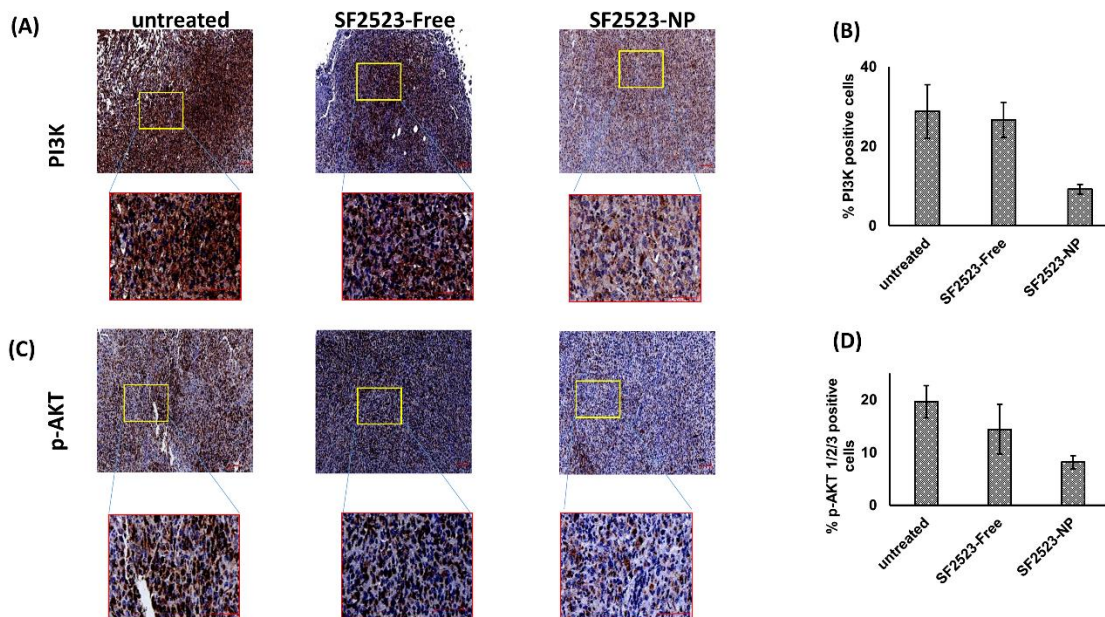
Figure 3.11 Immunohistochemical staining of tumor sections for PI3K and P-AKT proteins marker.

(A) Stains of tumor sections for the PI3Kproteins marker. **(B)** Quantification of PI3K positive cells in the tumor sections. **(C)** Stains of tumor sections p-AKT proteins marker.

(D) Quantification of pAKT positive cells in the tumor sections. The representative images were taken at 10X magnification and 40X for image with the red edges. All sections were quantified using Definiens Tissue Studio software. (*) $P < 0.05$
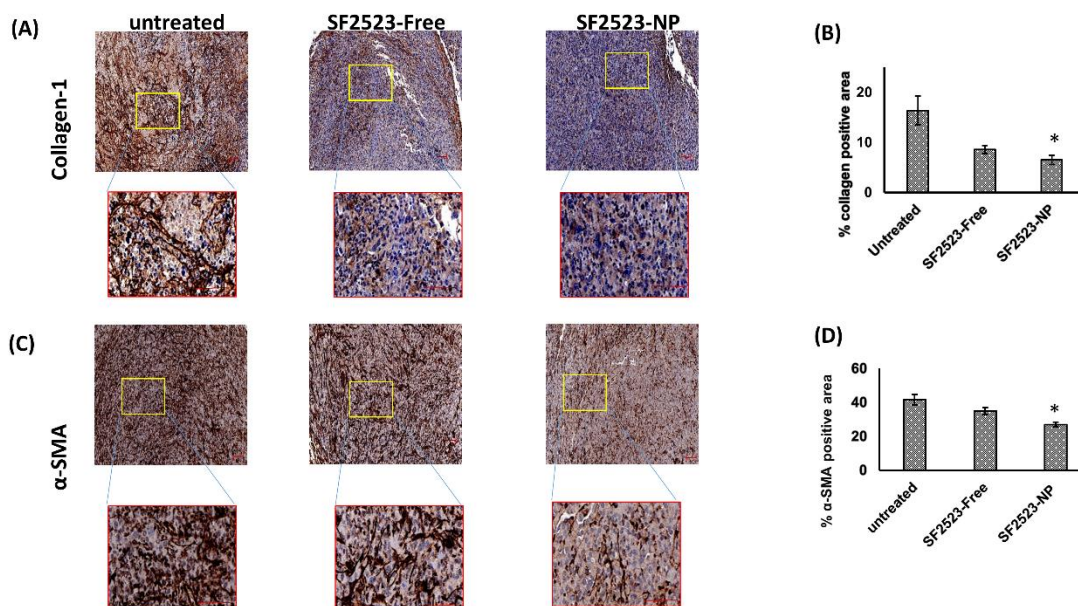
Figure 3.12 Immunohistochemical staining of tumor sections for Collagen-1 and α-SMA marker.

(A) Stains of tumor sections for desmoplasia marker collagen-1. **(B)** Quantification of collagen-1 positive area in the tumor sections. **(C)** Stains of tumor sections α-SMA marker. **(D)** Quantification of the α-SMA positive area in the tumor sections. The representative images were taken at 10X magnification and 40X for image with the red edges. All sections were quantified using Definiens Tissue Studio software. (*) $P < 0.05$

(16.34.82 ± 2.89%), respectively **[Figure 3.12]** . Moreover, The percentage of HIF-1a positive cells was significantly the lowest in SF2523-NP group (22.35 ± 6.05%) either compared to SF2523-Free group (36.38 ± 3.61%) or control group (39.88 ± 2.58%) **[Figure 3.13].**

3.4   Discussion

PC is a lethal malignancy with a 5-year survival rate of less than 8-10%, and survival time no more than six months [268, 269]. The absence of specific indications and symptoms similarities with other pancreatic diseases makes early diagnosis nearly impossible [270]. Many factors including genetic alterations, desmoplasia formation, and high interstitial fluid pressure lead to poor prognosis of PC patients. Another issue with PC treatments is ineffective drug delivery due to the short half-life of small drugs, low-water solubility, low drug penetration, and antagonistic effect of extensive co-solvents [271]. Both PI3K and BDR4 promote PC cell proliferation, regulate anti-apoptotic proteins, support the formation of desmoplasia that ultimately leads to elevate the IFP of tumor and treatment failure. Furthermore, It has been shown that c-MYC, which is downstream signal in BDR4 pathway, and PI3K are involved in development of chemoresistance [272-274]. Therefore, inhibiting these pathways using SF2523 a BDR4/PI3K inhibitor has the potential to improve efficacy through inhibiting tumor growth, reducing desmoplasia, and lowering IFP. However, SF2523 has low water-solubility, and short half-life, making it unfavorable for in vivo treatment. To improve these issues, NP approach is an excellent option because NP provides
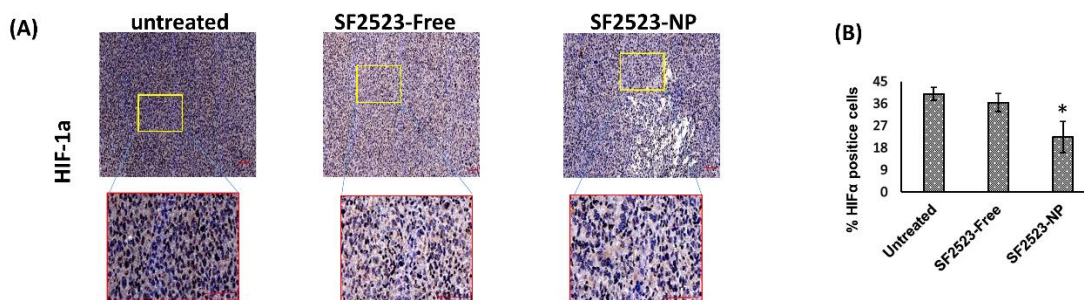
Figure 3.13 Immunohistochemical staining of tumor sections for HIF-1a marker

Stains of tumor sections for hypoxia marker HIF-1a. **(B)** Quantification of HIF-1 positive cells in the tumor sections. The representative images were taken at 10X magnification and 40X for the image with the red edges. All sections were quantified using Definiens Tissue Studio software. (*) P < 0.05

many advantages including protecting drug from metabolism and degradation, increasing water-solubility and circulation time of encapsulating drugs, improving drug delivery through enhanced permeability and retention (EPR) effect, providing better toxic profile compare to co-solvents such as CrEL.

In this study, our approach was to load SF2523 into NPs using mPEG-b-P(CB-co-LA) copolymer. This approach has two benefits. First, the NP formation allows to increase the SF2523 stability and to be delivered through intravenous injection. Seconds, the hydrophilic part of mPEG part of the polymer prevent aggregation of NPs, and reduce possible uptake by the reticuloendothelial system (RES), and thus increases their circulation times in the blood. We expected these attribution will ultimately contribute to enhance the therapeutic effect of SF2523-NP compared to SF2523 as a free drug . SF2523-NPs were stable at 25 $^{\circ}$C for one week with no precipitation of drug and no significant change in average particle size. These observations suggest that S2523-NP have a good stability profile at room temperature. NPs could load 5% w/w of drug with 82.15 ± 3.8 encapsulation efficiency and showed release of around 60% over three days [**Figure 3.1B**]. Moreover, NPs preserved loaded SF2523 from being metabolized by the liver enzyme and increased its half-life five folds as compared to SF2523 as free drug. . This finding are in line with reports from other groups. They have shown that polymeric NPs offered metabolic protection for lopinavir against liver microsomes [275]. SF2523-NP inhibited MIA PaCa-2 PANC-1 cell viability in dose-dependent manner and decreased the IC_{50} compared to SF253-Free. This could be due to the higher cellular uptake of SF2523-NP showed compared to SF2523-Free [**Figure 3.3C**] [275-277]. SF2523-NP showed significant increased cell cycle arrest at the G_0/G_1 phase. SF2523-NP significantly inhibited colony formation [Figure 3.4]. This result is in line with literature. Inhibition of BDR4/MYC pathway induce cell cycle arrest at G_0/G_1 phase, and suppress the colony

formation [278]. These in-vitro data suggested that SF2523-NP could be an attractive in vivo therapeutic approach.

In vivo efficacy assessment of SF2523-NP was evaluated in orthotopic desmoplastic pancreatic tumor-bearing mice. The model was generated by injecting a mixture of MIA PaCa-2-luc-GFP and PSC cells in the tip of pacrease in NSG mice. At the dose of 20 mg/kg, SF2523 was well tolerated by mice without any signs of toxicity (weight loss, activities, or eating/drinking habits). Mice treated with SF2523-NP showed a signification reduction in tumor size and tumor growth rate compared to either SF2523-Free or control groups [**Figure 3.6**].These promising findings could be explained by the significant drop in Ki-67 expression in mice treated SF2523-NP compared to mice treated with SF2523-Free [**Figure 3.9**]. The Ki-67 is involved in ribosomal RNA transcription and synthesis therapy. It is necessary for cellular proliferation and is also associated with a high survival rate of different kinds of tumors [225]. Moreover, we observed a significant increase in cleaved caspase-3 staining representing higher level of programmed cell death by apoptosis in tumor sections of mice treated with SF2523-NP compared to mice treated with SF2523- Free [**Figure 3.9**].

Further, the dual inhibitory effect of SF2523-NP on BDR4/PI3K pathway was determined using IHC staining. The significant reduction in the percentage of BDR4 and c-MYC positive cells was seen in tumor sections of mice treated with SF2523-NP compared to tumor section of mice treated with SF2523-Free [**Figure 3.10**]. There was a significant reduction in the percent of positive cells of PI3K and p-AKT in tumor section of mice treated with SF2523-NP compared to tumor section of mice treated with S2523-Free [**Figure 3.11**]. Moreover, the collagen-1 and α-SMA immunostaining experiments were performed to check where SF2523-NP has a superior effect on reducing desmoplasia component [**Figure 3.12**]. It has been reported that interaction between mitogen and

cholecystokinin and their receptor on PSC leads to the activation of PI3K signaling pathway that regulates fibrosis and collagen production[242]. Furthermore, another group showed that different BET proteins have different roles in collagen production; however, BRD4 positively regulates collagen production in primary and immortalized PSCs [255]

Additionally, it has been shown that desmoplasia plays a vital role in creating hypoxic microenvironment, which supports tumor progression, and limits chemotherapeutic agents delivery by activating the hypoxia-inducible factor-1a (HIF-1a) [279]. The percentage of HIF-1a positive cells in mice treated with SF2523-NP was significantly lower than other treated groups [**Figure 3.13**]. Many reports showed that pancreatic desmoplasia increases IFP therapy decreases the effectiveness of chemotherapies [241, 280-282]. Measurement of IFP of mice treated with SF2523-NP showed a significant reduction in the internal pressure of pancreas compared either SF2523-Free or control groups **[Figure 3.7B]**. These findings further highlight that SF2523-NP is more effective than other groups in decreasing desmoplasia component and IFP.

3.5 Conclusion

We have formulated SF2523, which is a dual inhibitor of BDR4/PI3K SF2523 polymeric NPs. These NPs successfully delivered SF2523 to tumor site through EPR effect and released in the sustained pattern, leading to high effect on inhibition of downstream pathway of BDR4/PI3K, reduction of desmoplasia component, and reduction of IFP. Therefore, SF2523-NP shows a high tumor inhibition compared to SF2523-Free. In future studies, SF2523-NP will be combined with other chemotherapies to improve their efficacy.

4   Chapter 4. Summary and Future Directions

4.1   Summary

The treatment of PDAC is still a challenge due to the difficulty of being diagnosed in the early stages and development of resistance to standard chemotherapies. Desmoplasia induces the chemoresistance in PDAC. There are many signaling pathways, which support and induce the formation desmoplasia. The Hh, PI3K, and BDR4 signaling pathways involved in supporting, developing desmoplasia, and pancreatic cancer progression. We used different strategies to overcome these challenges. In chapter one, The strategy was to combine to microtubules stabilizer (DTX) and Hh signaling pathway inhibitor (CYP) to overcome chemoresistance and improve the therapeutic effect. However, Both DTX and CYP are hydrophobic. Therefore, they need an appropriate delivery system to enhance their water solubilities, therapy improves therapeutic efficacy. Our approach was to synthesize PEG-based polymeric drug conjugate micelles. These polymeric-drug conjugate (P-DTX and P-CYP) can assemble into the micelles of less than 100 nm with drug loading more than 20% w/w. These combination micelles inhibited the tumor growth effectively when introduced into NSG mice bearing created orthotopically using MIA PaCa-2 cells compared to monotherapy micelles.

SF2523 is a dual inhibitor for PI3K/BDR4 pathways. These pathways play a crucial role in pancreatic cancer progression and resistance development by supporting pancreatic desmoplasia. The hydrophobicity of SF2523 had to use the toxic co-solvents to make it appropriate for systemic therapy. Our approach to improving the water solubility without using toxic co-solvents was to synthesize a biodegradable polymer with polyester and polycarbonate hydrophobic core. Methoxy polyethylene glycol-b-poly (carbonate-co-lactide) (mPEG-b-P(CB-co-LA)) was synthesized to encapsulate SF2523 in the polycarbonate hydrophobic core of the Biodegradable polymer. SF2523 was loading into the polymer using o/w emulsification method. Systemic administration of SF2523

encapsulated nanoparticles inhibited the tumor growth, decrease desmoplasia component, decrease the interstitial fluid pressure.

4.2 Future Directions

The findings presented in this dissertation showed that the combination therapy of tubulin stabilizer and Hh inhibitor has the potential to treat advanced pancreatic cancer associated with desmoplasia. The polymeric-drug conjugate micelles formulation can ensure the efficient delivery of hydrophobic anticancer agent (DTX&CYP). Therefore, the therapeutic efficacy would be improved compared to the parent drugs. However, different aspects could be used to further improve our delivery system. Our system relies on passive targeting, which is known as EPR phenomenon. This phenomenon is basically extravasation of nano-sized agents into tumor sites through damaged tumor vasculature; however, small portion of the drug could extravagate other organs (off targeting).

To further improve the current polymeric-drug conjugate platform, Attachment of targeting moiety such as G11 can decrease the off-targeting delivery and improve the delivery to the site of tumor. Moreover, the drug release profile is a limiting element for effective treatment. As next direction, we will fabricate the polymer with glutathione (GSH) responsive linker to be sensitive to the TME of PDAC.

Furthermore, we have shown that SF2523 that PI3K/BDR4 dual inhibitor had an excellent efficacy in a pancreatic cancer mouse model; however, the premature release of SF2523 might cause less tumor accumulation. In future studies, we plan to redesign polymers that have a function group, and synthesize drug analog with a functional group for conjugation that allows having high tumor accumulation and less toxic to other tissues after systemic administration

5   References

[1] R.L. Siegel, K.D. Miller, A. Jemal, Cancer statistics, 2016, CA Cancer. J. Clin. 66 (2016) 7-30.

[2] C.E. DeSantis, K.D. Miller, W. Dale, S.G. Mohile, H.J. Cohen, C.R. Leach, A. Goding Sauer, A. Jemal, R.L. Siegel, Cancer statistics for adults aged 85 years and older, 2019, CA Cancer. J. Clin. 69 (2019) 452-467.

[3] P. Rawla, T. Sunkara, V. Gaduputi, Epidemiology of Pancreatic Cancer: Global Trends, Etiology and Risk Factors, World J. Oncol. 10 (2019) 10-27.

[4] D.M. Parkin, L. Boyd, L.C. Walker, 16. The fraction of cancer attributable to lifestyle and environmental factors in the UK in 2010, Br. J. Cancer 105 Suppl 2 (2011) S77-81.

[5] W.C. Willett, Diet and cancer, Oncologist 5 (2000) 393-404.

[6] C. Bosetti, P. Bertuccio, E. Negri, C. La Vecchia, M.P. Zeegers, P. Boffetta, Pancreatic cancer: overview of descriptive epidemiology, Mol. Carcinog. 51 (2012) 3-13.

[7] P. Anand, A.B. Kunnumakkara, C. Sundaram, K.B. Harikumar, S.T. Tharakan, O.S. Lai, B. Sung, B.B. Aggarwal, Cancer is a preventable disease that requires major lifestyle changes, Pharm. Res. 25 (2008) 2097-2116.

[8] M. Ilic, I. Ilic, Epidemiology of pancreatic cancer, World J. Gastroenterol. 22 (2016) 9694-9705.

[9] J. Cicenas, K. Kvederaviciute, I. Meskinyte, E. Meskinyte-Kausiliene, A. Skeberdyte, J. Cicenas, KRAS, TP53, CDKN2A, SMAD4, BRCA1, and BRCA2 Mutations in Pancreatic Cancer, Cancers (Basel) 9 (2017) 10.3390/cancers9050042.

[10] V.T. Smit, A.J. Boot, A.M. Smits, G.J. Fleuren, C.J. Cornelisse, J.L. Bos, KRAS codon 12 mutations occur very frequently in pancreatic adenocarcinomas, Nucleic Acids Res. 16 (1988) 7773-7782.

[11] C. Caldas, S.A. Hahn, L.T. da Costa, M.S. Redston, M. Schutte, A.B. Seymour, C.L. Weinstein, R.H. Hruban, C.J. Yeo, S.E. Kern, Frequent somatic mutations and homozygous deletions of the p16 (MTS1) gene in pancreatic adenocarcinoma, Nat. Genet. 8 (1994) 27-32.

[12] M.S. Redston, C. Caldas, A.B. Seymour, R.H. Hruban, L. da Costa, C.J. Yeo, S.E. Kern, p53 mutations in pancreatic carcinoma and evidence of common involvement of homocopolymer tracts in DNA microdeletions, Cancer Res. 54 (1994) 3025-3033.

[13] M. Goggins, M. Schutte, J. Lu, C.A. Moskaluk, C.L. Weinstein, G.M. Petersen, C.J. Yeo, C.E. Jackson, H.T. Lynch, R.H. Hruban, S.E. Kern, Germline BRCA2 gene mutations in patients with apparently sporadic pancreatic carcinomas, Cancer Res. 56 (1996) 5360-5364.

[14] J. Carnevale, A. Ashworth, Assessing the Significance of BRCA1 and BRCA2 Mutations in Pancreatic Cancer, J. Clin. Oncol. 33 (2015) 3080-3081.

[15] J. Cicenas, L. Tamosaitis, K. Kvederaviciute, R. Tarvydas, G. Staniute, K. Kalyan, E. Meskinyte-Kausiliene, V. Stankevicius, M. Valius, KRAS, NRAS and BRAF mutations in colorectal cancer and melanoma, Med. Oncol. 34 (2017) 26-016-0879-9. Epub 2017 Jan 10.

[16] R. Marais, Y. Light, H.F. Paterson, C.J. Marshall, Ras recruits Raf-1 to the plasma membrane for activation by tyrosine phosphorylation, EMBO J. 14 (1995) 3136-3145.

[17] A. Gallo, C. Cuozzo, I. Esposito, M. Maggiolini, D. Bonofiglio, A. Vivacqua, M. Garramone, C. Weiss, D. Bohmann, A.M. Musti, Menin uncouples Elk-1, JunD and c-Jun phosphorylation from MAP kinase activation, Oncogene 21 (2002) 6434-6445.

[18] S. Bates, K.M. Ryan, A.C. Phillips, K.H. Vousden, Cell cycle arrest and DNA endoreduplication following p21Waf1/Cip1 expression, Oncogene 17 (1998) 1691-1703.

[19] R.F. Hwang, E.M. Gordon, W.F. Anderson, D. Parekh, Gene therapy for primary and metastatic pancreatic cancer with intraperitoneal retroviral vector bearing the wild-type p53 gene, Surgery 124 (1998) 143-50; discussion 150-1.

[20] S.E. Kern, J.A. Pietenpol, S. Thiagalingam, A. Seymour, K.W. Kinzler, B. Vogelstein, Oncogenic forms of p53 inhibit p53-regulated gene expression, Science 256 (1992) 827-830.

[21] J. Cicenas, K. Kvederaviciute, I. Meskinyte, E. Meskinyte-Kausiliene, A. Skeberdyte, J. Cicenas, KRAS, TP53, CDKN2A, SMAD4, BRCA1, and BRCA2 Mutations in Pancreatic Cancer, Cancers (Basel) 9 (2017) 10.3390/cancers9050042.

[22] M. Schutte, R.H. Hruban, J. Geradts, R. Maynard, W. Hilgers, S.K. Rabindran, C.A. Moskaluk, S.A. Hahn, I. Schwarte-Waldhoff, W. Schmiegel, S.B. Baylin, S.E. Kern, J.G. Herman, Abrogation of the Rb/p16 tumor-suppressive pathway in virtually all pancreatic carcinomas, Cancer Res. 57 (1997) 3126-3130.

[23] J.L. Dai, K.K. Turnacioglu, M. Schutte, A.Y. Sugar, S.E. Kern, Dpc4 transcriptional activation and dysfunction in cancer cells, Cancer Res. 58 (1998) 4592-4597.

[24] D. Cao, R. Ashfaq, M.G. Goggins, R.H. Hruban, S.E. Kern, C.A. Iacobuzio-Donahue, Differential expression of multiple genes in association with MADH4/DPC4/SMAD4 inactivation in pancreatic cancer, Int. J. Clin. Exp. Pathol. 1 (2008) 510-517.

[25] K. De Bosscher, C.S. Hill, F.J. Nicolas, Molecular and functional consequences of Smad4 C-terminal missense mutations in colorectal tumour cells, Biochem. J. 379 (2004) 209-216.

[26] A. Blackford, O.K. Serrano, C.L. Wolfgang, G. Parmigiani, S. Jones, X. Zhang, D.W. Parsons, J.C. Lin, R.J. Leary, J.R. Eshleman, M. Goggins, E.M. Jaffee, C.A. Iacobuzio-Donahue, A. Maitra, J.L. Cameron, K. Olino, R. Schulick, J. Winter, J.M. Herman, D. Laheru, A.P. Klein, B. Vogelstein, K.W. Kinzler, V.E. Velculescu, R.H. Hruban, SMAD4 gene mutations are associated with poor prognosis in pancreatic cancer, Clin. Cancer Res. 15 (2009) 4674-4679.

[27] P. Singh, R. Srinivasan, J.D. Wig, SMAD4 genetic alterations predict a worse prognosis in patients with pancreatic ductal adenocarcinoma, Pancreas 41 (2012) 541-546.

[28] S.J. Boulton, BRCA1-mediated ubiquitylation, Cell. Cycle 5 (2006) 1481-1486.

[29] C.X. Deng, R.H. Wang, Roles of BRCA1 in DNA damage repair: a link between development and cancer, Hum. Mol. Genet. 12 Spec No 1 (2003) R113-23.

[30] Z.K. Stadler, E. Salo-Mullen, S.M. Patil, M.C. Pietanza, J. Vijai, E. Saloustros, N.A. Hansen, N.D. Kauff, R.C. Kurtz, D.P. Kelsen, K. Offit, M.E. Robson, Prevalence of BRCA1 and BRCA2 mutations in Ashkenazi Jewish families with breast and pancreatic cancer, Cancer 118 (2012) 493-499.

[31] T.M. Rudkin, W.D. Foulkes, BRCA2: breaks, mistakes and failed separations, Trends Mol. Med. 11 (2005) 145-148.

[32] B. Friedenson, BRCA1 and BRCA2 pathways and the risk of cancers other than breast or ovarian, MedGenMed 7 (2005) 60.

[33] P.L. Welcsh, M.C. King, BRCA1 and BRCA2 and the genetics of breast and ovarian cancer, Hum. Mol. Genet. 10 (2001) 705-713.

[34] S. Jones, X. Zhang, D.W. Parsons, J.C. Lin, R.J. Leary, P. Angenendt, P. Mankoo, H. Carter, H. Kamiyama, A. Jimeno, S.M. Hong, B. Fu, M.T. Lin, E.S. Calhoun, M. Kamiyama, K. Walter, T. Nikolskaya, Y. Nikolsky, J. Hartigan, D.R. Smith, M. Hidalgo, S.D. Leach, A.P. Klein, E.M. Jaffee, M. Goggins, A. Maitra, C. Iacobuzio-Donahue, J.R. Eshleman, S.E. Kern, R.H. Hruban, R. Karchin, N. Papadopoulos, G. Parmigiani, B. Vogelstein, V.E. Velculescu, K.W. Kinzler, Core signaling pathways in human pancreatic cancers revealed by global genomic analyses, Science 321 (2008) 1801-1806.

[35] S.P. Thayer, M.P. di Magliano, P.W. Heiser, C.M. Nielsen, D.J. Roberts, G.Y. Lauwers, Y.P. Qi, S. Gysin, C. Fernandez-del Castillo, V. Yajnik, B. Antoniu, M. McMahon, A.L. Warshaw, M. Hebrok, Hedgehog is an early and late mediator of pancreatic cancer tumorigenesis, Nature 425 (2003) 851-856.

[36] D.M. Berman, S.S. Karhadkar, A. Maitra, R. Montes De Oca, M.R. Gerstenblith, K. Briggs, A.R. Parker, Y. Shimada, J.R. Eshleman, D.N. Watkins, P.A. Beachy, Widespread requirement for Hedgehog ligand stimulation in growth of digestive tract tumours, Nature 425 (2003) 846-851.

[37] R.L. Yauch, S.E. Gould, S.J. Scales, T. Tang, H. Tian, C.P. Ahn, D. Marshall, L. Fu, T. Januario, D. Kallop, M. Nannini-Pepe, K. Kotkow, J.C. Marsters, L.L. Rubin, F.J. de Sauvage, A paracrine requirement for hedgehog signalling in cancer, Nature 455 (2008) 406-410.

[38] H. Tian, C.A. Callahan, K.J. DuPree, W.C. Darbonne, C.P. Ahn, S.J. Scales, F.J. de Sauvage, Hedgehog signaling is restricted to the stromal compartment during pancreatic carcinogenesis, Proc. Natl. Acad. Sci. U. S. A. 106 (2009) 4254-4259.

[39] J.M. Bailey, B.J. Swanson, T. Hamada, J.P. Eggers, P.K. Singh, T. Caffery, M.M. Ouellette, M.A. Hollingsworth, Sonic hedgehog promotes desmoplasia in pancreatic cancer, Clin. Cancer Res. 14 (2008) 5995-6004.

[40] K. Walter, N. Omura, S.M. Hong, M. Griffith, A. Vincent, M. Borges, M. Goggins, Overexpression of smoothened activates the sonic hedgehog signaling pathway in pancreatic cancer-associated fibroblasts, Clin. Cancer Res. 16 (2010) 1781-1789.

[41] K.P. Olive, M.A. Jacobetz, C.J. Davidson, A. Gopinathan, D. McIntyre, D. Honess, B. Madhu, M.A. Goldgraben, M.E. Caldwell, D. Allard, K.K. Frese, G. Denicola, C. Feig, C. Combs, S.P. Winter, H. Ireland-Zecchini, S. Reichelt, W.J. Howat, A. Chang, M. Dhara, L. Wang, F. Ruckert, R. Grutzmann, C. Pilarsky, K. Izeradjene, S.R. Hingorani, P. Huang, S.E. Davies, W. Plunkett, M. Egorin, R.H. Hruban, N. Whitebread, K. McGovern, J. Adams, C. Iacobuzio-Donahue, J. Griffiths, D.A. Tuveson, Inhibition of Hedgehog signaling enhances delivery of chemotherapy in a mouse model of pancreatic cancer, Science 324 (2009) 1457-1461.

[42] A. Apelqvist, H. Li, L. Sommer, P. Beatus, D.J. Anderson, T. Honjo, M. Hrabe de Angelis, U. Lendahl, H. Edlund, Notch signalling controls pancreatic cell differentiation, Nature 400 (1999) 877-881.

[43] Y. Miyamoto, A. Maitra, B. Ghosh, U. Zechner, P. Argani, C.A. Iacobuzio-Donahue, V. Sriuranpong, T. Iso, I.M. Meszoely, M.S. Wolfe, R.H. Hruban, D.W. Ball, R.M. Schmid, S.D. Leach, Notch mediates TGF alpha-induced changes in epithelial differentiation during pancreatic tumorigenesis, Cancer. Cell. 3 (2003) 565-576.

[44] M.E. Mullendore, J.B. Koorstra, Y.M. Li, G.J. Offerhaus, X. Fan, C.M. Henderson, W. Matsui, C.G. Eberhart, A. Maitra, G. Feldmann, Ligand-dependent Notch signaling is involved in tumor initiation and tumor maintenance in pancreatic cancer, Clin. Cancer Res. 15 (2009) 2291-2301.

[45] P.K. Mazur, H. Einwachter, M. Lee, B. Sipos, H. Nakhai, R. Rad, U. Zimber-Strobl, L.J. Strobl, F. Radtke, G. Kloppel, R.M. Schmid, J.T. Siveke, Notch2 is required for progression of pancreatic intraepithelial neoplasia and development of pancreatic ductal adenocarcinoma, Proc. Natl. Acad. Sci. U. S. A. 107 (2010) 13438-13443.

[46] R. Plentz, J.S. Park, A.D. Rhim, D. Abravanel, A.F. Hezel, S.V. Sharma, S. Gurumurthy, V. Deshpande, C. Kenific, J. Settleman, P.K. Majumder, B.Z. Stanger, N. Bardeesy, Inhibition of gamma-secretase activity inhibits tumor progression in a mouse model of pancreatic ductal adenocarcinoma, Gastroenterology 136 (2009) 1741-9.e6.

[47] G. Zeng, M. Germinaro, A. Micsenyi, N.K. Monga, A. Bell, A. Sood, V. Malhotra, N. Sood, V. Midda, D.K. Monga, D.M. Kokkinakis, S.P. Monga, Aberrant Wnt/beta-catenin signaling in pancreatic adenocarcinoma, Neoplasia 8 (2006) 279-289.

[48] M. Pasca di Magliano, A.V. Biankin, P.W. Heiser, D.A. Cano, P.J. Gutierrez, T. Deramaudt, D. Segara, A.C. Dawson, J.G. Kench, S.M. Henshall, R.L. Sutherland, A. Dlugosz, A.K. Rustgi, M. Hebrok, Common activation of canonical Wnt signaling in pancreatic adenocarcinoma, PLoS One 2 (2007) e1155.

[49] Z. Zhang, B. Rigas, NF-kappaB, inflammation and pancreatic carcinogenesis: NF-kappaB as a chemoprevention target (review), Int. J. Oncol. 29 (2006) 185-192.

[50] D. Malka, P. Hammel, F. Maire, P. Rufat, I. Madeira, F. Pessione, P. Levy, P. Ruszniewski, Risk of pancreatic adenocarcinoma in chronic pancreatitis, Gut 51 (2002) 849-852.

[51] W. Wang, J.L. Abbruzzese, D.B. Evans, L. Larry, K.R. Cleary, P.J. Chiao, The nuclear factor-kappa B RelA transcription factor is constitutively activated in human pancreatic adenocarcinoma cells, Clin. Cancer Res. 5 (1999) 119-127.

[52] N.M. Chandler, J.J. Canete, M.P. Callery, Increased expression of NF-kappa B subunits in human pancreatic cancer cells, J. Surg. Res. 118 (2004) 9-14.

[53] G.I. Evan, T.D. Littlewood, The role of c-myc in cell growth, Curr. Opin. Genet. Dev. 3 (1993) 44-49.

[54] S. Adhikary, M. Eilers, Transcriptional regulation and transformation by Myc proteins, Nat. Rev. Mol. Cell Biol. 6 (2005) 635-645.

[55] E.P. Sandgren, C.J. Quaife, A.G. Paulovich, R.D. Palmiter, R.L. Brinster, Pancreatic tumor pathogenesis reflects the causative genetic lesion, Proc. Natl. Acad. Sci. U. S. A. 88 (1991) 93-97.

[56] C. Schleger, C. Verbeke, R. Hildenbrand, H. Zentgraf, U. Bleyl, c-MYC activation in primary and metastatic ductal adenocarcinoma of the pancreas: incidence, mechanisms, and clinical significance, Mod. Pathol. 15 (2002) 462-469.

[57] M. Buchholz, A. Schatz, M. Wagner, P. Michl, T. Linhart, G. Adler, T.M. Gress, V. Ellenrieder, Overexpression of c-myc in pancreatic cancer caused by ectopic activation of NFATc1 and the Ca2+/calcineurin signaling pathway, EMBO J. 25 (2006) 3714-3724.

[58] A. Koenig, T. Linhart, K. Schlengemann, K. Reutlinger, J. Wegele, G. Adler, G. Singh, L. Hofmann, S. Kunsch, T. Buch, E. Schafer, T.M. Gress, M.E. Fernandez-Zapico, V. Ellenrieder, NFAT-induced histone acetylation relay switch promotes c-Myc-dependent growth in pancreatic cancer cells, Gastroenterology 138 (2010) 1189-99.e1-2.

[59] A.L. McCleary-Wheeler, R. McWilliams, M.E. Fernandez-Zapico, Aberrant signaling pathways in pancreatic cancer: a two compartment view, Mol. Carcinog. 51 (2012) 25-39.

[60] T.M. Williams, D.B. Weiner, M.I. Greene, H.C. Maguire Jr, Expression of c-erbB-2 in human pancreatic adenocarcinomas, Pathobiology 59 (1991) 46-52.

[61] K. Satoh, H. Sasano, T. Shimosegawa, M. Koizumi, T. Yamazaki, F. Mochizuki, N. Kobayashi, T. Okano, T. Toyota, T. Sawai, An immunohistochemical study of the c-erbB-2 oncogene product in intraductal mucin-hypersecreting neoplasms and in ductal cell carcinomas of the pancreas, Cancer 72 (1993) 51-56.

[62] J.D. Day, J.A. Digiuseppe, C. Yeo, M. Lai-Goldman, S.M. Anderson, S.N. Goodman, S.E. Kern, R.H. Hruban, Immunohistochemical evaluation of HER-2/neu expression in pancreatic adenocarcinoma and pancreatic intraepithelial neoplasms, Hum. Pathol. 27 (1996) 119-124.

[63] V.M. Bondar, B. Sweeney-Gotsch, M. Andreeff, G.B. Mills, D.J. McConkey, Inhibition of the phosphatidylinositol 3'-kinase-AKT pathway induces apoptosis in pancreatic carcinoma cells in vitro and in vivo, Mol. Cancer. Ther. 1 (2002) 989-997.

[64] M.G. Schlieman, B.N. Fahy, R. Ramsamooj, L. Beckett, R.J. Bold, Incidence, mechanism and prognostic value of activated AKT in pancreas cancer, Br. J. Cancer 89 (2003) 2110-2115.

[65] T.L. Yuan, L.C. Cantley, PI3K pathway alterations in cancer: variations on a theme, Oncogene 27 (2008) 5497-5510.

[66] C. Schild, M. Wirth, M. Reichert, R.M. Schmid, D. Saur, G. Schneider, PI3K signaling maintains c-myc expression to regulate transcription of E2F1 in pancreatic cancer cells, Mol. Carcinog. 48 (2009) 1149-1158.

[67] L.C. Cantley, The phosphoinositide 3-kinase pathway, Science 296 (2002) 1655-1657.

[68] B. Vanhaesebroeck, J. Guillermet-Guibert, M. Graupera, B. Bilanges, The emerging mechanisms of isoform-specific PI3K signalling, Nat. Rev. Mol. Cell Biol. 11 (2010) 329-341.

[69] M.D. Fesinmeyer, M.A. Austin, C.I. Li, A.J. De Roos, D.J. Bowen, Differences in survival by histologic type of pancreatic cancer, Cancer Epidemiol. Biomarkers Prev. 14 (2005) 1766-1773.

[70] T.J. Grant, K. Hua, A. Singh, Molecular Pathogenesis of Pancreatic Cancer, Prog. Mol. Biol. Transl. Sci. 144 (2016) 241-275.

[71] B. Ren, X. Liu, A.A. Suriawinata, Pancreatic Ductal Adenocarcinoma and Its Precursor Lesions: Histopathology, Cytopathology, and Molecular Pathology, Am. J. Pathol. 189 (2019) 9-21.

[72] R.H. Hruban, M. Goggins, J. Parsons, S.E. Kern, Progression model for pancreatic cancer, Clin. Cancer Res. 6 (2000) 2969-2972.

[73] M.A. Khan, S. Azim, H. Zubair, A. Bhardwaj, G.K. Patel, M. Khushman, S. Singh, A.P. Singh, Molecular Drivers of Pancreatic Cancer Pathogenesis: Looking Inward to Move Forward, Int. J. Mol. Sci. 18 (2017) 10.3390/ijms18040779.

[74] R. Ferro, M. Falasca, Emerging role of the KRAS-PDK1 axis in pancreatic cancer, World J. Gastroenterol. 20 (2014) 10752-10757.

[75] S. Weissmueller, E. Manchado, M. Saborowski, J.P. Morris 4th, E. Wagenblast, C.A. Davis, S.H. Moon, N.T. Pfister, D.F. Tschaharganeh, T. Kitzing, D. Aust, E.K. Markert, J. Wu, S.M. Grimmond, C. Pilarsky, C. Prives, A.V. Biankin, S.W. Lowe, Mutant p53 drives pancreatic cancer metastasis through cell-autonomous PDGF receptor beta signaling, Cell 157 (2014) 382-394.

[76] T. Golan, Z.S. Kanji, R. Epelbaum, N. Devaud, E. Dagan, S. Holter, D. Aderka, S. Paluch-Shimon, B. Kaufman, R. Gershoni-Baruch, D. Hedley, M.J. Moore, E. Friedman, S. Gallinger, Overall survival and clinical characteristics of pancreatic cancer in BRCA mutation carriers, Br. J. Cancer 111 (2014) 1132-1138.

[77] T.L. Tinder, D.B. Subramani, G.D. Basu, J.M. Bradley, J. Schettini, A. Million, T. Skaar, P. Mukherjee, MUC1 enhances tumor progression and contributes toward

immunosuppression in a mouse model of spontaneous pancreatic adenocarcinoma, J. Immunol. 181 (2008) 3116-3125.

[78] C.J. Whatcott, C.H. Diep, P. Jiang, A. Watanabe, J. LoBello, C. Sima, G. Hostetter, H.M. Shepard, D.D. Von Hoff, H. Han, Desmoplasia in Primary Tumors and Metastatic Lesions of Pancreatic Cancer, Clin. Cancer Res. 21 (2015) 3561-3568.

[79] M. Xu, B.P. Zhou, M. Tao, J. Liu, W. Li, The Role of Stromal Components in Pancreatic Cancer Progression, Anticancer Agents Med. Chem. 16 (2016) 1117-1124.

[80] K.P. Olive, Stroma, Stroma Everywhere (Far More Than You Think), Clin. Cancer Res. 21 (2015) 3366-3368.

[81] A.P. Singh, S. Arora, A. Bhardwaj, S.K. Srivastava, M.P. Kadakia, B. Wang, W.E. Grizzle, L.B. Owen, S. Singh, CXCL12/CXCR4 protein signaling axis induces sonic hedgehog expression in pancreatic cancer cells via extracellular regulated kinase- and Akt kinase-mediated activation of nuclear factor kappaB: implications for bidirectional tumor-stromal interactions, J. Biol. Chem. 287 (2012) 39115-39124.

[82] S. Arora, A. Bhardwaj, S. Singh, S.K. Srivastava, S. McClellan, C.S. Nirodi, G.A. Piazza, W.E. Grizzle, L.B. Owen, A.P. Singh, An undesired effect of chemotherapy: gemcitabine promotes pancreatic cancer cell invasiveness through reactive oxygen species-dependent, nuclear factor kappaB- and hypoxia-inducible factor 1alpha-mediated up-regulation of CXCR4, J. Biol. Chem. 288 (2013) 21197-21207.

[83] K.P. Olive, M.A. Jacobetz, C.J. Davidson, A. Gopinathan, D. McIntyre, D. Honess, B. Madhu, M.A. Goldgraben, M.E. Caldwell, D. Allard, K.K. Frese, G. Denicola, C. Feig, C. Combs, S.P. Winter, H. Ireland-Zecchini, S. Reichelt, W.J. Howat, A. Chang, M. Dhara, L.

Wang, F. Ruckert, R. Grutzmann, C. Pilarsky, K. Izeradjene, S.R. Hingorani, P. Huang, S.E. Davies, W. Plunkett, M. Egorin, R.H. Hruban, N. Whitebread, K. McGovern, J. Adams, C. Iacobuzio-Donahue, J. Griffiths, D.A. Tuveson, Inhibition of Hedgehog signaling enhances delivery of chemotherapy in a mouse model of pancreatic cancer, Science 324 (2009) 1457-1461.

[84] A.D. Rhim, P.E. Oberstein, D.H. Thomas, E.T. Mirek, C.F. Palermo, S.A. Sastra, E.N. Dekleva, T. Saunders, C.P. Becerra, I.W. Tattersall, C.B. Westphalen, J. Kitajewski, M.G. Fernandez-Barrena, M.E. Fernandez-Zapico, C. Iacobuzio-Donahue, K.P. Olive, B.Z. Stanger, Stromal elements act to restrain, rather than support, pancreatic ductal adenocarcinoma, Cancer. Cell. 25 (2014) 735-747.

[85] M. Gnanamony, C.S. Gondi, Chemoresistance in pancreatic cancer: Emerging concepts, Oncol. Lett. 13 (2017) 2507-2513.

[86] K.S. Sherlach, P.D. Roepe, "Drug resistance associated membrane proteins", Front. Physiol. 5 (2014) 108.

[87] B. Mansoori, A. Mohammadi, S. Davudian, S. Shirjang, B. Baradaran, The Different Mechanisms of Cancer Drug Resistance: A Brief Review, Adv. Pharm. Bull. 7 (2017) 339-348.

[88] T.W. Synold, I. Dussault, B.M. Forman, The orphan nuclear receptor SXR coordinately regulates drug metabolism and efflux, Nat. Med. 7 (2001) 584-590.

[89] Y.Y. Liu, T.Y. Han, A.E. Giuliano, M.C. Cabot, Ceramide glycosylation potentiates cellular multidrug resistance, FASEB J. 15 (2001) 719-730.

[90] M.M. Gottesman, Mechanisms of cancer drug resistance, Annu. Rev. Med. 53 (2002) 615-627.

[91] M. Ilmer, A.R. Boiles, I. Regel, K. Yokoi, C.W. Michalski, I.I. Wistuba, J. Rodriguez, E. Alt, J. Vykoukal, RSPO2 Enhances Canonical Wnt Signaling to Confer Stemness-Associated Traits to Susceptible Pancreatic Cancer Cells, Cancer Res. 75 (2015) 1883-1896.

[92] M. Herreros-Villanueva, T.K. Er, L. Bujanda, Retinoic Acid Reduces Stem Cell-Like Features in Pancreatic Cancer Cells, Pancreas 44 (2015) 918-924.

[93] C. Ma, Y.C. Ding, W. Yu, Q. Wang, B. Meng, T. Huang, MicroRNA-200c overexpression plays an inhibitory role in human pancreatic cancer stem cells by regulating epithelial-mesenchymal transition, Minerva Med. 106 (2015) 193-202.

[94] S. Meidhof, S. Brabletz, W. Lehmann, B.T. Preca, K. Mock, M. Ruh, J. Schuler, M. Berthold, A. Weber, U. Burk, M. Lubbert, M. Puhr, Z. Culig, U. Wellner, T. Keck, P. Bronsert, S. Kusters, U.T. Hopt, M.P. Stemmler, T. Brabletz, ZEB1-associated drug resistance in cancer cells is reversed by the class I HDAC inhibitor mocetinostat, EMBO Mol. Med. 7 (2015) 831-847.

[95] J. Xu, T. Wang, Z. Cao, H. Huang, J. Li, W. Liu, S. Liu, L. You, L. Zhou, T. Zhang, Y. Zhao, MiR-497 downregulation contributes to the malignancy of pancreatic cancer and associates with a poor prognosis, Oncotarget 5 (2014) 6983-6993.

[96] C. Liang, X.J. Yu, X.Z. Guo, M.H. Sun, Z. Wang, Y. Song, Q.X. Ni, H.Y. Li, N. Mukaida, Y.Y. Li, MicroRNA-33a-mediated downregulation of Pim-3 kinase expression renders

human pancreatic cancer cells sensitivity to gemcitabine, Oncotarget 6 (2015) 14440-14455.

[97] S. Trehoux, F. Lahdaoui, Y. Delpu, F. Renaud, E. Leteurtre, J. Torrisani, N. Jonckheere, I. Van Seuningen, Micro-RNAs miR-29a and miR-330-5p function as tumor suppressors by targeting the MUC1 mucin in pancreatic cancer cells, Biochim. Biophys. Acta 1853 (2015) 2392-2403.

[98] P.A. Toste, L. Li, B.E. Kadera, A.H. Nguyen, L.M. Tran, N. Wu, D.L. Madnick, S.G. Patel, D.W. Dawson, T.R. Donahue, p85alpha is a microRNA target and affects chemosensitivity in pancreatic cancer, J. Surg. Res. 196 (2015) 285-293.

[99] S. Hasegawa, H. Eguchi, H. Nagano, M. Konno, Y. Tomimaru, H. Wada, N. Hama, K. Kawamoto, S. Kobayashi, N. Nishida, J. Koseki, T. Nishimura, N. Gotoh, S. Ohno, N. Yabuta, H. Nojima, M. Mori, Y. Doki, H. Ishii, MicroRNA-1246 expression associated with CCNG2-mediated chemoresistance and stemness in pancreatic cancer, Br. J. Cancer 111 (2014) 1572-1580.

[100] Q. Xu, P. Li, X. Chen, L. Zong, Z. Jiang, L. Nan, J. Lei, W. Duan, D. Zhang, X. Li, H. Sha, Z. Wu, Q. Ma, Z. Wang, miR-221/222 induces pancreatic cancer progression through the regulation of matrix metalloproteinases, Oncotarget 6 (2015) 14153-14164.

[101] M. Cioffi, S.M. Trabulo, Y. Sanchez-Ripoll, I. Miranda-Lorenzo, E. Lonardo, J. Dorado, C. Reis Vieira, J.C. Ramirez, M. Hidalgo, A. Aicher, S. Hahn, B. Sainz Jr, C. Heeschen, The miR-17-92 cluster counteracts quiescence and chemoresistance in a distinct subpopulation of pancreatic cancer stem cells, Gut 64 (2015) 1936-1948.

[102] J.A. Moir, J. Mann, S.A. White, The role of pancreatic stellate cells in pancreatic cancer, Surg. Oncol. 24 (2015) 232-238.

[103] M. Schober, R. Jesenofsky, R. Faissner, C. Weidenauer, W. Hagmann, P. Michl, R.L. Heuchel, S.L. Haas, J.M. Lohr, Desmoplasia and chemoresistance in pancreatic cancer, Cancers (Basel) 6 (2014) 2137-2154.

[104] B.C. Ozdemir, T. Pentcheva-Hoang, J.L. Carstens, X. Zheng, C.C. Wu, T.R. Simpson, H. Laklai, H. Sugimoto, C. Kahlert, S.V. Novitskiy, A. De Jesus-Acosta, P. Sharma, P. Heidari, U. Mahmood, L. Chin, H.L. Moses, V.M. Weaver, A. Maitra, J.P. Allison, V.S. LeBleu, R. Kalluri, Depletion of carcinoma-associated fibroblasts and fibrosis induces immunosuppression and accelerates pancreas cancer with reduced survival, Cancer. Cell. 25 (2014) 719-734.

[105] C. Duluc, S. Moatassim-Billah, M. Chalabi-Dchar, A. Perraud, R. Samain, F. Breibach, M. Gayral, P. Cordelier, M.B. Delisle, M.P. Bousquet-Dubouch, R. Tomasini, H. Schmid, M. Mathonnet, S. Pyronnet, Y. Martineau, C. Bousquet, Pharmacological targeting of the protein synthesis mTOR/4E-BP1 pathway in cancer-associated fibroblasts abrogates pancreatic tumour chemoresistance, EMBO Mol. Med. 7 (2015) 735-753.

[106] F. Cao, J. Li, H. Sun, S. Liu, Y. Cui, F. Li, HES 1 is essential for chemoresistance induced by stellate cells and is associated with poor prognosis in pancreatic cancer, Oncol. Rep. 33 (2015) 1883-1889.

[107] H. Zhang, H. Wu, J. Guan, L. Wang, X. Ren, X. Shi, Z. Liang, T. Liu, Paracrine SDF-1alpha signaling mediates the effects of PSCs on GEM chemoresistance through an IL-6 autocrine loop in pancreatic cancer cells, Oncotarget 6 (2015) 3085-3097.

[108] M.H. Sherman, R.T. Yu, D.D. Engle, N. Ding, A.R. Atkins, H. Tiriac, E.A. Collisson, F. Connor, T. Van Dyke, S. Kozlov, P. Martin, T.W. Tseng, D.W. Dawson, T.R. Donahue, A. Masamune, T. Shimosegawa, M.V. Apte, J.S. Wilson, B. Ng, S.L. Lau, J.E. Gunton, G.M. Wahl, T. Hunter, J.A. Drebin, P.J. O'Dwyer, C. Liddle, D.A. Tuveson, M. Downes, R.M. Evans, Vitamin D receptor-mediated stromal reprogramming suppresses pancreatitis and enhances pancreatic cancer therapy, Cell 159 (2014) 80-93.

[109] J.J. Kwon, S.C. Nabinger, Z. Vega, S.S. Sahu, R.K. Alluri, Z. Abdul-Sater, Z. Yu, J. Gore, G. Nalepa, R. Saxena, M. Korc, J. Kota, Pathophysiological role of microRNA-29 in pancreatic cancer stroma, Sci. Rep. 5 (2015) 11450.

[110] C. Sessa, S. Aamdal, I. Wolff, R. Eppelbaum, J.F. Smyth, A. Sulkes, W. Ten Bokkel Huinink, J. Vermorken, J. Wanders, H. Franklin, Gemcitabine in patients with advanced malignant melanoma or gastric cancer: phase II studies of the EORTC Early Clinical Trials Group, Ann. Oncol. 5 (1994) 471-472.

[111] W. Plunkett, P. Huang, Y.Z. Xu, V. Heinemann, R. Grunewald, V. Gandhi, Gemcitabine: metabolism, mechanisms of action, and self-potentiation, Semin. Oncol. 22 (1995) 3-10.

[112] H. Burris, A.M. Storniolo, Assessing clinical benefit in the treatment of pancreas cancer: gemcitabine compared to 5-fluorouracil, Eur. J. Cancer 33 Suppl 1 (1997) S18-22.

[113] J. Dai, Y. Zhang, H. Li, Y. Deng, A.A. Elzatahry, A. Alghamdi, D. Fu, Y. Jiang, D. Zhao, Enhancement of gemcitabine against pancreatic cancer by loading in mesoporous silica vesicles, Chinese Chemical Letters 28 (2017) 531-536.

[114] L. Wang, Y. An, C. Yuan, H. Zhang, C. Liang, F. Ding, Q. Gao, D. Zhang, GEM-loaded magnetic albumin nanospheres modified with cetuximab for simultaneous targeting, magnetic resonance imaging, and double-targeted thermochemotherapy of pancreatic cancer cells, Int. J. Nanomedicine 10 (2015) 2507-2519.

[115] H.A. Burris 3rd, M.J. Moore, J. Andersen, M.R. Green, M.L. Rothenberg, M.R. Modiano, M.C. Cripps, R.K. Portenoy, A.M. Storniolo, P. Tarassoff, R. Nelson, F.A. Dorr, C.D. Stephens, D.D. Von Hoff, Improvements in survival and clinical benefit with gemcitabine as first-line therapy for patients with advanced pancreas cancer: a randomized trial, J. Clin. Oncol. 15 (1997) 2403-2413.

[116] T. Conroy, F. Desseigne, M. Ychou, O. Bouche, R. Guimbaud, Y. Becouarn, A. Adenis, J.L. Raoul, S. Gourgou-Bourgade, C. de la Fouchardiere, J. Bennouna, J.B. Bachet, F. Khemissa-Akouz, D. Pere-Verge, C. Delbaldo, E. Assenat, B. Chauffert, P. Michel, C. Montoto-Grillot, M. Ducreux, Groupe Tumeurs Digestives of Unicancer, PRODIGE Intergroup, FOLFIRINOX versus gemcitabine for metastatic pancreatic cancer, N. Engl. J. Med. 364 (2011) 1817-1825.

[117] D.D. Von Hoff, T. Ervin, F.P. Arena, E.G. Chiorean, J. Infante, M. Moore, T. Seay, S.A. Tjulandin, W.W. Ma, M.N. Saleh, M. Harris, M. Reni, S. Dowden, D. Laheru, N. Bahary, R.K. Ramanathan, J. Tabernero, M. Hidalgo, D. Goldstein, E. Van Cutsem, X. Wei, J. Iglesias, M.F. Renschler, Increased survival in pancreatic cancer with nab-paclitaxel plus gemcitabine, N. Engl. J. Med. 369 (2013) 1691-1703.

[118] M.T. Saung, L. Zheng, Current Standards of Chemotherapy for Pancreatic Cancer, Clin. Ther. 39 (2017) 2125-2134.

[119] T. Alcindor, N. Beauger, Oxaliplatin: a review in the era of molecularly targeted therapy, Curr. Oncol. 18 (2011) 18-25.

[120] K. Fujita, Y. Kubota, H. Ishida, Y. Sasaki, Irinotecan, a key chemotherapeutic drug for metastatic colorectal cancer, World J. Gastroenterol. 21 (2015) 12234-12248.

[121] S. Mullany, P.A. Svingen, S.H. Kaufmann, C. Erlichman, Effect of adding the topoisomerase I poison 7-ethyl-10-hydroxycamptothecin (SN-38) to 5-fluorouracil and folinic acid in HCT-8 cells: elevated dTTP pools and enhanced cytotoxicity, Cancer Chemother. Pharmacol. 42 (1998) 391-399.

[122] V. Pavillard, P. Formento, P. Rostagno, J.L. Formento, J.L. Fischel, M. Francoual, M.C. Etienne, G. Milano, Combination of irinotecan (CPT11) and 5-fluorouracil with an analysis of cellular determinants of drug activity, Biochem. Pharmacol. 56 (1998) 1315-1322.

[123] D.R. Mans, I. Grivicich, G.J. Peters, G. Schwartsmann, Sequence-dependent growth inhibition and DNA damage formation by the irinotecan-5-fluorouracil combination in human colon carcinoma cell lines, Eur. J. Cancer 35 (1999) 1851-1861.

[124] R.G. Azrak, S. Cao, H.K. Slocum, K. Toth, F.A. Durrani, M.B. Yin, L. Pendyala, W. Zhang, H.L. McLeod, Y.M. Rustum, Therapeutic synergy between irinotecan and 5-fluorouracil against human tumor xenografts, Clin. Cancer Res. 10 (2004) 1121-1129.

[125] N. Zeghari-Squalli, E. Raymond, E. Cvitkovic, F. Goldwasser, Cellular pharmacology of the combination of the DNA topoisomerase I inhibitor SN-38 and the diaminocyclohexane platinum derivative oxaliplatin, Clin. Cancer Res. 5 (1999) 1189-1196.

[126] M. Ducreux, E. Mitry, M. Ould-Kaci, V. Boige, J.F. Seitz, R. Bugat, J.L. Breau, O. Bouche, P.L. Etienne, J.M. Tigaud, F. Morvan, E. Cvitkovic, P. Rougier, Randomized phase II study evaluating oxaliplatin alone, oxaliplatin combined with infusional 5-FU, and infusional 5-FU alone in advanced pancreatic carcinoma patients, Ann. Oncol. 15 (2004) 467-473.

[127] H. Ueno, T. Okusaka, A. Funakoshi, H. Ishii, K. Yamao, O. Ishikawa, S. Ohkawa, S. Saitoh, A phase II study of weekly irinotecan as first-line therapy for patients with metastatic pancreatic cancer, Cancer Chemother. Pharmacol. 59 (2007) 447-454.

[128] D.J. Wagener, H.E. Verdonk, L.Y. Dirix, G. Catimel, P. Siegenthaler, M. Buitenhuis, A. Mathieu-Boue, J. Verweij, Phase II trial of CPT-11 in patients with advanced pancreatic cancer, an EORTC early clinical trials group study, Ann. Oncol. 6 (1995) 129-132.

[129] S. Gourgou-Bourgade, C. Bascoul-Mollevi, F. Desseigne, M. Ychou, O. Bouche, R. Guimbaud, Y. Becouarn, A. Adenis, J.L. Raoul, V. Boige, J. Berille, T. Conroy, Impact of FOLFIRINOX compared with gemcitabine on quality of life in patients with metastatic pancreatic cancer: results from the PRODIGE 4/ACCORD 11 randomized trial, J. Clin. Oncol. 31 (2013) 23-29.

[130] T.L. Fitzgerald, K. Lertpiriyapong, L. Cocco, A.M. Martelli, M. Libra, S. Candido, G. Montalto, M. Cervello, L. Steelman, S.L. Abrams, J.A. McCubrey, Roles of EGFR and KRAS and their downstream signaling pathways in pancreatic cancer and pancreatic cancer stem cells, Adv. Biol. Regul. 59 (2015) 65-81.

[131] M. Guo, G. Luo, C. Liu, H. Cheng, Y. Lu, K. Jin, Z. Liu, J. Long, L. Liu, J. Xu, D. Huang, Q. Ni, X. Yu, The Prognostic and Predictive Role of Epidermal Growth Factor

Receptor in Surgical Resected Pancreatic Cancer, Int. J. Mol. Sci. 17 (2016) 10.3390/ijms17071090.

[132] M.J. Moore, D. Goldstein, J. Hamm, A. Figer, J.R. Hecht, S. Gallinger, H.J. Au, P. Murawa, D. Walde, R.A. Wolff, D. Campos, R. Lim, K. Ding, G. Clark, T. Voskoglou-Nomikos, M. Ptasynski, W. Parulekar, National Cancer Institute of Canada Clinical Trials Group, Erlotinib plus gemcitabine compared with gemcitabine alone in patients with advanced pancreatic cancer: a phase III trial of the National Cancer Institute of Canada Clinical Trials Group, J. Clin. Oncol. 25 (2007) 1960-1966.

[133] A. Ottaiano, M. Capozzi, C. De Divitiis, A. De Stefano, G. Botti, A. Avallone, S. Tafuto, Gemcitabine mono-therapy versus gemcitabine plus targeted therapy in advanced pancreatic cancer: a meta-analysis of randomized phase III trials, Acta Oncol. 56 (2017) 377-383.

[134] R.K. Ramanathan, R.L. Korn, J.C. Sachdev, G.J. Fetterly, K. Marceau, V. Marsh, J.M. Neil, R.G. Newbold, N. Raghunand, J. Prey, Abstract CT224: Pilot study in patients with advanced solid tumors to evaluate feasibility of ferumoxytol (FMX) as tumor imaging agent prior to MM-398, a nanoliposomal irinotecan (nal-IRI) (2014) .

[135] A.V. Kalra, J. Kim, S.G. Klinz, N. Paz, J. Cain, D.C. Drummond, U.B. Nielsen, J.B. Fitzgerald, Preclinical activity of nanoliposomal irinotecan is governed by tumor deposition and intratumor prodrug conversion, Cancer Res. 74 (2014) 7003-7013.

[136] A. Wang-Gillam, R.A. Hubner, J.T. Siveke, D.D. Von Hoff, B. Belanger, F.A. de Jong, B. Mirakhur, L.T. Chen, NAPOLI-1 phase 3 study of liposomal irinotecan in metastatic pancreatic cancer: Final overall survival analysis and characteristics of long-term survivors, Eur. J. Cancer 108 (2019) 78-87.

[137] R.A. Freitas Jr, What is nanomedicine? Nanomedicine 1 (2005) 2-9.

[138] J.H. Myung, K.A. Tam, S.J. Park, A. Cha, S. Hong, Recent advances in nanotechnology-based detection and separation of circulating tumor cells, Wiley Interdiscip. Rev. Nanomed Nanobiotechnol 8 (2016) 223-239.

[139] A.S. Chadha, A. Khoo, M.L. Aliru, H.K. Arora, J.R. Gunther, S. Krishnan, Recent Advances and Prospects for Multimodality Therapy in Pancreatic Cancer, Semin. Radiat. Oncol. 26 (2016) 320-337.

[140] C. Buzea, I.I. Pacheco, K. Robbie, Nanomaterials and nanoparticles: sources and toxicity, Biointerphases 2 (2007) MR17-71.

[141] A. Manzur, A. Oluwasanmi, D. Moss, A. Curtis, C. Hoskins, Nanotechnologies in Pancreatic Cancer Therapy, Pharmaceutics 9 (2017) 10.3390/pharmaceutics9040039.

[142] K. Greish, Enhanced permeability and retention (EPR) effect for anticancer nanomedicine drug targeting, Methods Mol. Biol. 624 (2010) 25-37.

[143] J.D. Byrne, T. Betancourt, L. Brannon-Peppas, Active targeting schemes for nanoparticle systems in cancer therapeutics, Adv. Drug Deliv. Rev. 60 (2008) 1615-1626.

[144] T.T. Goodman, J. Chen, K. Matveev, S.H. Pun, Spatio-temporal modeling of nanoparticle delivery to multicellular tumor spheroids, Biotechnol. Bioeng. 101 (2008) 388-399.

[145] V.P. Chauhan, Z. Popovic, O. Chen, J. Cui, D. Fukumura, M.G. Bawendi, R.K. Jain, Fluorescent nanorods and nanospheres for real-time in vivo probing of nanoparticle shape-dependent tumor penetration, Angew. Chem. Int. Ed Engl. 50 (2011) 11417-11420.

[146] F. Yuan, M. Leunig, S.K. Huang, D.A. Berk, D. Papahadjopoulos, R.K. Jain, Microvascular permeability and interstitial penetration of sterically stabilized (stealth) liposomes in a human tumor xenograft, Cancer Res. 54 (1994) 3352-3356.

[147] C. Chittasupho, S. Anuchapreeda, N. Sarisuta, CXCR4 targeted dendrimer for anti-cancer drug delivery and breast cancer cell migration inhibition, Eur. J. Pharm. Biopharm. 119 (2017) 310-321.

[148] C.Y. Yeh, J.K. Hsiao, Y.P. Wang, C.H. Lan, H.C. Wu, Peptide-conjugated nanoparticles for targeted imaging and therapy of prostate cancer, Biomaterials 99 (2016) 1-15.

[149] T.K. Motawi, S.A. El-Maraghy, A.N. ElMeshad, O.M. Nady, O.A. Hammam, Cromolyn chitosan nanoparticles as a novel protective approach for colorectal cancer, Chem. Biol. Interact. 275 (2017) 1-12.

[150] Y.H. Shih, T.Y. Luo, P.F. Chiang, C.J. Yao, W.J. Lin, C.L. Peng, M.J. Shieh, EGFR-targeted micelles containing near-infrared dye for enhanced photothermal therapy in colorectal cancer, J. Control. Release 258 (2017) 196-207.

[151] D. Luong, P. Kesharwani, H.O. Alsaab, S. Sau, S. Padhye, F.H. Sarkar, A.K. Iyer, Folic acid conjugated polymeric micelles loaded with a curcumin difluorinated analog for targeting cervical and ovarian cancers, Colloids Surf. B Biointerfaces 157 (2017) 490-502.

[152] R. Xu, G. Zhang, J. Mai, X. Deng, V. Segura-Ibarra, S. Wu, J. Shen, H. Liu, Z. Hu, L. Chen, Y. Huang, E. Koay, Y. Huang, J. Liu, J.E. Ensor, E. Blanco, X. Liu, M. Ferrari, H. Shen, An injectable nanoparticle generator enhances delivery of cancer therapeutics, Nat. Biotechnol. 34 (2016) 414-418.

[153] F. Canal, J. Sanchis, M.J. Vicent, Polymer--drug conjugates as nano-sized medicines, Curr. Opin. Biotechnol. 22 (2011) 894-900.

[154] L. Wang, X. Liu, Q. Zhou, M. Sui, Z. Lu, Z. Zhou, J. Tang, Y. Miao, M. Zheng, W. Wang, Y. Shen, Terminating the criminal collaboration in pancreatic cancer: Nanoparticle-based synergistic therapy for overcoming fibroblast-induced drug resistance, Biomaterials 144 (2017) 105-118.

[155] M.J. Ernsting, B. Hoang, I. Lohse, E. Undzys, P. Cao, T. Do, B. Gill, M. Pintilie, D. Hedley, S.D. Li, Targeting of metastasis-promoting tumor-associated fibroblasts and modulation of pancreatic tumor-associated stroma with a carboxymethylcellulose-docetaxel nanoparticle, J. Control. Release 206 (2015) 122-130.

[156] V. Bala, S. Rao, B.J. Boyd, C.A. Prestidge, Prodrug and nanomedicine approaches for the delivery of the camptothecin analogue SN38, J. Control. Release 172 (2013) 48-61.

[157] M.I. Gibson, R.K. O'Reilly, To aggregate, or not to aggregate? considerations in the design and application of polymeric thermally-responsive nanoparticles, Chem. Soc. Rev. 42 (2013) 7204-7213.

[158] K. Letchford, H. Burt, A review of the formation and classification of amphiphilic block copolymer nanoparticulate structures: micelles, nanospheres, nanocapsules and polymersomes, Eur. J. Pharm. Biopharm. 65 (2007) 259-269.

[159] K. Prompruk, T. Govender, S. Zhang, C.D. Xiong, S. Stolnik, Synthesis of a novel PEG-block-poly(aspartic acid-stat-phenylalanine) copolymer shows potential for formation of a micellar drug carrier, Int. J. Pharm. 297 (2005) 242-253.

[160] R.T. Chan, H. Marçal, R.A. Russell, P.J. Holden, L.J.R. Foster, Application of polyethylene glycol to promote cellular biocompatibility of polyhydroxybutyrate films, International Journal of Polymer Science 2011 (2011) .

[161] P.G. Millili, J.A. Selekman, K.M. Blocker, D.A. Johnson, U.P. Naik, M.O. Sullivan, Structural and functional consequences of poly(ethylene glycol) inclusion on DNA condensation for gene delivery, Microsc. Res. Tech. 73 (2010) 866-877.

[162] J.W. Yoo, E. Chambers, S. Mitragotri, Factors that control the circulation time of nanoparticles in blood: challenges, solutions and future prospects, Curr. Pharm. Des. 16 (2010) 2298-2307.

[163] A. Veeren, A. Bhaw-Luximon, D. Mukhopadhyay, D. Jhurry, Mixed poly(vinyl pyrrolidone)-based drug-loaded nanomicelles shows enhanced efficacy against pancreatic cancer cell lines, Eur. J. Pharm. Sci. 102 (2017) 250-260.

[164] C. Hoskins, P.K. Thoo-Lin, W.P. Cheng, A review on comb-shaped amphiphilic polymers for hydrophobic drug solubilization, Ther. Deliv. 3 (2012) 59-79.

[165] X. Bao, W. Wang, C. Wang, Y. Wang, J. Zhou, Y. Ding, X. Wang, Y. Jin, A chitosan-graft-PEI-candesartan conjugate for targeted co-delivery of drug and gene in anti-angiogenesis cancer therapy, Biomaterials 35 (2014) 8450-8466.

[166] Y. Niu, L.K. Yeung, R.M. Crooks, Size-selective hydrogenation of olefins by dendrimer-encapsulated palladium nanoparticles, J. Am. Chem. Soc. 123 (2001) 6840-6846.

[167] A. Topp, B.J. Bauer, J.W. Klimash, R. Spindler, D.A. Tomalia, E.J. Amis, Probing the location of the terminal groups of dendrimers in dilute solution, Macromolecules 32 (1999) 7226-7231.

[168] E. Ladd, A. Sheikhi, N. Li, T.G.M. van de Ven, A. Kakkar, Design and Synthesis of Dendrimers with Facile Surface Group Functionalization, and an Evaluation of Their Bactericidal Efficacy, Molecules 22 (2017) 10.3390/molecules22060868.

[169] F. Chiba, L.J. Twyman, Effect of Terminal-Group Functionality on the Ability of Dendrimers to Bind Proteins, Bioconjug. Chem. 28 (2017) 2046-2050.

[170] K.T. Al-Jamal, C. Ramaswamy, A.T. Florence, Supramolecular structures from dendrons and dendrimers, Adv. Drug Deliv. Rev. 57 (2005) 2238-2270.

[171] S. Svenson, Dendrimers as versatile platform in drug delivery applications, Eur. J. Pharm. Biopharm. 71 (2009) 445-462.

[172] P. Kesharwani, L. Xie, S. Banerjee, G. Mao, S. Padhye, F.H. Sarkar, A.K. Iyer, Hyaluronic acid-conjugated polyamidoamine dendrimers for targeted delivery of 3,4-difluorobenzylidene curcumin to CD44 overexpressing pancreatic cancer cells, Colloids Surf. B Biointerfaces 136 (2015) 413-423.

[173] R. Teranishi, R. Matsuki, E. Yuba, A. Harada, K. Kono, Doxorubicin Delivery Using pH and Redox Dual-Responsive Hollow Nanocapsules with a Cationic Electrostatic Barrier, Pharmaceutics 9 (2016) 10.3390/pharmaceutics9010004.

[174] E. Cabane, X. Zhang, K. Langowska, C.G. Palivan, W. Meier, Stimuli-responsive polymers and their applications in nanomedicine, Biointerphases 7 (2012) 9-011-0009-3. Epub 2012 Feb 11.

[175] N. Rapoport, Physical stimuli-responsive polymeric micelles for anti-cancer drug delivery, Progress in Polymer Science 32 (2007) 962-990.

[176] E.S. Gil, S.M. Hudson, Stimuli-reponsive polymers and their bioconjugates, Progress in polymer science 29 (2004) 1173-1222.

[177] J. Li, B. Wang, P. Liu, Possibility of active targeting to tumor by local hyperthermia with temperature-sensitive nanoparticles, Med. Hypotheses 71 (2008) 249-251.

[178] M. Emamzadeh, D. Desmaële, P. Couvreur, G. Pasparakis, Dual controlled delivery of squalenoyl-gemcitabine and paclitaxel using thermo-responsive polymeric micelles for pancreatic cancer, Journal of Materials Chemistry B 6 (2018) 2230-2239.

[179] N. Wiradharma, Y. Zhang, S. Venkataraman, J.L. Hedrick, Y.Y. Yang, Self-assembled polymer nanostructures for delivery of anticancer therapeutics, Nano Today 4 (2009) 302-317.

[180] X. Li, M.R. Szewczuk, C. Malardier-Jugroot, Folic acid-conjugated amphiphilic alternating copolymer as a new active tumor targeting drug delivery platform, Drug Des. Devel. Ther. 10 (2016) 4101-4110.

[181] B. Kim, B. Seo, S. Park, C. Lee, J.O. Kim, K.T. Oh, E.S. Lee, H.G. Choi, Y.S. Youn, Albumin nanoparticles with synergistic antitumor efficacy against metastatic lung cancers, Colloids Surf. B Biointerfaces 158 (2017) 157-166.

[182] T. Peters Jr, All about albumin: biochemistry, genetics, and medical applications, Academic press, 1995.

[183] G. Ciofani, A. Menciassi, Piezoelectric nanomaterials for biomedical applications, Springer, 2012.

[184] S. Banerjee, T. Hemraj-Benny, S.S. Wong, Covalent surface chemistry of single-walled carbon nanotubes, Adv Mater 17 (2005) 17-29.

[185] C. Klumpp, K. Kostarelos, M. Prato, A. Bianco, Functionalized carbon nanotubes as emerging nanovectors for the delivery of therapeutics, Biochim. Biophys. Acta 1758 (2006) 404-412.

[186] S. Wang, Q. Lin, J. Chen, H. Gao, D. Fu, S. Shen, Biocompatible polydopamine-encapsulated gadolinium-loaded carbon nanotubes for MRI and color mapping guided photothermal dissection of tumor metastasis, Carbon 112 (2017) 53-62.

[187] C.T. Matea, T. Mocan, F. Tabaran, T. Pop, O. Mosteanu, C. Puia, C. Iancu, L. Mocan, Quantum dots in imaging, drug delivery and sensor applications, Int. J. Nanomedicine 12 (2017) 5421-5431.

[188] S.Q. Chang, Y.D. Dai, B. Kang, W. Han, L. Mao, D. Chen, UV-enhanced cytotoxicity of thiol-capped CdTe quantum dots in human pancreatic carcinoma cells, Toxicol. Lett. 188 (2009) 104-111.

[189] K.H. Lee, J.F. Galloway, J. Park, C.M. Dvoracek, M. Dallas, K. Konstantopoulos, A. Maitra, P.C. Searson, Quantitative molecular profiling of biomarkers for pancreatic cancer with functionalized quantum dots, Nanomedicine 8 (2012) 1043-1051.

[190] E.U. Saritas, P.W. Goodwill, L.R. Croft, J.J. Konkle, K. Lu, B. Zheng, S.M. Conolly, Magnetic particle imaging (MPI) for NMR and MRI researchers, J. Magn. Reson. 229 (2013) 116-126.

[191] J. Xie, S. Lee, X. Chen, Nanoparticle-based theranostic agents, Adv. Drug Deliv. Rev. 62 (2010) 1064-1079.

[192] J.E. Rosen, L. Chan, D.B. Shieh, F.X. Gu, Iron oxide nanoparticles for targeted cancer imaging and diagnostics, Nanomedicine 8 (2012) 275-290.

[193] P.B. Santhosh, N.P. Ulrih, Multifunctional superparamagnetic iron oxide nanoparticles: promising tools in cancer theranostics, Cancer Lett. 336 (2013) 8-17.

[194] M.P. Arachchige, S.S. Laha, A.R. Naik, K.T. Lewis, R. Naik, B.P. Jena, Functionalized nanoparticles enable tracking the rapid entry and release of doxorubicin in human pancreatic cancer cells, Micron 92 (2017) 25-31.

[195] A.K. Rochani, S. Balasubramanian, A. Ravindran Girija, S. Raveendran, A. Borah, Y. Nagaoka, Y. Nakajima, T. Maekawa, D.S. Kumar, Dual mode of cancer cell destruction for pancreatic cancer therapy using Hsp90 inhibitor loaded polymeric nano magnetic formulation, Int. J. Pharm. 511 (2016) 648-658.

[196] Y. Guo, Z. Zhang, D.H. Kim, W. Li, J. Nicolai, D. Procissi, Y. Huan, G. Han, R.A. Omary, A.C. Larson, Photothermal ablation of pancreatic cancer cells with hybrid iron-oxide core gold-shell nanoparticles, Int. J. Nanomedicine 8 (2013) 3437-3446.

[197] A. Oluwasanmi, M. Malekigorji, S. Jones, A. Curtis, C. Hoskins, Potential of hybrid iron oxide–gold nanoparticles as thermal triggers for pancreatic cancer therapy, RSC Advances 6 (2016) 95044-95054.

[198] W. Wang, Q.Q. Wei, J. Wang, B.C. Wang, S.H. Zhang, Z. Yuan, Role of thiol-containing polyethylene glycol (thiol-PEG) in the modification process of gold

nanoparticles (AuNPs): stabilizer or coagulant? J. Colloid Interface Sci. 404 (2013) 223-229.

[199] S. Zhang, L. Berguiga, J. Elezgaray, T. Roland, C. Faivre-Moskalenko, F. Argoul, Surface plasmon resonance characterization of thermally evaporated thin gold films, Surf. Sci. 601 (2007) 5445-5458.

[200] S. Verma, B.T. Rao, S. Rai, V. Ganesan, L. Kukreja, Influence of process parameters on surface plasmon resonance characteristics of densely packed gold nanoparticle films grown by pulsed laser deposition, Appl. Surf. Sci. 258 (2012) 4898-4905.

[201] L. Vigderman, E.R. Zubarev, Therapeutic platforms based on gold nanoparticles and their covalent conjugates with drug molecules, Adv. Drug Deliv. Rev. 65 (2013) 663-676.

[202] L. Mocan, I. Ilie, F.A. Tabaran, B. Dana, F. Zaharie, C. Zdrehus, C. Puia, T. Mocan, V. Muntean, P. Teodora, M. Ofelia, T. Marcel, C. Iancu, Surface plasmon resonance-induced photoactivation of gold nanoparticles as mitochondria-targeted therapeutic agents for pancreatic cancer, Expert Opin. Ther. Targets 17 (2013) 1383-1393.

[203] S. Saha, X. Xiong, P.K. Chakraborty, K. Shameer, R.R. Arvizo, R.A. Kudgus, S.K. Dwivedi, M.N. Hossen, E.M. Gillies, J.D. Robertson, J.T. Dudley, R.A. Urrutia, R.G. Postier, R. Bhattacharya, P. Mukherjee, Gold Nanoparticle Reprograms Pancreatic Tumor Microenvironment and Inhibits Tumor Growth, ACS Nano 10 (2016) 10636-10651.

[204] R.L. Siegel, K.D. Miller, A. Jemal, Cancer statistics, 2015, CA Cancer. J. Clin. 65 (2015) 5-29.

[205] A.L. Warshaw, C. Fernandez-del Castillo, Pancreatic carcinoma, N. Engl. J. Med. 326 (1992) 455-465.

[206] T.M. Gall, M. Tsakok, H. Wasan, L.R. Jiao, Pancreatic cancer: current management and treatment strategies, Postgrad. Med. J. 91 (2015) 601-607.

[207] L. Rahib, B.D. Smith, R. Aizenberg, A.B. Rosenzweig, J.M. Fleshman, L.M. Matrisian, Projecting cancer incidence and deaths to 2030: the unexpected burden of thyroid, liver, and pancreas cancers in the United States, Cancer Res. 74 (2014) 2913-2921.

[208] E. Moysan, G. Bastiat, J.P. Benoit, Gemcitabine versus Modified Gemcitabine: a review of several promising chemical modifications, Mol. Pharm. 10 (2013) 430-444.

[209] S. Mohammed, G. Van Buren 2nd, W.E. Fisher, Pancreatic cancer: advances in treatment, World J. Gastroenterol. 20 (2014) 9354-9360.

[210] M. Erkan, S. Hausmann, C.W. Michalski, A.A. Fingerle, M. Dobritz, J. Kleeff, H. Friess, The role of stroma in pancreatic cancer: diagnostic and therapeutic implications, Nat. Rev. Gastroenterol. Hepatol. 9 (2012) 454-467.

[211] V. Heinemann, M. Reni, M. Ychou, D.J. Richel, T. Macarulla, M. Ducreux, Tumour-stroma interactions in pancreatic ductal adenocarcinoma: rationale and current evidence for new therapeutic strategies, Cancer Treat. Rev. 40 (2014) 118-128.

[212] B. Zhang, T. Jiang, S. Shen, X. She, Y. Tuo, Y. Hu, Z. Pang, X. Jiang, Cyclopamine disrupts tumor extracellular matrix and improves the distribution and efficacy of nanotherapeutics in pancreatic cancer, Biomaterials 103 (2016) 12-21.

[213] G. Feldmann, S. Dhara, V. Fendrich, D. Bedja, R. Beaty, M. Mullendore, C. Karikari, H. Alvarez, C. Iacobuzio-Donahue, A. Jimeno, K.L. Gabrielson, W. Matsui, A. Maitra, Blockade of hedgehog signaling inhibits pancreatic cancer invasion and metastases: a

new paradigm for combination therapy in solid cancers, Cancer Res. 67 (2007) 2187-2196.

[214] M.W. Saif, K. Syrigos, R. Penney, K. Kaley, Docetaxel second-line therapy in patients with advanced pancreatic cancer: a retrospective study, Anticancer Res. 30 (2010) 2905-2909.

[215] K.L. Hennenfent, R. Govindan, Novel formulations of taxanes: a review. Old wine in a new bottle? Ann. Oncol. 17 (2006) 735-749.

[216] N. Larson, H. Ghandehari, Polymeric conjugates for drug delivery, Chem. Mater. 24 (2012) 840-853.

[217] K. Tsukigawa, L. Liao, H. Nakamura, J. Fang, K. Greish, M. Otagiri, H. Maeda, Synthesis and therapeutic effect of styrene-maleic acid copolymer-conjugated pirarubicin, Cancer. Sci. 106 (2015) 270-278.

[218] R. Yang, G. Mondal, D. Wen, R.I. Mahato, Combination therapy of paclitaxel and cyclopamine polymer-drug conjugates to treat advanced prostate cancer, Nanomedicine 13 (2017) 391-401.

[219] F. Li, M. Danquah, R.I. Mahato, Synthesis and characterization of amphiphilic lipopolymers for micellar drug delivery, Biomacromolecules 11 (2010) 2610-2620.

[220] B.N. Singh, J. Fu, R.K. Srivastava, S. Shankar, Hedgehog signaling antagonist GDC-0449 (Vismodegib) inhibits pancreatic cancer stem cell characteristics: molecular mechanisms, PLoS One 6 (2011) e27306.

[221] N.A. Franken, H.M. Rodermond, J. Stap, J. Haveman, C. van Bree, Clonogenic assay of cells in vitro, Nat. Protoc. 1 (2006) 2315-2319.

[222] K. Kattel, G. Mondal, F. Lin, V. Kumar, R.I. Mahato, Biodistribution of Self-Assembling Polymer-Gemcitabine Conjugate after Systemic Administration into Orthotopic Pancreatic Tumor Bearing Mice, Mol. Pharm. 14 (2017) 1365-1372.

[223] G. Mondal, V. Kumar, S.K. Shukla, P.K. Singh, R.I. Mahato, EGFR-Targeted Polymeric Mixed Micelles Carrying Gemcitabine for Treating Pancreatic Cancer, Biomacromolecules 17 (2016) 301-313.

[224] D. Chitkara, A. Mittal, S.W. Behrman, N. Kumar, R.I. Mahato, Self-assembling, amphiphilic polymer-gemcitabine conjugate shows enhanced antitumor efficacy against human pancreatic adenocarcinoma, Bioconjug. Chem. 24 (2013) 1161-1173.

[225] A.L. Johannessen, S.H. Torp, The clinical value of Ki-67/MIB-1 labeling index in human astrocytomas, Pathol. Oncol. Res. 12 (2006) 143-147.

[226] J. Verweij, M. Clavel, B. Chevalier, Paclitaxel (Taxol) and docetaxel (Taxotere): not simply two of a kind, Ann. Oncol. 5 (1994) 495-505.

[227] A. Dimou, K.N. Syrigos, M.W. Saif, Overcoming the stromal barrier: technologies to optimize drug delivery in pancreatic cancer, Ther. Adv. Med. Oncol. 4 (2012) 271-279.

[228] D. Mahadevan, D.D. Von Hoff, Tumor-stroma interactions in pancreatic ductal adenocarcinoma, Mol. Cancer. Ther. 6 (2007) 1186-1197.

[229] H.L. Kindler, Front-line therapy of advanced pancreatic cancer, Semin. Oncol. 32 (2005) S33-6.

[230] D.T. Chang, D. Schellenberg, J. Shen, J. Kim, K.A. Goodman, G.A. Fisher, J.M. Ford, T. Desser, A. Quon, A.C. Koong, Stereotactic radiotherapy for unresectable adenocarcinoma of the pancreas, Cancer 115 (2009) 665-672.

[231] Q. Xu, T.P. Zhang, Y.P. Zhao, Advances in early diagnosis and therapy of pancreatic cancer, Hepatobiliary. Pancreat. Dis. Int. 10 (2011) 128-135.

[232] K.L. Hennenfent, R. Govindan, Novel formulations of taxanes: a review. Old wine in a new bottle? Ann. Oncol. 17 (2006) 735-749.

[233] M.V. Apte, S. Park, P.A. Phillips, N. Santucci, D. Goldstein, R.K. Kumar, G.A. Ramm, M. Buchler, H. Friess, J.A. McCarroll, G. Keogh, N. Merrett, R. Pirola, J.S. Wilson, Desmoplastic reaction in pancreatic cancer: role of pancreatic stellate cells, Pancreas 29 (2004) 179-187.

[234] J.A. McCarroll, S. Naim, G. Sharbeen, N. Russia, J. Lee, M. Kavallaris, D. Goldstein, P.A. Phillips, Role of pancreatic stellate cells in chemoresistance in pancreatic cancer, Front. Physiol. 5 (2014) 141.

[235] M.V. Apte, P.S. Haber, S.J. Darby, S.C. Rodgers, G.W. McCaughan, M.A. Korsten, R.C. Pirola, J.S. Wilson, Pancreatic stellate cells are activated by proinflammatory cytokines: implications for pancreatic fibrogenesis, Gut 44 (1999) 534-541.

[236] B. Uzunparmak, I.H. Sahin, Pancreatic cancer microenvironment: a current dilemma, Clin. Transl. Med. 8 (2019) 2-019-0221-1.

[237] P.P. Provenzano, C. Cuevas, A.E. Chang, V.K. Goel, D.D. Von Hoff, S.R. Hingorani, Enzymatic targeting of the stroma ablates physical barriers to treatment of pancreatic ductal adenocarcinoma, Cancer. Cell. 21 (2012) 418-429.

[238] V.P. Chauhan, J.D. Martin, H. Liu, D.A. Lacorre, S.R. Jain, S.V. Kozin, T. Stylianopoulos, A.S. Mousa, X. Han, P. Adstamongkonkul, Z. Popovic, P. Huang, M.G. Bawendi, Y. Boucher, R.K. Jain, Angiotensin inhibition enhances drug delivery and potentiates chemotherapy by decompressing tumour blood vessels, Nat. Commun. 4 (2013) 2516.

[239] C. Voutouri, C. Polydorou, P. Papageorgis, V. Gkretsi, T. Stylianopoulos, Hyaluronan-Derived Swelling of Solid Tumors, the Contribution of Collagen and Cancer Cells, and Implications for Cancer Therapy, Neoplasia 18 (2016) 732-741.

[240] P.P. Provenzano, S.R. Hingorani, Hyaluronan, fluid pressure, and stromal resistance in pancreas cancer, Br. J. Cancer 108 (2013) 1-8.

[241] C.H. Heldin, K. Rubin, K. Pietras, A. Ostman, High interstitial fluid pressure - an obstacle in cancer therapy, Nat. Rev. Cancer. 4 (2004) 806-813.

[242] M.J. Berna, O. Seiz, J.F. Nast, D. Benten, M. Blaker, J. Koch, A.W. Lohse, A. Pace, CCK1 and CCK2 receptors are expressed on pancreatic stellate cells and induce collagen production, J. Biol. Chem. 285 (2010) 38905-38914.

[243] J.P. Smith, T.K. Cooper, C.O. McGovern, E.L. Gilius, Q. Zhong, J. Liao, A.A. Molinolo, J.S. Gutkind, G.L. Matters, Cholecystokinin receptor antagonist halts progression of pancreatic cancer precursor lesions and fibrosis in mice, Pancreas 43 (2014) 1050-1059.

[244] Y. Mao, L. Xi, Q. Li, Z. Cai, Y. Lai, X. Zhang, C. Yu, Regulation of cell apoptosis and proliferation in pancreatic cancer through PI3K/Akt pathway via Polo-like kinase 1, Oncol. Rep. 36 (2016) 49-56.

[245] A. Puissant, S.M. Frumm, G. Alexe, C.F. Bassil, J. Qi, Y.H. Chanthery, E.A. Nekritz, R. Zeid, W.C. Gustafson, P. Greninger, M.J. Garnett, U. McDermott, C.H. Benes, A.L. Kung, W.A. Weiss, J.E. Bradner, K. Stegmaier, Targeting MYCN in neuroblastoma by BET bromodomain inhibition, Cancer. Discov. 3 (2013) 308-323.

[246] W.W. Lockwood, K. Zejnullahu, J.E. Bradner, H. Varmus, Sensitivity of human lung adenocarcinoma cell lines to targeted inhibition of BET epigenetic signaling proteins, Proc. Natl. Acad. Sci. U. S. A. 109 (2012) 19408-19413.

[247] J.E. Delmore, G.C. Issa, M.E. Lemieux, P.B. Rahl, J. Shi, H.M. Jacobs, E. Kastritis, T. Gilpatrick, R.M. Paranal, J. Qi, M. Chesi, A.C. Schinzel, M.R. McKeown, T.P. Heffernan, C.R. Vakoc, P.L. Bergsagel, I.M. Ghobrial, P.G. Richardson, R.A. Young, W.C. Hahn, K.C. Anderson, A.L. Kung, J.E. Bradner, C.S. Mitsiades, BET bromodomain inhibition as a therapeutic strategy to target c-Myc, Cell 146 (2011) 904-917.

[248] J. Zuber, J. Shi, E. Wang, A.R. Rappaport, H. Herrmann, E.A. Sison, D. Magoon, J. Qi, K. Blatt, M. Wunderlich, M.J. Taylor, C. Johns, A. Chicas, J.C. Mulloy, S.C. Kogan, P. Brown, P. Valent, J.E. Bradner, S.W. Lowe, C.R. Vakoc, RNAi screen identifies Brd4 as a therapeutic target in acute myeloid leukaemia, Nature 478 (2011) 524-528.

[249] P. Filippakopoulos, J. Qi, S. Picaud, Y. Shen, W.B. Smith, O. Fedorov, E.M. Morse, T. Keates, T.T. Hickman, I. Felletar, M. Philpott, S. Munro, M.R. McKeown, Y. Wang, A.L. Christie, N. West, M.J. Cameron, B. Schwartz, T.D. Heightman, N. La Thangue, C.A. French, O. Wiest, A.L. Kung, S. Knapp, J.E. Bradner, Selective inhibition of BET bromodomains, Nature 468 (2010) 1067-1073.

[250] X. Tang, R. Peng, Y. Ren, S. Apparsundaram, J. Deguzman, C.M. Bauer, A.F. Hoffman, S. Hamilton, Z. Liang, H. Zeng, M.E. Fuentes, J.A. Demartino, C. Kitson, C.S.

Stevenson, D.C. Budd, BET bromodomain proteins mediate downstream signaling events following growth factor stimulation in human lung fibroblasts and are involved in bleomycin-induced pulmonary fibrosis, Mol. Pharmacol. 83 (2013) 283-293.

[251] V. Sahai, A.J. Redig, K.A. Collier, F.D. Eckerdt, H.G. Munshi, Targeting BET bromodomain proteins in solid tumors, Oncotarget 7 (2016) 53997-54009.

[252] S. Shu, C.Y. Lin, H.H. He, R.M. Witwicki, D.P. Tabassum, J.M. Roberts, M. Janiszewska, S.J. Huh, Y. Liang, J. Ryan, E. Doherty, H. Mohammed, H. Guo, D.G. Stover, M.B. Ekram, J. Brown, C. D'Santos, I.E. Krop, D. Dillon, M. McKeown, C. Ott, J. Qi, M. Ni, P.K. Rao, M. Duarte, S.Y. Wu, C.M. Chiang, L. Anders, R.A. Young, E. Winer, A. Letai, W.T. Barry, J.S. Carroll, H. Long, M. Brown, X.S. Liu, C.A. Meyer, J.E. Bradner, K. Polyak, Response and resistance to BET bromodomain inhibitors in triple-negative breast cancer, Nature 529 (2016) 413-417.

[253] V. Sahai, K. Kumar, L.M. Knab, C.R. Chow, S.S. Raza, D.J. Bentrem, K. Ebine, H.G. Munshi, BET bromodomain inhibitors block growth of pancreatic cancer cells in three-dimensional collagen, Mol. Cancer. Ther. 13 (2014) 1907-1917.

[254] K. Kumar, S.S. Raza, L.M. Knab, C.R. Chow, B. Kwok, D.J. Bentrem, R. Popovic, K. Ebine, J.D. Licht, H.G. Munshi, GLI2-dependent c-MYC upregulation mediates resistance of pancreatic cancer cells to the BET bromodomain inhibitor JQ1, Sci. Rep. 5 (2015) 9489.

[255] K. Kumar, B.T. DeCant, P.J. Grippo, R.F. Hwang, D.J. Bentrem, K. Ebine, H.G. Munshi, BET inhibitors block pancreatic stellate cell collagen I production and attenuate fibrosis in vivo, JCI Insight 2 (2017) e88032.

[256] F.H. Andrews, A.R. Singh, S. Joshi, C.A. Smith, G.A. Morales, J.R. Garlich, D.L. Durden, T.G. Kutateladze, Dual-activity PI3K-BRD4 inhibitor for the orthogonal inhibition of MYC to block tumor growth and metastasis, Proc. Natl. Acad. Sci. U. S. A. 114 (2017) E1072-E1080.

[257] J.X. Zhu, J.R. Xiao, SF2523 inhibits human chondrosarcoma cell growth in vitro and in vivo, Biochem. Biophys. Res. Commun. 511 (2019) 559-565.

[258] G. Shen, M. Jiang, J. Pu, Dual inhibition of BRD4 and PI3K by SF2523 suppresses human prostate cancer cell growth in vitro and in vivo, Biochem. Biophys. Res. Commun. 495 (2018) 567-573.

[259] R. Gilabert-Oriol, G.M. Ryan, A.W.Y. Leung, N.S. Firmino, K.L. Bennewith, M.B. Bally, Liposomal Formulations to Modulate the Tumour Microenvironment and Antitumour Immune Response, Int. J. Mol. Sci. 19 (2018) 10.3390/ijms19102922.

[260] V. Mundra, Y. Lu, M. Danquah, W. Li, D.D. Miller, R.I. Mahato, Formulation and characterization of polyester/polycarbonate nanoparticles for delivery of a novel microtubule destabilizing agent, Pharm. Res. 29 (2012) 3064-3074.

[261] V. Mundra, Y. Peng, V. Kumar, W. Li, D.D. Miller, R.I. Mahato, Systemic delivery of nanoparticle formulation of novel tubulin inhibitor for treating metastatic melanoma, Drug Deliv. Transl. Res. 5 (2015) 199-208.

[262] J. Bariwal, V. Kumar, H. Chen, R.S. Bhattarai, Y. Peng, W. Li, R.I. Mahato, Nanoparticulate delivery of potent microtubule inhibitor for metastatic melanoma treatment, J. Control. Release 309 (2019) 231-243.

[263] M. Vandana, S.K. Sahoo, Long circulation and cytotoxicity of PEGylated gemcitabine and its potential for the treatment of pancreatic cancer, Biomaterials 31 (2010) 9340-9356.

[264] V. Kumar, V. Mundra, Y. Peng, Y. Wang, C. Tan, R.I. Mahato, Pharmacokinetics and biodistribution of polymeric micelles containing miRNA and small-molecule drug in orthotopic pancreatic tumor-bearing mice, Theranostics 8 (2018) 4033-4049.

[265] U. Ozerdem, A.R. Hargens, A simple method for measuring interstitial fluid pressure in cancer tissues, Microvasc. Res. 70 (2005) 116-120.

[266] C.B. Thompson, H.M. Shepard, P.M. O'Connor, S. Kadhim, P. Jiang, R.J. Osgood, L.H. Bookbinder, X. Li, B.J. Sugarman, R.J. Connor, S. Nadjsombati, G.I. Frost, Enzymatic depletion of tumor hyaluronan induces antitumor responses in preclinical animal models, Mol. Cancer. Ther. 9 (2010) 3052-3064.

[267] V. Kumar, V. Mundra, R.I. Mahato, Nanomedicines of Hedgehog inhibitor and PPAR-gamma agonist for treating liver fibrosis, Pharm. Res. 31 (2014) 1158-1169.

[268] A. Sultana, C. Tudur Smith, D. Cunningham, N. Starling, J.P. Neoptolemos, P. Ghaneh, Meta-analyses of chemotherapy for locally advanced and metastatic pancreatic cancer: results of secondary end points analyses, Br. J. Cancer 99 (2008) 6-13.

[269] R.L. Siegel, S.A. Fedewa, K.D. Miller, A. Goding-Sauer, P.S. Pinheiro, D. Martinez-Tyson, A. Jemal, Cancer statistics for Hispanics/Latinos, 2015, CA Cancer. J. Clin. 65 (2015) 457-480.

[270] X. Sun, X. Zhou, Y. Zhang, X. Zhu, H. Liu, Systematic Review and Meta-Analysis of Diagnostic Accuracy of miRNAs in Patients with Pancreatic Cancer, Dis. Markers 2018 (2018) 6292396.

[271] J.E. Liebmann, J.A. Cook, C. Lipschultz, D. Teague, J. Fisher, J.B. Mitchell, Cytotoxic studies of paclitaxel (Taxol) in human tumour cell lines, Br. J. Cancer 68 (1993) 1104-1109.

[272] N. Dey, B. Leyland-Jones, P. De, MYC-xing it up with PIK3CA mutation and resistance to PI3K inhibitors: summit of two giants in breast cancers, Am. J. Cancer. Res. 5 (2014) 1-19.

[273] J.C. Bendell, J. Rodon, H.A. Burris, M. de Jonge, J. Verweij, D. Birle, D. Demanse, S.S. De Buck, Q.C. Ru, M. Peters, M. Goldbrunner, J. Baselga, Phase I, dose-escalation study of BKM120, an oral pan-Class I PI3K inhibitor, in patients with advanced solid tumors, J. Clin. Oncol. 30 (2012) 282-290.

[274] F. Janku, J.J. Wheler, S.N. Westin, S.L. Moulder, A. Naing, A.M. Tsimberidou, S. Fu, G.S. Falchook, D.S. Hong, I. Garrido-Laguna, R. Luthra, J.J. Lee, K.H. Lu, R. Kurzrock, PI3K/AKT/mTOR inhibitors in patients with breast and gynecologic malignancies harboring PIK3CA mutations, J. Clin. Oncol. 30 (2012) 777-782.

[275] P.R. Ravi, R. Vats, V. Dalal, N. Gadekar, Design, optimization and evaluation of poly-ε-caprolactone (PCL) based polymeric nanoparticles for oral delivery of lopinavir, Drug Dev. Ind. Pharm. 41 (2015) 131-140.

[276] Y. Wang, X. Liang, R. Tong, J. Yang, Y. Yang, J. Zhong, Q. Wu, C. Gong, J. Yu, L. Cai, Gambogic Acid-Loaded Polymeric Micelles for Improved Therapeutic Effect in Breast Cancer, J. Biomed. Nanotechnol 14 (2018) 1695-1704.

[277] J. Huang, H. Zhang, Y. Yu, Y. Chen, D. Wang, G. Zhang, G. Zhou, J. Liu, Z. Sun, D. Sun, Y. Lu, Y. Zhong, Biodegradable self-assembled nanoparticles of poly (D,L-lactide-

co-glycolide)/hyaluronic acid block copolymers for target delivery of docetaxel to breast cancer, Biomaterials 35 (2014) 550-566.

[278] Y. Tan, L. Wang, Y. Du, X. Liu, Z. Chen, X. Weng, J. Guo, H. Chen, M. Wang, X. Wang, Inhibition of BRD4 suppresses tumor growth in prostate cancer via the enhancement of FOXO1 expression, Int. J. Oncol. 53 (2018) 2503-2517.

[279] T.R. Spivak-Kroizman, G. Hostetter, R. Posner, M. Aziz, C. Hu, M.J. Demeure, D. Von Hoff, S.R. Hingorani, T.B. Palculict, J. Izzo, G.M. Kiriakova, M. Abdelmelek, G. Bartholomeusz, B.P. James, G. Powis, Hypoxia triggers hedgehog-mediated tumor-stromal interactions in pancreatic cancer, Cancer Res. 73 (2013) 3235-3247.

[280] C. Bouzin, O. Feron, Targeting tumor stroma and exploiting mature tumor vasculature to improve anti-cancer drug delivery, Drug Resist Updat 10 (2007) 109-120.

[281] R.K. Jain, Transport of molecules across tumor vasculature, Cancer Metastasis Rev. 6 (1987) 559-593.

[282] O. Tredan, C.M. Galmarini, K. Patel, I.F. Tannock, Drug resistance and the solid tumor microenvironment, J. Natl. Cancer Inst. 99 (2007) 1441-1454.